The reverse flow adsorption technology for the process integrated recycling of homogeneous catalysts

THE REVERSE FLOW ADSORPTION TECHNOLOGY FOR THE PROCESS INTEGRATED RECYCLING OF HOMOGENEOUS CATALYSTS

Tanja Đekić Živković

Graduation committee

Chairman:	Prof.dr. Niemandsverdriet	Eindhoven University of Technology
Promoter:	Prof.dr.ir. A.B. de Haan	Eindhoven University of Technology
Assistant promoter:	Dr.ir. A.G.J. van der Ham	University of Twente
Committee members:	Prof.dr.ir. M. Petkovska	University of Belgrade
	Prof.dr. P.W.N.M van Leeuwen	University of Amsterdam
	Prof.dr.ir. F. Kapteijn	Delft University of Technology
	Prof.dr. D. Vögt	Eindhoven University of Technology
	Prof.dr.ir. J.C. Schouten	Eindhoven University of Technology

The Reverse Flow Adsorption Technology for the Process Integrated Recycling of Homogeneous Catalysts
T. Đekić Živković

Cover design by N. Jovičić

The Reverse Flow Adsorption Technology for the Process Integrated Recycling of Homogeneous Catalysts

PROEFSCHRIFT

ter verkrijging van de graad van doctor aan de
Technische Universiteit Eindhoven, op gezag van de
Rector Magnificus, prof.dr.ir. C.J. van Duijn, voor een
commissie aangewezen door het College voor
Promoties in het openbaar te verdedigen
op woensdag 20 februari 2008 om 16.00 uur

door

Tanja Đekić Živković

geboren te Virovitica, Kroatië

Dit proefschrift is goedgekeurd door de promotor:

prof.dr.ir. A.B. de Haan

Copromotor:
dr.ir. A.G.J. van der Ham

To my parents/ Mojim roditeljima

Acknowledgments

My gratitude to everyone who was there for me in the last four years and helped me to finish this work*.

My Dependence

by *Rabindranath Tagore*

*I like to be dependent, and so for ever
with warmth and care of my mother
my father, to love, kiss and embrace
wear life happily in all their grace.*

*I like to be dependent, and so for ever
on my kith and kin, for they all shower
harsh and warm advices, complaints
full wondering, true and info giants.*

*I like to be dependent, and so for ever
for my friends, chat and want me near
with domestic, family and romantic tips
colleagues as well, guide me work at risks.*

*I like to be dependent, and so for ever
for my neighbours too, envy at times
when at my rise of fortune like to hear
my daily steps, easy and odd things too.*

*My promoter, assistant promoter, graduation committee members, members of the user's committee meetings, reviewers of my articles, my master students, colleagues, as well as my friends, relatives and mostly my family.

I

II

The Reverse Flow Adsorption Technology for the Process Integrated Recycling of Homogeneous Catalysts

Catalysis is nowadays an essential part of many industrial processes. Researchers and scientists still struggle with a choice between heterogeneous and homogeneous catalysis. Although homogeneous catalysis offers better selectivity, activity and milder reaction conditions, on a volume basis most of the chemical reactions are performed in the presence of heterogeneous catalysts. The reason for selecting heterogeneous catalysts is simple: difficult and expensive methods for the recovery of homogeneous catalysts that lead to a unavoidable loss of precious metals, and catalyst deactivation.

To understand why this occurs, we primarily focused on the structure and the composition of homogeneous catalyst precursors that are complex compounds that are always in equilibrium with their free metal, free ligand and other complex forms. The ratios between different species are defined by the stability constants, which are influenced by different parameters such as the type of metal, ligand, counter ion or solvent. Thus, determination of the stability constants for a range of different complexes as well as the concentration of each species present in the solution was initially studied. Cobalt, nickel and palladium halogens with triphenylphosphine as a ligand were selected as complexes since they are commonly used in industrial processes. The results were analyzed with a stability constant model developed for 1:2 complexation. The stability constants of the selected complex systems increase in order: $[PdCl_2(OPPh_3)_2]_{MeCN} \approx [CoCl_2(PPh_3)_2]_{butanol} < [CoBr_2(PPh_3)_2]_{MeCN} < [CoCl_2(PPh_3)_2]_{MeCN} < [NiBr_2(PPh_3)_2]_{MeCN} < [PdCl_2(PPh_3)_2]_{DMF} < [PdCl_2(PPh_3)_2]_{MeCN}$. The obtained results show that even for the very high overall stability constants (range of 10^{12}) there are still free metal forms remaining. Since many recovery methods are designed just for the catalyst form, residual free metal is very often left to leach.

Therefore in this thesis we propose a new method for recovery and recycling of homogeneous catalysts: ***Reverse Flow Adsorption***. Reverse flow adsorption (RFA) combines separation by adsorption with the reverse flow technology. In this set-up the catalytic reaction takes place in the homogeneous phase where the full advantage of the high rates and selectivity of such systems is taken. The homogeneous catalyst is separated from the outlet reaction mixture by adsorption on beds downstream the reactor. On the first bed all metal contained forms are adsorbed, and the second bed adsorbs free ligand. In the subsequent step, the inlet feed changes its direction and enters the adsorption beds with previously recovered homogenous catalyst. Catalyst is desorbed and recycled back to the reactor. Leaving the reactor the product stream enters the second pair of adsorption beds

where the homogeneous catalyst is again recovered. In this process four adsorption beds are required, two for recovery of all metal containing species and two for recovery of the free ligand. With this concept drawbacks of other recovery methods can be overcome:

- Leaching of the homogenous catalyst by changing flow direction before the appearance of breakthrough at the exit of adsorption bed;
- Deactivation of the catalyst due to temperature shift since the adsorption process can run at very mild conditions.
- The process should be economically feasible by reaching high number of cycles before the adsorbent is renewed.

After defining a recovery approach, the selection of suitable adsorbents was studied. Silica was selected as a carrier of functionalized groups due to its rigid and uniform pore structure. A wide range of commercially available and self-made functionalized silica was evaluated. As model complexes we selected $CoCl_2(PPh_3)_2$, $PdCl_2(PPh_3)_2$ and $RhCl(PPh_3)_3$. Twelve functionalized groups selected from four classes containing one or more N-, O-, P- or S- atoms were evaluated for adsorption of metal centres and five functionalized groups are selected for adsorption of the ligand. A preliminary selection of the adsorbents was done by investigating the adsorption of the metal salts for the cobalt and the palladium complex. The results are explained by the Hard and Soft Acid Base (HSAB) theory. 2-(2-pyridyl)ethyl- functionalized silica is selected as an adsorbent for adsorption of the $CoCl_2(PPh_3)_2$ from acetonitrile, while 3-(mercapto)propyl-functionalized silica is selected as adsorbent for adsorption of the $PdCl_2(PPh_3)_2$ and $RhCl(PPh_3)_3$ from DMF. Functionalized silica containing propyl-sulphonic acid is selected as adsorbent for adsorption of the triphenylphosphine.

For $CoCl_2$ adsorption on 2-(2-pyridyl)ethyl-functionalized silica and 3-(1-morpholino)propyl-functionalized silica equilibrium experiments were extended by introducing the triphenylphosphine ligand in the system which promoted the competition of the functionalized groups on the adsorbent and the ligands present in solution. Therefore we have developed a model which can describe the competitive adsorption of complex species. Since in a solution $CoCl_2(PPh_3)_2$ (ML_2) is always in equilibrium with its free metal centre $CoCl_2$ (M), free ligand PPh_3 (L) and complex form $CoCl_2(PPh_3)$ (ML), three models were evaluated (M, M-ML and M-ML-ML_2). They combine the equilibrium of the complex forms present in a solution with its competitive adsorption on the functionalized silica. Comparison of the model results with the experimental adsorption data shows that the model which takes all three forms M, ML and ML_2, into account is needed to describe the experimental results consistently.

After selection of suitable functionalized groups on the silica based adsorbent, we directed our research to the determination of the intraparticle diffusion coefficients of

CoCl$_2$ in the mezoporous functionalized silica. The adsorption kinetics is investigated with the Zero Length Column (ZLC) method. Initially, experiments were performed at different flow rates to eliminate the effect of external mass transfer. The effect of pore size (60Å and 90Å), particle size (40 μm -1000 μm) and initial CoCl$_2$ concentration (1 mmol/l -2.0 mmol/l) on the mass transfer was investigated. A model was developed to determine the effective pore diffusion coefficient of CoCl$_2$ by fitting the model to the experimental data. The effective pore diffusion coefficients determined for two different pore sizes of silica are D$_p$(60Å)=1.95·10^{-10} [m^2/s] and D$_p$(90Å)=5.8·10^{-10} [m^2/s]. The particle size and the initial CoCl$_2$ concentration do not influence the value of the diffusion coefficient. In comparison with polymer adsorbents, silica based adsorbents have higher effective diffusion coefficients, as well as a more uniform and stable pore structure.

In this thesis two models are developed to describe the reversible adsorption. One describes the adsorption of the metal containing species and a second model describes adsorption of the free ligand. Models are built to demonstrate the stability of the RFA process, to study the influence of catalyst and to mathematically optimize the design of the silica adsorbent. Performing numerous simulations it is shown that stable operation is reached, where leaching of both metal and ligand is prevented. The RFA process can be applied for a wide range of the catalyst stability constants (10^0-10^{12} (dm^3/mol)^2) and it is specially applicable for the recovery of homogeneous catalysts from system that have a low metal concentration. It is also shown that the binding strength between the adsorbing catalyst and the selected adsorbent should be around 0.8 l/mmol; the adsorbent capacity and the diffusion coefficient should be maximal; and the particle size and the bed porosity minimal. Material and process limitations are also pointed out. In a simulation of the rhodium recovery in the BASF hydroformylation process a total adsorption bed volume of 6% of the reactor volume is required for recovery of the metal species.

Finally, the stability of the reverse flow adsorption and activity of the catalyst after several cycles of reversible adsorption/desorption of the catalyst precursor are studied. The Heck reaction is selected as a test reaction to measure the catalytic activity of PdCl$_2$(PPh$_3$)$_2$ in acetonitrile at very low concentrations. The RFA set-up is built to continuously adsorb and desorb PdCl$_2$ and the Heck reaction is used in the subsequent step to test the activity. Leaching was observed in the RFA experiments. This leaching is closely related with the particular chemistry and especially for metals changing their valence state in catalysis, as palladium often does. Thus, overall 96% process efficiency is achieved in the experimental study of the reversible adsorption and desorption. The results also show that after multiple cycles of continuous adsorption and desorption of PdCl$_2$, the activity of the homogeneous catalyst remains constant.

From the above stated and in spite of the leaching of the $PdCl_2$ in the reverse flow experiments the major outcome of this work is that ***Reverse Flow Adsorption*** is a promising concept for the recovery and recycling of homogeneous catalysts.

Contents

VIII

Introduction to the Reverse Flow Adsorption technology for the process integrated recycling and recovery of homogeneous catalysts

1.1 Catalysis

Nowadays the use of catalysts is essential for many industrial processes and applications. Between 85 and 90% of the products of the chemical industry is produced with catalytic processes [1]. Without catalysts many reactions would not be possible because catalysts offer energetically favourable mechanisms. In the beginning catalysts were used for the production of liquid fuels and bulk chemistry, but with time catalysts became also essential for the production of fine chemicals. Besides the use for production purposes, catalysts are also beneficial in the field of green chemistry, where they are used for pollution prevention by avoiding waste formation [1].

About 150 years ago Berzelius was the first person who mentioned the word 'catalyst' [2]. Since then scientists came up with many definitions for the word catalyst making it more precise and accurate. The most common definition today is that a catalyst is a substance that increases the rate at which chemical reaction approaches equilibrium without becoming permanently involved itself [2]. On the other hand, Sabatier was the first who gave a rough classification of the different catalytic reactions. He defined homogeneous systems as systems where all compounds present or at least one of them are miscible with the catalyst; and heterogeneous systems as systems that are based upon a solid catalyst which is in contact with a reactive liquid or gas [3].

Heterogeneous catalysts are still more applied in industry than homogeneous, but this situation is gradually changing with time. Due to many prerequisites that a good catalyst should fulfil, the overall approach of the research for suitable catalysts is changing in favour of homogenous catalysts. As can be seen from Table 1.1 homogeneous catalysts, compared to heterogeneous, have several advantages such as high activity, better selectivity, no diffusion/mass transfer problems, etc.

In spite of all these advantages, homogeneous catalysts have a major problem: their recovery. Although many scientists have been working on solving this problem there is still no universal solution. The most common techniques that have been investigated are distillation, extraction, membrane technology, precipitation/filtration, biphasic catalysis, ion exchange and adsorption [17-52]. Major drawbacks of these methods are the incomplete complex recovery and/or decomposition of the catalyst which leads to its deactivation [4]. Therefore *Reverse Flow Adsorption* technology is proposed as a novel concept for the recovery of the homogeneous catalysts. It combines adsorption as a separation method with reverse flow technology [5].

1

Table 1.1. Homogeneous versus heterogeneous catalysis [3]

	Homogeneous catalysis	Heterogeneous catalysis
Activity	High	Variable
Selectivity	High	Variable
Reaction conditions	Mild	Mild, Harsh
Service life of catalysts	Variable	Long
Sensitivity toward catalyst poisons	Medium	High
Diffusion problems	None	May be important
Variability of steric and electronic properties of catalysts	Possible	Not possible
Mechanistic understanding	Plausible under random conditions	Limited
Catalyst recycling	Expensive	Easy

This chapter focuses on three main subjects: homogeneous catalysts, present recovery methods and objectives of this thesis. First the structure of homogeneous catalysts such as effects of the metals and ligands will be discussed. Hereafter, the recovery methods that have already been investigated are reviewed and reverse flow adsorption technology will be presented as a novel concept for the recovery of homogeneous catalysts. At the end of this chapter the scope of this project will be set, explaining the goal of the project and necessary steps to reach it. Finally, the outline of the thesis is presented.

1.2 Homogeneous catalysts

Homogeneous catalysts are compounds that are in the same phase as the reactant or the product, and that phase is mostly a liquid. They are typically used at reaction temperatures less than 250°C [6]. Those mild conditions are more energetically favourable than the severe conditions often used for heterogeneous catalysts. Other important favourable properties of homogeneous catalysts are high activity and improved selectivity. The reaction rate is proportional to the activity of the catalyst at equivalent temperatures, pressures, reaction volumes and mole fractions [7]. Improved selectivity of homogeneous catalyst is observed with respect to chemoselectivity, regioselectivity, diastereoselectivity and enantioselectivity [2]. Besides the preferable activity and selectivity, homogeneous catalysts are less susceptible to the poisoning by sulfur-containing compounds. Furthermore the performance of the catalysis can be explained at the molecular level that gives an insight into the all steps of the reactions [6].

Organometallic catalysts belong to the group of homogenous catalysts. Coordination complexes are often catalyst precursor forms of organometallic catalysts. Both forms consist of a central metal which is surrounded by organic and sometimes also inorganic ligands. In solution these metal-ligand complexes are always in equilibrium with their free metal centre (metal atom or metal salt), ligands and other complex forms. This equilibrium is described by stability constants:
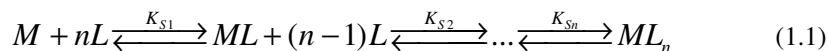
$$M + nL \xrightleftharpoons{K_{S1}} ML + (n-1)L \xrightleftharpoons{K_{S2}} ... \xrightleftharpoons{K_{Sn}} ML_n \qquad (1.1)$$

where M, L, ML, ML_n represent the free metal salt, free ligand, and different forms of the complex respectively, and n represents a number of surrounding ligands. This equilibrium is described by stability constants or complexation constants defined as the ratio between the concentrations of the complex form of the catalyst $[ML_i]$ and the concentrations of free metal $[M]$ and free ligands $[L]$:

$$K_{s1} = \frac{[ML]}{[M] \cdot [L]} \qquad (1.2)$$

…

$$K_{sn} = \frac{[ML_n]}{[ML_{n-1}] \cdot [L]} . \qquad (1.3)$$

where K_{s1} and K_{sn} present the stability constants for each of the individual complexation steps.

1.2.1 Metals used in the catalytic processes

Both metal and ligand determine the properties of the catalyst. Transition metals such as cobalt, palladium, rhodium, nickel, etc., are the most commonly encountered metals in the catalytic processes [2]. Cobalt or rhodium as a metal centre together with phosphine ligands are used as the catalyst in hydroformylation processes [3]. Despite the fact that cobalt is less expensive than rhodium, the mild process conditions and the use of arylphosphines with rhodium make cobalt the second choice. Production of the terephthalic acid where Co is selected as a catalyst is one of the largest homogenous catalyzed processes [2]. The palladium-triphenylphosphine complex is used mostly in coupling reaction such as for instance the Suzuki, Sonogashira and Heck reactions [8]. In this work oxidation processes employing Co, Pd or Ti with oxygenate ligands will not be considered.

1.2.2   Ligands

The amount and type of the ligand are very often crucial for the rate of reaction and the selectivity. Ligand effects are extremely important in homogeneous catalysis since they determine properties of the metal complex. The same transition metal can give a variety of products depending on the type of ligands that surround the metal centre. Whether the product will be linear or branched, cis or trans, depends on the type of ligand used through its electronic and steric properties.

Electronic effects describe the donor/acceptor properties of the ligand. It tells us how strong or weak the ligand is as σ-donor or π-acceptor. Strong σ-donor ligands provide a high electron density around the metal, and strong π-acceptors compete with other ligands for electron back donation. To describe steric parameters of the ligands Tolman's cone angle, θ, is used for monodentate ligands (Figure 1.1) and the bite angle is used for bidentate ligands since Tolman's cone angle is very often not straightforward (Figure 1.2) [2].
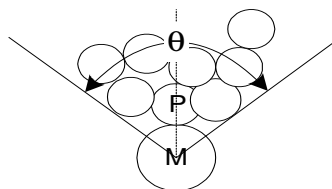
Figure 1.1. Tolman's cone angle
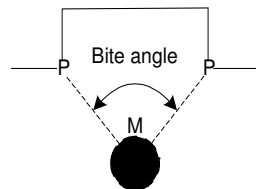
Figure 1.2. Bite angle

Ligands that have been most commonly utilized in catalysis are phosphines, amines, imines and cyclopentadienyl anions [2]. Phosphine ligands have the broadest industrial application. A general formula of phosphine ligands is PR_3, where R=alkyl, aryl, H, etc. Alkyl and aryl phosphines form complexes of high stability constants with many non-transition atoms and with many transition metals in a wide range of oxidation states [9]. Phosphine ligands are in general very good σ-donors and weak and good π-acceptors. They are neutral two electron donors and bind with metals via their lone pair. The binding of the phosphine ligand with the metal consists of two parts [10]. The first part is the sigma donation of the lone pair of the phosphine ligand to the free metal orbital. The second part is the back donation between the filled d-orbital of the metal and the empty phosphine orbital that is described as the empty d-orbital or anti-bonding σ-orbital (see Figure 1.3). Alkyl phosphines are strong bases and therefore very good σ-donors, while aryl phosphines are medium σ-donors. Steric effects can be easily controlled, by changing the phosphine ligands which are generally not complicated to synthesize [10]. The Tolman's cone angle

4

differs for every phosphine ligands, and varies from 87° for PH$_3$, over 145° for PPh$_3$, to 212° for P(mesityl)$_3$.

The negative side of the phosphine ligands is their sensitivity for oxidation that deactivates the metal centre. If a phosphine ligand is a good σ-donor it will also show the tendency to share its two electrons with oxygen, and will form a P-O bond. If so, the phosphor atom is losing its bond with the metal atom, leading to deactivation of the complex. Aryl phosphines are more air stable than alkyl phosphine[2]. This degradation of the phosphine ligand can limit its industrial application.

σ bond   **π backbond**

M ◄———: PR$_3$ M PR$_3$

Empty d or p- orbital   Filled σ-orbital   Filled d or p- orbital   Empty σ*-orbital
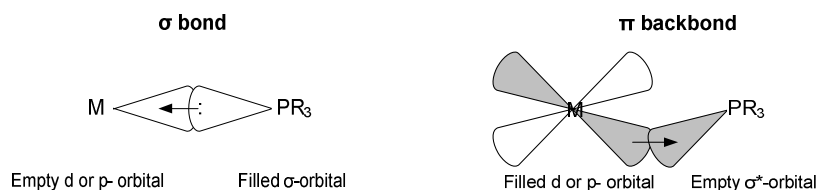
Figure 1.3. Bonding between metal and phosphine ligand [6]

1.2.3   Catalytic processes-Heck reaction

Homogeneous catalysis is equally used for production of bulk and fine chemicals. The Heck reaction is a homogeneously catalyzed reaction used for generating new C-C bonds (see Figure 1.4) [11-13]. The importance of the solvent type on the Heck vinylation reactions has been widely studied [11-16]. Palladium complexes with triphenylphosphine (PPh$_3$) as a ligand are often used in the Heck reaction. The influence of the PPh$_3$/Pd ratio has been studied and reported in the work of Zhao et al. [11] and Hermann et al. [16]. They observed that with increase of this ratio the rate of reaction significantly drops. Therefore the ratio of the metal and ligand should be strictly controlled at a PPh$_3$/Pd ratio range of 0 to 4 depending on the solvent type.

+ H$_2$C=CHCOOMe $\xrightarrow{Pd(OAC)_2(PPh_3)_2}$ H C=CHCOOMe
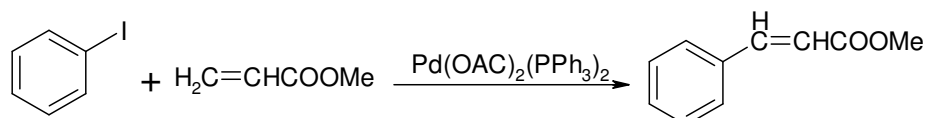
Figure 1.4. Heck reaction-vinylation of iodobenzene with methyl acrylate [11]

1.3   Technologies for the recovery of homogeneous catalysts

Nowadays many techniques are used to recover homogeneous catalysts. The most common separation methods used in industrial applications to recover homogeneous catalysts are distillation, extraction, membrane separations, precipitation/filtration, ion-

exchange and adsorption (heterogenization) (Figure 1.5). These recovery methods are both used on a large and small scale, already applied in industry for production of fine and bulk chemicals, or are still a subject of research. In the following paragraphs the present recovery methods will be reviewed as well as some of their applications and reported drawbacks. Biphasic catalysis is also addressed here as a method where homogeneous catalyst and reaction mixture are in two different phases.
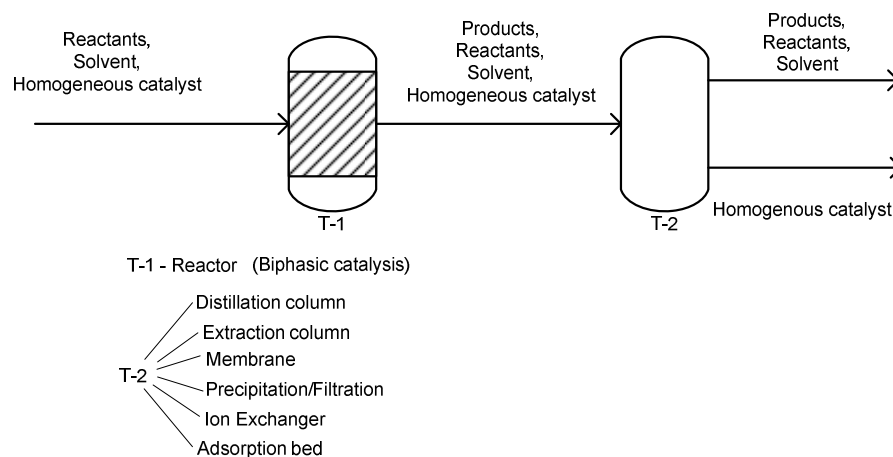
Figure 1.5. Recovery of homogeneous catalysts

1.3.1   Flash/Evaporation/Distillation

Single stage flash, evaporation and distillation are widely used operation methods for the separation of the catalyst from the principal product of the reaction [47]. In the Monsanto process for production of acetic acid by rhodium catalyzed methanol carbonylation, the catalyst is separated by conducting a simple flash and recycling it to the reactor. It is observed that catalyst is lost due to precipitation. To overcome these limitations a broad study is done on immobilizating the catalyst [47]. Distillation was for instance selected for the preparation of esters of beta., gamma.-unsaturated carboxylic acids by the carbonylation of conjugated dienes with carbon monoxide in the presence of a palladium catalyst [17]. Unfortunately they don't mention anything about its consequences, such as catalyst decomposition and deactivation. Keim et al. combines the use of ionic liquids together with distillation as an extension of Chauvin's work, who introduced ionic liquids in catalytic processes [18-23]. Ionic liquids significantly enhance the catalyst life time since they stabilize the catalyst against the thermal stress of distillation. The main drawback of using non volatile ionic liquids is that for some reactions accumulation of

6

high-boiling by-products in the non-volatile catalyst layer after several distillation cycles may become a problem [18].

Flash, evaporation and distillation are commonly used for the recycling of the catalyst since they do not require large investment costs. In combination with ionic liquids they can reduce common drawbacks such as deactivation due to temperature changes, vaporisation and precipitation [4]. This method is limited to processes with volatile products and by-products.

1.3.2   Extraction

Extraction is another method for recovery of homogeneous catalysts, very often used in industrial applications of companies as Shell, BASF, Mitsubishi [24-27]. The extraction process is performed usually in several steps. First, the product mixture containing a catalyst goes to the extraction column. There the mixture is contacted with an extractant which forms a complex with the catalyst and separates it from the product mixture. In the following step the catalyst can be separated from the extractant using one of the conventional methods such as distillation, decantation, etc, [24].   Edwin H. Homeier et al., described in their patent the recovery of the active metal catalyst by treating the product mixture with a nitrogen-containing compounds which extracted the catalyst [24].   In patents of BASF AG the rhodium catalyst is recovered from the products of a hydroformylation reaction by water soluble polymers [25] and aqueous solutions of weak acids [26]. For the recovery of ruthenium catalysts applied in the process for producing adamantanols by hydroxylation of adamantane compounds an aqueous alkali solution was selected [27]. Extraction is also used for recovery of homogeneous catalysts in combination with distillation [26].

Homogeneous catalyst can be recovered with a proper extractant to less than parts per million levels [48]. The problem occurs if the extractant is very expensive or the total amount of an extractant is large and therefore also economically unfavourable.

1.3.3   Membrane technology

In recent years, the application of membrane technology in homogeneous catalyst recycling has received widespread attention since it can lead to faster, cleaner and highly selective green industrial processes. Commonly the membrane is compartmentalized in the reactor. Reactants continuously enter the reactor. Products and unreacted materials permeate through the membrane while the catalyst remains inside the reactor [28]. Also a nano-filtration membrane can be placed after the reactor where the solvent containing the catalyst is separated from the reactants and recycled back to the reactor. The homogeneous catalyst can also be heterogenized on a solid support in order to use conventional filtration

[29,30]. For recovery of soluble homogeneous catalysts ultra- and nano-filtration is a selected as potential methods [28,32].

Recovery methods by ultra- or nano-filtration do not require additional solvents and can be operated at the same process conditions as the reactor. Therefore they are presented as a green method to recover homogeneous catalysts. The limitations occur for example in the production of bulk chemicals since the capacity of the membrane is determined by product flow instead of catalyst recovery. Also the process conditions can be very harsh for the polymeric membranes, while the inorganic ones are far too expensive. Furthermore, free catalyst metals can either leach through the membrane or accumulate inside [49].

1.3.4   Precipitation/Filtration

Conventional filtration as a method for separation of the homogenous catalyst is used when precipitation of the catalyst is applied. Precipitation of a homogeneous catalyst occurs when the solubility of the catalyst drastically decreases when one reagent is consumed or if the temperature is changed after completion of the reaction [52]. Furthermore filtration is commonly used when the catalysts are coupled to soluble polymers [33-36]. Heterogenization of homogeneous catalysts to different supports, inorganic material or organic polymers, provides easy separation by simple filters or operation in fixed bed reactors [33]. Although precipitation combined with filtration as a method to recover homogenous catalysts belongs to the group "green chemistry" methods, a homogeneous catalyst should completely precipitate or the remains of the soluble catalyst should be recovered in combination with other recovery techniques which increases its costs.

The other way to recover homogeneous catalyst from product stream by filtration is precipitation of the product and recycling of the catalyst back to the reactor. The typical example of such a recovery is production of terephthalic acid [2]. In that process terephthalic acid precipitates due to low solubility, and cobalt catalyst is recycled back to the reactor.

1.3.5   Biphasic catalysis

Biphasic catalysis is a liquid-liquid two phase system where the catalyst is retained in one phase and the other phase is used for delivery and/or removal of reactants [33]. Strategies studied so far include:

-aqueous/ organic biphasic systems where the catalyst is water soluble, for example Rh/TPPTS (tri(m-sulfonyl)triphenylhosphine)[37],

-fluorous biphasic systems, where the use of fluorinated ligands solubilises the catalyst in the fluorinated phase. An investigated catalyst is rhodium trialkylphosphine complex appended with fluorous ponytails such as $RhH(CO)[P(CH2CH_2C_6F_{13})_3]$ [38],

-use of molten salts as ionic liquids for separation of the rhodium complexes (e.g. $[Rh(nbd)(PPh_3)_2]$) [39],

-use of ternary mixtures which can be interchanged between homogenous and biphasic regions by either composition or temperature changes as it is explained by da Rosa et al. [40] where poly(ethylene oxide), CH_2Cl_2 and heptane were selected as a ternary mixture.

The advantages of this recovery method are simplicity in terms of the apparatus and process operation, constant activity of the catalyst and simple recycle of the homogeneous catalyst. Biphasic recovery of homogeneous catalyst has a standard drawback of metal leaching to the organic phase [37]. Also common problem is for example leaching of ionic liquids. Solubility of the catalyst in the organic solvent limits its wide industrial application.

1.3.6   *Ion exchange*

Ion exchange is a technique to recover transition metals from homogeneous catalyst by contacting the catalyst first with a resin, separating it from the reactor effluent, and in the next step freeing the homogeneous catalyst complex from the resin by displacement with a suitable ligand [41]. This technique is also used to recover the active rhodium complex and separate impurities from inactive rhodium complexes and the hydroformylation stream [42]. The active rhodium complex and impurities are bound to the resin, and separately removed. Ion exchange methods have been used to recover group VIII metal from aqueous solutions as described in US patents No: 2,945,743 and 3,567,368 [43]. Ion exchange resins used for recovery of the rhodium catalyst are strongly acidic resins containing sulfonic acid [43] or amine containing resins [44].

One of the limitations of this method can be a type of solvent. Some solvents either influence the kinetics of ion exchange or do not allow the ion exchange process by simply keeping the metal in solution surrounded with its atoms [44].

1.3.7.   *Adsorption*

Adsorption of the homogeneous catalysts was applied as a method for the heterogenization of the homogenous catalyst [45]. Those catalysts have combined properties of homogeneous and heterogeneous catalysts. Heterogeneous catalyst do not have a problem with solubility which can govern reactor capacity [47]. Since it stays inside the reactor, problems as vaporisation or precipitation of the catalyst are avoided. If the

immobilisation procedure is not proper the leaching of the catalyst is observed. Also the decomposition of the resins is observed if they can not stand the process conditions [50-51]. By immobilizing, the homogeneous catalyst can lose its properties and therefore reduce its activation and selectivity properties.

1.3.8. *Summary of the present methods*

A summary of the present recovery methods is shown in Table 1.2. Five aspects are addressed: activity of the catalyst after the recycle, leaching of the catalyst's species during the recovery process, costs of the process, application range and environmental aspects of the process. Each aspect of every process is marked with:

- "−" if the process mostly cannot fulfil the aspect;
- "±"if the process partially can fulfil the aspect;
- "+"if the process mostly can fulfil the aspect.

Table 1.2. Summary of the present recovery methods and a novel RFA concept

	Activity of the catalyst	Leaching of the catalyst's species	Costs of the process	Application range	Green engineering
Flash/ Evaporation/ Distillation	±	±	±	±	±
Extraction	±	+	±	±	−
Membrane	±	±	−	±	+
Precipitation/ Filtration	±	±	±	±	+
Biphasic catalysis	+	±	+	±	+
Ion exchange	±	±	±	±	±
Adsorption	±	±	+	±	+
Reverse Flow Adsorption	±	+	±	+	+

As it can be seen from the Table 1.2, most of the recovery methods very often can not keep a constant activity of the homogeneous catalysts. Examples of metal leaching are

found in all proposed methods. Some of the processes are economically more acceptable then the others. Due to high energy costs and the usage of a wide range of waste solvents, some processes are not environmentally friendly. To overcome these drawbacks a new separation process has to be developed. This method should prevent leaching of any complex species, not influence either activity or selectivity of the catalytic process and be economically suitable for industrial scale processes. Therefore a novel concept is proposed for the recovery of homogenous catalysts: **Reverse Flow Adsorption** [5].

Reverse flow adsorption (RFA) is a novel concept for the recovery of homogenous catalysts that combines separation by adsorption with reverse flow technology [5]. In reverse flow adsorption, the feed (reactants, homogeneous catalyst and solvent) changes periodically the flow direction. The homogeneous catalyst is separated from the reaction mixture by adsorption downstream of the reactor (Figure 1.6). In the subsequent step the homogenous catalyst is desorbed again and used in the reactor.

With this concept several drawbacks often found in other recovery methods can be either reduced or completely overcome:

- The feed is changing direction before the breakthrough at the exit of the adsorption bed to prevent leaching of the homogenous catalyst;
- Deactivation of the catalyst is expected to be negligible since the adsorption process properties can be either at the reaction conditions or at the conditions more favourable for constant activity of the catalyst.
- The process should be economically feasible if a high number of cycles can be reached before the adsorbent is renewed and low cost adsorbents are used.
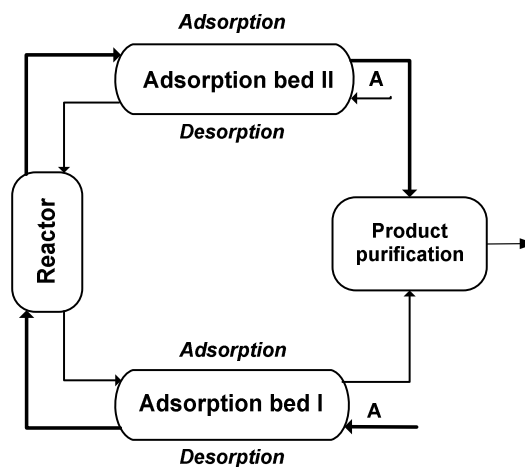
Figure 1.6. Adsorption by reverse flow for the recovery of homogeneous catalyst

1.4 Approach and goal of the project

The goal of this project is to demonstrate the feasibility of the reverse flow adsorption technology for the recovery of homogenous catalysts. The knowledge necessary to achieve this has to be established in several steps. First the adsorption method should be selected. For this insight into the catalyst structure/composition is necessary. In this first step of the process development we selected coordination compounds for studying the complex behaviour of compounds such as catalysts are. The next step is selection of suitable affinity adsorbents for the recovery of coordination compounds, followed by modelling of the adsorption isotherms and determination of the diffusion coefficient within the adsorbent particle. An ideal adsorbent should reversibly adsorb and desorb the catalyst and have particle properties that will result in an optimal design of an adsorption bed. A test reaction should be selected which will show preservation of the catalyst activity after reversible adsorption and desorption of catalyst precoursor form. Finally, a design of the representative industrial process would lead to the major conclusions of this work.

1.4.1   Affinity adsorbents

In this work we study coordination complexes where metal centre is surrounded with monodenate ligands. They are complex compounds mostly found in solution as free metal, free ligands and different complex forms (see Figure 1.7).
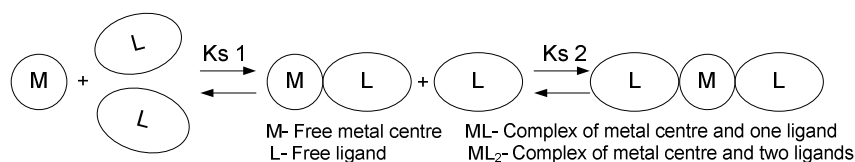
Figure 1.7. Homogeneous catalyst

Since several forms of the complex are found we propose recovery of the catalyst using the two step adsorption approach: separately adsorbing the metal containing species from the excess of ligand. To apply this method two types of adsorbents are needed: a "metal adsorbent" and a "ligand adsorbent" (Figure 1.8). The metal adsorbent is in the first adsorption bed after the reactor and it should adsorb all metal containing species. The remaining free ligand is adsorbed in the second adsorption bed. For this reason four adsorption beds are needed for the adsorption of homogenous catalysts by the two step adsorption approach.

Nowadays a wide spectrum of commercial materials that can be used as adsorbent is available. Both, polymeric and inorganic types of a carrier are used. In previous research

[5], the polymeric materials were selected as carrier of functional groups. Using these materials the first estimations of groups suitable to adsorb $CoCl_2$ and PPh_3 were performed. However, at the same time some major drawbacks, such as high mass transfer resistance and swelling of the adsorbent were detected. The slow diffusion inside of particles and unstable particle properties caused by swelling require longer residence time and larger bed volumes.
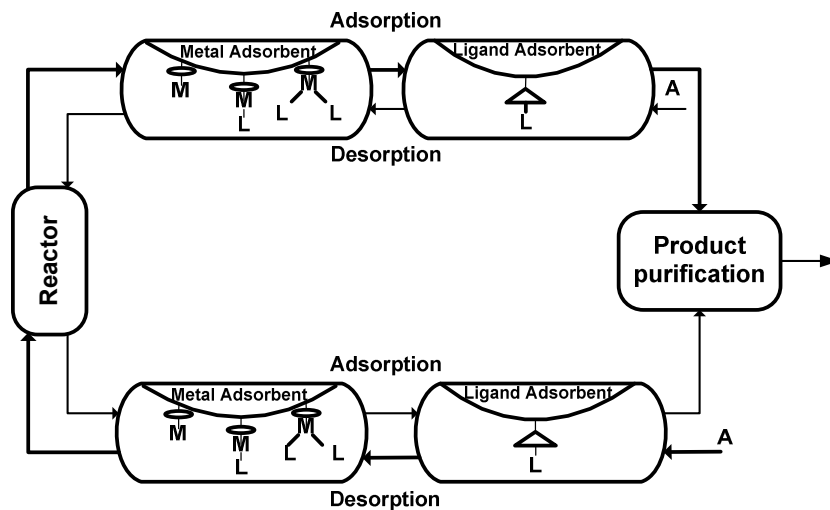
Figure 1.8. Reverse flow adsorption applying two step adsorption approach

To overcome these limitations silica was selected as a carrier of different functionalized groups. Silica gel is a chemically inert, non-toxic material widely used as a chromatographic adsorbent. It is used for adsorption of vapours and gases, and as a dehydrating agent. Silica gel is composed of amorphous silica dioxide. A large surface area, a wide range of pore sizes and a stable structure make silica a potentially ideal carrier. Pure silica doesn't have the required properties for adsorption of homogeneous catalysts. Therefore the silica should be functionalized with suitable groups but also the free –OH groups should be capped to avoid hydrophilic properties of the silica.

For the two step adsorption approach silica needs to be functionalized with motives that will selectively bind either the metal centre or the ligand molecule. The binding strength between the motif functionalized on adsorbent and its complementary motif on the catalyst should be balanced to obtain optimal adsorption and desorption characteristics. Additionally, pore size and particle size of the silica are varied to optimize the mass transfer properties and consequently the process performance of the silica adsorbent.

13

1.4.2   The RFA process

A basic model of the RFA process has already been developed by Dunnewijk [46]. It contains two adsorption beds and a continuous stirred reactor where only a metal salt, $CoCl_2$, is continuously adsorbed and desorbed. The model shows the stability of the RFA process for this system. Since in this work the homogenous catalyst is treated as a complex mixture where different species are present in solution, two models are needed to completely describe the feasibility of the RFA process. One model describes the adsorption of metal containing species, and the other model describes the adsorption of the free ligand. In this case the model for the bed containing "metal adsorbent" is more complex than the model for "ligand adsorbent" bed due to the competitive adsorption of different metal species. In the first model interactions between catalyst species in solution are incorporated and described by stability constants. Also a competitive adsorption of the metal containing species is taken into account. The complete model also describes the reverse flow adsorption process excluding reactor designed. It is developed to find the optimal adsorbent and process parameters which will lead to a stable and feasible process.

A simple reverse flow adsorption set-up is built for the proof of principle. Due to complicity of the actual system the present RFA set-up contains only one column where a metal centre is periodically adsorbed and desorbed. Adsorption of the metal centre is selected since it is the one that gets deactivated during the recovery process.   These experiments are selected to prove stable operation without leaching of the metal and with a metal concentration after each desorption cycle equal to the initial feed concentration. This set-up is also used to demonstrate the activity of the catalyst after several cycles of reversible adsorption and desorption of the catalyst precursor.

1.4.3   Catalyst activity

Besides the leaching of catalyst species, deactivation of the catalyst is also a common problem that occurs in different recovery processes. Therefore a Heck reaction (Figure 4) is selected to check the catalyst activity after several cycles of adsorption and desorption in the RFA set-up. To demonstrate that the conversion of the reaction is constant is one of the crucial points of this research.

1.5   The outlines of the thesis

The first step in our research is to determine the amount of different complex species present in solution and how this ratio can be changed. This is discussed in **Chapter 2** where stability constants for cobalt, nickel and palladium coordination complexes containing triphenylphosphine ligands are determined depending on counter ion, ligand, solvent and concentration.

In **Chapter 3** the selection of suitable affinity adsorbents used for adsorption due to binding with the metal and ligand part is presented. Three different complexes were selected: $CoCl_2(PPh_3)_2$, $PdCl_2(PPh_3)_2$ and $RhCl(PPh_3)_3$ for which the influences of the excess of ligands, type of solvent and temperature effect on the adsorption of the metal part are investigated.

Chapter 4 describes a model established to evaluate the competitive adsorption of the metal containing species in the presence of ligands. The developed model combines the stability constant equations together with a competitive Langmuir isotherm.

In **Chapter 5** mass transfer kinetics are studied. A Zero Length Column (ZLC) set-up is developed to determine the effective diffusivity, D_{eff}, inside the particles. A wide range of particle sizes (40-1000 μm) and different pore sizes (60 and 90 Å) are separately evaluated to design an optimal particle.

In **Chapter 6** Dunnewijk's model for the RFA process is upgraded. This model is used to predict the optimal values of the adsorption parameters, to demonstrate stable operation, and to describe the overall dynamics of the RFA process.

Catalyst stability through the Heck reaction and reverse flow adsorption experiments are reported in **Chapter 7**. The Heck reaction is performed after the reversible adsorption/desorption cycles of $PdCl_2$ in the RFA set-up to demonstrate catalyst activity after several continuous cycles.

Finally in the last chapter, **Chapter 8**, the major conclusions are given as well as future outlook.

1.6　Reference:

[1]　L. Chorkendorf, J.W. Niemantsverdriet, *Concept of Modern Catalysis and Kinetics*, Wiley-VCH Weinheim, 2003, p.1

[2]　P.W.N.M van Leeuwen, *Homogeneous Catalysis- Understanding the Art*, Kluwer Academic Publishers, 2004

[3]　B. Cornils, W. A. Hermann *Applied Homogeneous Catalysis with Organometallic Compounds,* Wiley-VCH, 2000

[4]　P. Arnoldy, C. M. Bolinger et al., Patent No: EP 0922691A1, Shell Internationale Research maatschappij B. V., (1998)

[5]　J. Dunnewijk, H. Bosch, A.B. de Haan, Sep. and Purif. Technol. 40 (3), 317-320, 2004

[6]　S. Bhaduri, et al, *Homogeneous Catalyst: Mechanisms and Industrial Applications,* Wiley-Interscience, 2001

[7]　Johnson Matthey, http://www.synetix.com/technical/applications-kinetic. htm, (2006)

[8]　M. Beller, Chem. Ing. Tech. 78 8 (2006) 1061-1067

[9]　C.A. McAuliffe, *Transition Metal Complexes of Phosphorus, Arsenic and Antimony ligands*, Macmillan, 1973

[10]   R. Toreki, http://www.ilpi.com/organomet/phosphine.html, (2006)

[11]   F. Zhao, B.M. Bhanage, M. Shirai, M.Arai, J. Mol. Catal. A 142 (1999) 383-388

[12]   A. de Meijere, F.E. Meyer, Angew. Chem. 106 (1994) 2473, Angew. Chem., Int. Ed. Engl. 33(1994) 2379

[13]   W. Cabri, I. Candiani, Acc. Chem. Res. 28 (1995) 2

[14]   A.A. Kelkar, T. Hanaoka, Y. Kubota, Y. Sugi, Catal. Lett. 29 (1994) 69

[15]   W.A. Hermann, C. Brossmer, C.P. Reisinger, T.H. Riermeier, K. Ofele, M. Beller, Chem. Eur. J. 3 (1997) 1357

[16]   W.A. Hermann, C. Brossmer, K. Ofele, M. Beller, H. Fischer, J. Mol. Catal. A 103 (1995) 133

[17]   J. Jean, Patent No: US4454333, Rhone Poulenc Chim Base, 1984

[18]   W. Keim, D. Vogt, H. Waffenschmidt, and P. Wasserscheid, J. of Catal, 1999, 186, 481-484

[19]   P. Wasserscheid and W. Keim, Angew. Chem. Int.Ed., 2000, 39, 3772-3789

[20]   K.R. Seddon, J.Chem. Tech. Biotechnology 1997,68, 351

[21]   K.R. Seddon, ionic liquid database, QUB School of Chemistry homepage, http://www.ch.qub.ac.uk

[22]   J. S. Wilkes, and J. Zawarotko, Chem. Soc. Chem. Commun., (1992), 965

[23]   Y. Chauvin, and H. Oliver- Bourbigou, Chemtech, 26, (1995)

[24]   E. H. Homeier, Maywood; A. R. Dodds, Elgin; Tamotsu Imai, Mt. Prospect, all of Ill, Patent No: US4292196, (1981)

[25]   G. Bernhard, H. J. Kneuper et al., Patent No: US6225507, BASF AG (US), (2001)

[26]   G. Bernhard, H. J. Kneuper et al., Patent No:US6107524, BASF AG (US), (1997)

[27]   M. Kakuda, T. Okamato, T. Onozawa, H. Kurata, Patent No: EP 1 069 103 A1, Mitsubishi Gas Chemical Company, INC, Tokyo, (2000)

[28]   H. P. Dijkstra, G. P. M. van Klink, G. van Koten, Acc. Chem. Res, 35 (2000) 798-810

[29]   S. J. Shuttleworth, S. M. Allin, P. K. Sharma, Synthesis 1217, (1997)

[30]   D. E. de Vos, I. F. J. Vankelecom, P. A. Jacobs (Eds.), *Chiral Catalyst Immobilization and Recycling*, Wiley-VCH, Weinheim, (2000)

[31]   T. Dwars, J. Haberland, et al., J. of Mol. Catal A: Chemical , 168 (2001) 81-86,

[32]   R.P. Tooze, K. Whiston, A. P. Malyan, et al., J. of Chem. Soc., 19 (2000) 3441-3444

[33]   U. Kragl, T. Dwars, Trends in Biotechnol., 19 (2001) 11

[34]   C. Bolm, A. Gerlach, Angew. Chem., Int. Ed. Eng., 36 (1997) 741-743

[35]   L.E. Martinez, J. Am. Chem. Soc., 117 (1995) 5897-5898

[36]   S. Crosignani et al., Tetrahedron, 54 (1998) 15721-15730

[37]   C. W. Kohlpaintner, R. W. Fischer, B. Cornils, Appl. Catal. A, 221 (2001) 219-225

[38]   W. Chen, L. Xu, J. Xian, Chem. Commun., (2000), 837-838

[39]   H.Oliver, J. of Mol. Cat. A: Chemicals, (1999), 146, 285-289

[40]   R.G. da Rossa, L. Martinelli, et al., Chem. Commun., (2000), 33-34

[41]   A.L. Forman, European patent office, Publication no: 0 186 409

[42]   G. S. Silverman, P. Mercando, PO:WO9703938, (1997)

16

[43]   R. Pitchai, T.S. Zak, K.E. Soring, PO:5.208.194 (1993)

[44]   J. Kramer et al., Eur.J. Inorg.Chem, (2002),1488-1494

[45]   B. Sandee, *Tailor-made Catalysts Immobilized on Silica*, Theses, Unniversity of Amsterdam, (2001)

[46]   J. Dunnewijk, *Reverse Flow Adsorption Technology for Homogeneous Catalyst Recycling,* thesis, University of Twente, (2006)

[47]   N. Yoneda, S. Kusano, et al., Appl Catal A: General 221, (2001), p. 253-265

[48]   J. Haggin, 209th ACS national Meeting, Anaheim, C&EN, (1995), p. 25-26

[49]   J.T. Scarpello, D. Nair et al., J. Membr. Sci. 5180 (2002) p. 1-15

[50]   R.S. Drago, E.D. Nyberg et al., Inorg. Chem. 20 (181) p. 641

[51]   M.S. Jarrel, B.C. Gates, J. Catal. 40 (1975) p.255

[52]   V.K. Dioumaev, R.M. Bullock, Nature, 424, (2000), p. 530-532

Determination of the stability constants for cobalt, nickel and palladium homogeneous complexes containing triphenylphosphine ligands

Abstract

Coordination complexes are often catalyst precursor forms of organometallic catalysts. They are compounds that are always in equilibrium with their free metal, free ligand and other forms of complexes. The ratios between different species are defined by the stability constants, which are influenced by different parameters such as the type of metal, ligand, counter ion or solvent. The main goal of this chapter is the determination of the stability constants for a range of different homogeneous metal complexes and the concentration of the different co-existing species present in solution. This information is needed for the modelling and design of reverse flow adsorption (RFA) technology, a novel concept for the recovery and recycling of homogeneous catalysts [1,3]. Cobalt, nickel and palladium halide salts with triphenylphosphine as a ligand are selected as complexes since they are commonly used in homogeneous catalysis. Titration experiments with UV-Visible spectroscopy as analytical technique have been carried out. The results were analyzed with a stability constant model developed for 1:2 complexation and adjusted for easy handling using Microsoft Excel. The stability constants of the selected complex systems increase in order: $[PdCl_2(OPPh_3)_2]_{MeCN} \approx \approx [CoCl_2(PPh_3)_2]_{butanol} < [CoBr_2(PPh_3)_2]_{MeCN} < [CoCl_2(PPh_3)_2]_{MeCN} < [NiBr_2(PPh_3)_2]_{MeCN} < < [PdCl_2(PPh_3)_2]_{DMF} < [PdCl_2(PPh_3)_2]_{MeCN}$. The obtained results for the stability constants could be explained with the Hard and Soft Acid Base theory in combination with the natural order of different species theory.

19

2.1 Introduction

By definition homogeneous catalysts are substances that are in the same phase as the substrates of the reaction, most often the liquid phase. Recently chemists refer to homogeneous catalysts as organometallic complexes [2]. Coordination complexes are often catalyst precursor forms of organometallic catalysts. In this work we study coordination complexes where metal centre is surrounded with monodenate ligands. They consist of a central metal which is surrounded by organic and sometimes also inorganic ligands. These metal-ligand complexes are always in equilibrium with their free metal centre (metal atom or metal salt), ligands and various complex species (Figure 2.1). Therefore it was decided to use two steps approach in the Reverse Flow Adsorption (RFA) process to recover the catalyst: separately adsorbing the metal and the ligand part [3].
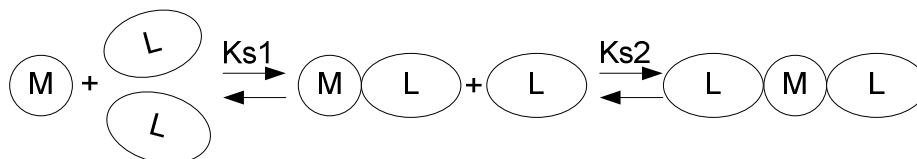
Figure 2.1. Schematic representation of the homogeneous catalyst in solution

The first step in understanding and modelling the RFA concept is to obtain insight in the interactions of all species present in the liquid phase. If one metal centre forms a complex with n ligands then the equilibrium can be presented as [4]:
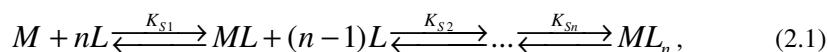
$$M + nL \xrightleftharpoons{K_{S1}} ML + (n-1)L \xrightleftharpoons{K_{S2}} ... \xrightleftharpoons{K_{Sn}} ML_n, \qquad (2.1)$$

where M, L, ML, ML_n represent the free metal salt, free ligand, and different forms of the complex respectively. This equilibrium is described by stability constants or complexation constants defined as the ratio between the concentrations of the complex form of the catalyst $[ML_i]$ and the concentrations of free metal $[M]$ and free ligands $[L]$:

$$K_{s1} = \frac{[ML]}{[M] \cdot [L]} \qquad (2.2)$$

$$K_{s2} = \frac{[ML_2]}{[ML] \cdot [L]} \qquad (2.3)$$

…

$$K_{sn} = \frac{[ML_n]}{[ML_{n-1}] \cdot [L]} .$$ (2.4)

where K_{s1}, K_{s2} and K_{sn} present the stability constants for each of the individual complexation steps. Equations (2.2)-(2.4) clearly demonstrate that understanding of the stability constants and the parameters that influence the system (metal, counter ion, ligand, solvent) is crucial for describing the amount of each species present in the system both quantitatively and qualitatively. In this chapter $CoCl_2(PPh_3)_2$, $CoBr_2(PPh_3)_2$, $NiBr_2(PPh_3)_2$, $PdCl_2(PPh_3)_2$, $PdCl_2(OPPh_3)_2$ are selected as model complexes, with 1-butanol, acetonitrile (MeCN) and N,N- dimethylformamide (DMF) as the solvents. For these complexes 1:2 complexation is valid, but stability constants are not available in literature and therefore need to be determined. To explain interaction metal-ligand binding several theories can be applied. For an example molecular orbital theory is a modern theory nowadays often used for profound and accurate insight in metal-ligand interactions. However, we selected the older theory, the Hard and Soft Acid Base theory [4], since it can in a simple way and still accurate enough describe the interactions of our systems. Co^{2+}, Ni^{2+}, Pd^{2+} were selected as metal ions because according to the Hard and Soft Acid Base theory (HSAB theory) Co^{2+} and Ni^{2+} belong to the borderline group of metals, and Pd^{2+} belongs to the soft acid metals [4]. It is expected that palladium will bind significantly stronger to the triphenylphosphine ligand than nickel or cobalt. On the other hand nickel will bind stronger than cobalt with a same ligand due to its natural order [4]. As counter ion Cl^- was selected as it is commonly found in catalyst precursor complexes. Br^- was selected to investigate the effect of the counter ion on the stability constant. As a model ligand we selected triphenylphosphine, PPh_3, because of its great relevance in catalysis and its relatively high air stability. In solution PPh_3 will only slowly oxidize. Therefore we also selected its oxidized form $OPPh_3$ as another ligand to compare binding strengths. As solvents we selected:

- 1-butanol which is a polar solvent and excellent electron donor,
- N,N-dimethylformamide which is a dipolar aprotic solvent and an excellent electron donor and
- acetonitrile which is also a dipolar aprotic solvent but medium electron donor [5].

Chemists in the field of homogeneous catalysis have studied binding interactions in the metal-ligand systems and applied terminology of host-guest interaction as well as binding constant [6]. These general names refer, in our case, to the metal-ligand interaction and the stability constants respectively. Several computer programs were developed to determine the stability constants by fitting potentiometric [7-8] or spectroscopic data [9-10]

with a mathematical model. Hirose [6] described the general approach to determine the stability constants by combining titration and spectroscopic methods, UV-Visible and NMR, and gave an example for 1:1 complexation modelling. Huskens [9], Hynes [10], and Bisson et al. [11] developed computer models to determine the stability constants based on NMR as an analytical technique. Hunter's software [11] for calculating stability constants is for both 1:1 and 1:2 complexation, but data handling appeared to be inconvenient and the amount of complex forms present were not calculated. Therefore we decided to develop our own software in Excel which calculates in addition to the stability constants also the concentration of each species present in solution. This is essential for the modelling of the RFA process since it provides the concentration of each species for different metal-ligand ratios. In this study we extend the work of Hirose [6] by applying his approach to 1:2 complexation of the metal salt with the ligand. The derived model determines stability constants by fitting data obtained by titration experiments using UV-Visible spectroscopy. UV-Visible spectroscopy is selected as the analytical technique because it is next to NMR the most common technique [7] and it is (unlike NMR) able to measure cobalt complexes. NMR is not feasible since cobalt is paramagnetic. Furthermore, our software is using the analytical solution (see appendix) while the Hunter's model is based on an iterative procedure. Both programs give the same values for the stability constants.

This chapter starts by first describing the development of the model used to determine the stability constants values for 1:2 complexation. The calculated stability constants for different systems are presented. The influence of metal, ligand, counter ion, solvent and concentration on the stability constant values is discussed. With this knowledge the concentrations of all species present at different metal-ligand ratios for the investigated systems can be compared. Finally, the sensitivity of the fitting model parameters depending on the changes in measured absorbance by the UV-Visible spectrometer is discussed.

2.2   Stability constants model
To develop the stability constant model for the 1:2 complexation the stability constant equations, the total mass balances and the observed absorbance of the UV-Visible spectrometer need to be combined.

2.2.1   Stability constants
For the 1:2 metal, M, to ligand, L, ratio, equation (2.1) can be modified:

$$M + 2L \xrightleftharpoons{K_{S1}} ML + L \xrightleftharpoons{K_{S2}} ML_2 \qquad\qquad (2.5)$$
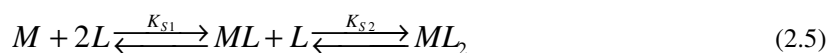
where K_{S1} and K_{S2} are defined by (2.2) and (2.3). The overall stability constant, β_2 , is defined as:

$$M + 2L \xrightarrow{\beta_2} ML_2 \qquad (2.6)$$

$$\beta_2 = K_{s1} \cdot K_{s2} \qquad (2.7)$$

2.2.2.   Total mass balances

In the system both the metal and the ligand are present in different forms: free metal salt, free ligand, metal salt complexed with one ligand, and metal salt complexed with two ligands. The total mass balance applied to the metal and the ligand will give:

$$[M_t] = [M] + [ML] + [ML_2] \qquad (2.8)$$

$$[L_t] = [L] + [ML] + 2 \cdot [ML_2] \qquad (2.9)$$

where $[M_t]$ and $[L_t]$ are total concentrations of metal and ligand present in all their forms.

2.2.3.   UV-Visible spectroscopy

With the UV-Vis spectrophotometer the sum of the absorbencies of all species in solution can be measured (Figure 2.2). For each wave length the contribution of the absorbance of each component A_i adds up to the total absorbance value A_{obs}:

$$A_{obs} = A_{ML_2} + A_{ML} + A_M + A_L . \qquad (2.10)$$

If the absorbance is a linear function of concentration for each species, equation (2.10) will become:

$$A_{obs} = \varepsilon_{ML_2} \cdot [ML_2] + \varepsilon_{ML} \cdot [ML] + \varepsilon_M \cdot [M] + \varepsilon_L \cdot [L], \qquad (2.11)$$

where A_{ML2}, A_{ML}, A_M, and A_L are absorbencies and ε_{ML2}, ε_{ML}, ε_M, and ε_L are molar absorptivities [M^{-1}] of respectively catalyst, metal with one ligand, free metal and free ligand.
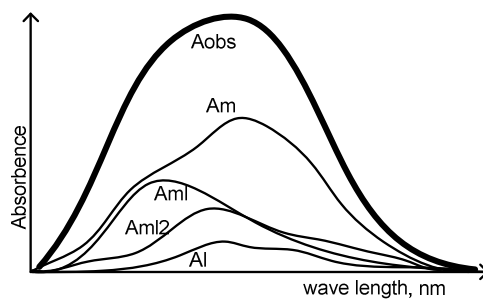
Figure 2.2. Schematic representation of absorption spectrum of the compounds present in the mixture and the sum curve

2.2.4. Modelling of the stability constants

The model that we developed consists of six equations ((2.2), (2.3), (2.7), (2.8), (2.9), (2.11)) with ten unknowns. Therefore four parameters need to be adjusted to fit the model to the data. Hence we can define three types of parameters:

1. Known parameters ([M_t], [L_t], $A_{obs,exp}$, ε_m and ε_l)
2. Fitting parameters (K_{S1}, K_{S2}, ε_{ml2} and ε_{ml})
3. Calculated parameters ($A_{obs, mod}$, [M],[L],[ML],[ML_2], β_2).

1.   Known parameters

[M_t] and [L_t] are controlled by the experimenter, $A_{obs,exp}$ is measured for different combinations of [M_t]and [L_t]by the UV-Visible spectrometer, and ε_M and ε_L can be determined by fitting the calibration curves with the equation: $A_M = \varepsilon_M \cdot [M]$ and $A_L = \varepsilon_L \cdot [L]$, where ε_M and ε_L are the slopes. Those calibration curves are calculated from separate experiments where only concentration of metal or ligand was varied.

2.   Fitting parameters

The values of K_{S1}, K_{S2}, ε_{ML2} and ε_{ML} were adjusted to minimize the objective function:

$$\Sigma(\Delta = (A_{obs,\mathrm{mod}} - A_{obs,\exp})^2) . \tag{2.12}$$

3.   Calculated parameters

The model equations are used to calculate other unknown parameters at each point of the titration. For further modelling and design of the RFA it is essential to know the

concentrations of each species at different metal to ligand ratios. A detailed explanation of the stability constant model is given in the appendix.

2.3   Material

Chemicals $PdCl_2$(99.9%), $NiBr_2$(99%), $CoCl_2$(anhydrous), $CoBr_2$(99%), triphenylphosphine, triphenylphosphine oxide 98%, 1-butanol, N,N-dimethylformamide (DMF) and acetonitrile (MeCN) used for the experiments were obtained by Sigma-Aldrich. The absorption of the mixtures was measured with a UV-Vis spectrometer (Varian Cary 300 Conc).

2.4   Experimental

Titration combined with the UV-Visible spectroscopy for analysis is the applied experimental procedure often called "the method of inverse titration" [12]. All titration experiments were performed identically: 50 ml of a metal salt solution (solution I) was prepared with concentration of approximately 2 mM for Co, 0.2 mM for Ni, and 0.04-2 mM for Pd experiments 25 ml of starting solution was separated and loaded with a large excess of triphenylphosphine ligands (solution II). After dissolving PPh_3, the titration experiments were performed in a closed cuvet, starting with a 2 ml of solution I, and subsequently after each absorption measurement by the UV-Vis spectrometer 8 μl of solution II was added and mixed with the rest. The solution was left for one minute to reach equilibrium. Fast equilibration time is confirmed by monitoring formation of $CoCl_2(PPh_3)_2$ in 1-butanol over 3h and a increase of the UV-Vis spectra is observed to be 1.5% compared to the time after 1 minute. Each titration experiment consists of 20 to 25 points. All experiments were done at the room temperature. The kinetics of complex formation was experimentally checked and the results showed that equilibrium was reached within one minute.

A_{obs} was selected at the wave lengths where the highest change in A_{obs} was detected (Figures 2.3). In Table 2.1 the wave lengths for each system are shown. At those wave lengths the contribution of PPh_3 and $OPPh_3$ was not detected and therefore ε_L is set to zero. Linearity was verified by the calibration lines for only metal present in the solution and applies for absorbance $A_{obs}<3$ and all species present in the system.

Table 2.1. Wavelengths at which Aobs was measured to determine the stability constants

Complex	Solvent	Wave Length, nm
$CoCl_2(PPh_3)_2$	1-Butanol	585
$CoCl_2(PPh_3)_2$	Acetonitrile	683
$CoBr_2(PPh_3)_2$	Acetonitrile	633
$NiBr_2(PPh_3)_2$	Acetonitrile	378
$PdCl_2(PPh_3)_2$	Acetonitrile	343
$PdCl_2(PPh_3)_2$	DMF	343
$PdCl_2(OPPh_3)_2$	Acetonitrile	330

(a)   (b)
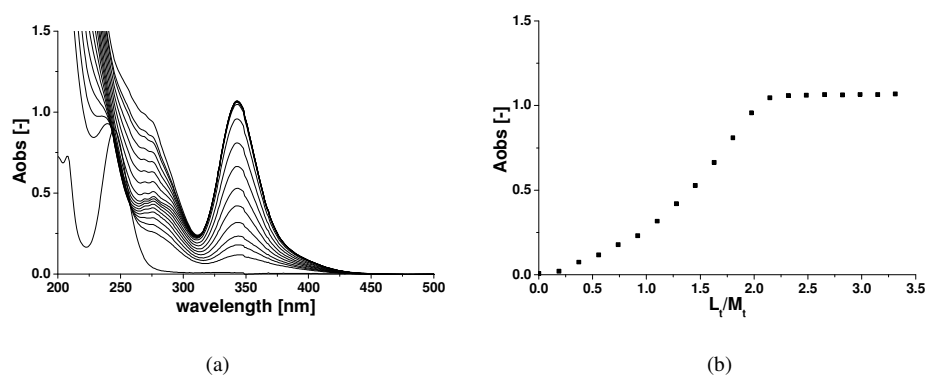
Figure 2.3. Variation of the observed absorption during titration experiments of $PdCl_2(PPh_3)_2$: (a) as a function of wavelength and (b) at the wavelength of 343 nm for different metal to ligand ratio

2.5   Results and discussion

The results for the different combinations of metal, counter ion, ligand and solvent which were investigated are given in Table 2.2. The last columns list the stability constants obtained by fitting the model to the experimental data. Concentrations of the free metal form and the complex forms of the metal for the measured range of metal-ligand ratios are calculated by the model and shown in Figures 2.4-2.7 (similar to the "[L]-control maps" by Heimbach and Schenkluhn [12]).

Table 2.2. Overview of stability constants for different complex systems at room temperature

No	Metal	Counter ion	Ligand	Solvent	K_{S1}, M^{-1}	K_{S2}, M^{-1}	β_2, M^{-2}
1	Co	Cl	PPh$_3$	1-butanol	≈ 2	$\approx 3\cdot 10^1$	$\approx 6\cdot 10^1$
2	Co	Cl	PPh$_3$	MeCN	6.6	$2.8\cdot 10^2$	$1.9\cdot 10^3$
3	Co	Br	PPh$_3$	MeCN	$2.3\cdot 10^1$	$5.0\cdot 10^1$	$1.1\cdot 10^3$
4	Ni	Br	PPh$_3$	MeCN	$1.0\cdot 10^3$	$5.3\cdot 10^2$	$5.3\cdot 10^5$
5-1	Pd	Cl	PPh$_3$	MeCN	$3.2\cdot 10^7$	$8.0\cdot 10^6$	$2.6\cdot 10^{14}$
5-2	Pd	Cl	PPh$_3$	MeCN	$3.2\cdot 10^7$	$8.0\cdot 10^6$	$2.6\cdot 10^{14}$
5-3	Pd	Cl	PPh$_3$	MeCN	$3.5\cdot 10^7$	$8.8\cdot 10^6$	$3.1\cdot 10^{14}$
6	Pd	Cl	PPh$_3$	DMF	$1.3\cdot 10^5$	$3.3\cdot 10^4$	$4.3\cdot 10^9$
7	Pd	Cl	OPPh$_3$	MeCN	2.4	5.8	$1.4\cdot 10^1$

2.5.1 Influence of the metal

According to the soft and hard acid and base theory Pd^{2+} belongs to the group of soft acids and Co^{2+} belongs to the borderline group. PPh$_3$ belongs to the group of soft bases. Therefore it is easy to predict that binding between Pd^{2+} and PPh$_3$ will be stronger than between Co^{2+} and PPh$_3$. This is experimentally validated and shown in Figure 2.4(a) and (b). It is clear that formation of the palladium complex is much stronger than the cobalt complex. For example at a metal to ligand ratio 1:2 only around 5% of the total amount of cobalt is present as a complex with two ligands and 9% as a complex with one ligand, and in a case of palladium already 98.4% is a complex with two ligands, and 1.6% is a complex with one ligand.

The effect of replacing Co^{2+} by Ni^{2+} on the stability constant of the PPh$_3$ complex is not covered by the HSAB theory since both metal ions belong to the borderline acids. Therefore it is more convenient to compare them by their natural order which is also mentioned in the introduction. From this sequence it is expected that the nickel complex is more stable than the cobalt complex. Experimental results confirm this as can be seen (Figure 2.5(a) and (b)). For the ligand-metal ratio Lt/Mt=4 50% of the total metal is present as a free metal in the case of Ni-complex and 80% in the case of Co-complex.

(a)   (b)

Figure 2.4. Relative amount of free metal and the complex forms as a function of the total ligand to metal ratio for
(a) $CoCl_2(PPh_3)_2$ in MeCN and (b) $PdCl_2(PPh_3)_2$ in MeCN

(a)   (b)

Figure 2.5. Relative amount of free metal and the complex forms as a function of the total ligand to metal ratio for
(a) $CoBr_2(PPh_3)_2$ in MeCN and (b) $NiBr_2(PPh_3)_2$ in MeCN

2.5.2   *Influence of the counter ion*

The influence of the counter ion can be seen by comparing the $CoCl_2(PPh_3)_2$ and $CoBr_2(PPh_3)_2$ complex. The difference between Cl^- and Br^- ions as counter ions is not large because they belong both to the same periodic group of elements. However, there is a difference in their electronegativites. Cl^- as more electronegative than Br^- ion will form a stronger ionic bond with cobalt, and therefore cobalt will be more attracted to the lone electron pair of triphenylphosphine than in the case of the $CoBr_2(PPh_3)_2$ complex. The 'influence of electronegativity' is noticed in the values of the stability constants (Table 2.2). Although it is not large (the same order of magnitude), it gives difference in the values of the concentrations of free metals and complex forms: for ratio Lt/Mt=4 70% of the total metal concentration is in its free form in a case of $CoCl_2(PPh_3)_2$ (Figure 2.4(a)) and 80% in a case of $CoBr_2(PPh_3)_2$ (Figure 2.5(a)).

2.5.3 Influence of the ligand

To compare the influence of the ligand we selected $PdCl_2(PPh_3)_2$ and $PdCl_2(OPPh_3)_2$ as model complexes. In the oxidized form triphenylphosphine is changing from a P-ligand to an O-ligand [13]. Therefore in a complex form an oxidized phosphine is now binding with its oxygen atom to the metal. Experiments show that the O-Pd bond is very weak, and there is almost no complex formation (see also Figure 2.6 and Table 2.2). For a ratio Lt/Mt=2 only 0.2% of the complex form, ML_2, is present for the oxidized triphenylphosphine form, while 98.4% of the palladium is present in the complex form, ML_2, for the non-oxidized ligand (Figure 2.4(b)).
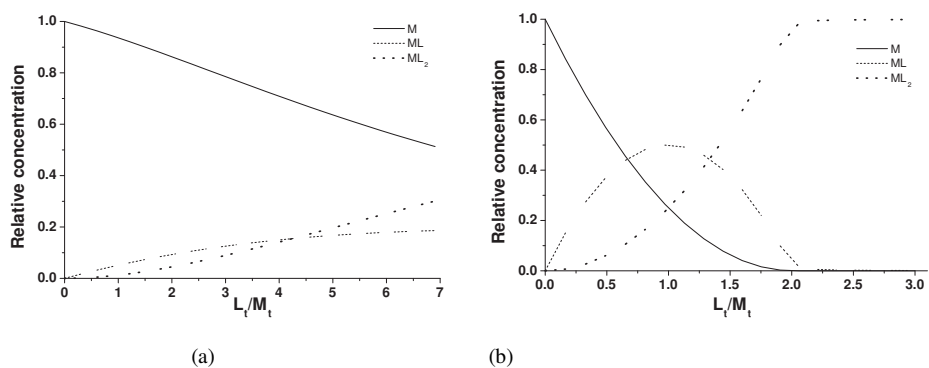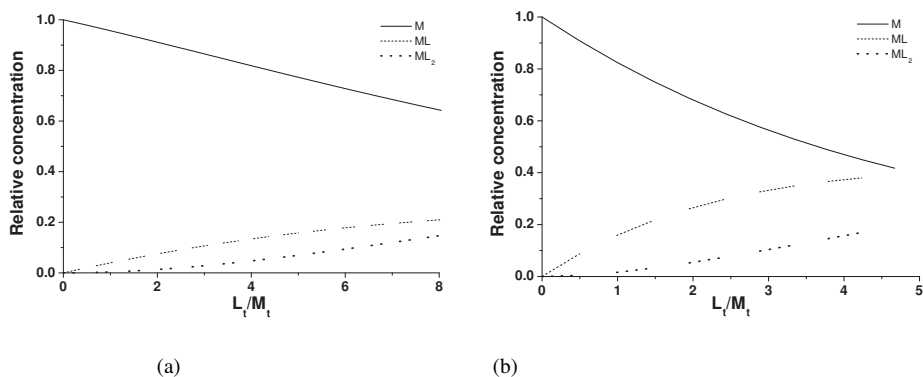

Figure 2.6. Relative amount of free metal and the complex forms as a function of the total ligand to metal ratio for $PdCl_2(OPPh_3)_2$ in MeCN

2.5.4 Influence of the solvent

To investigate the influence of the solvent on the stability of the complex $CoCl_2(PPh_3)_2$ was selected in the solvents 1-butanol and acetonitrile and $PdCl_2(PPh_3)_2$ in the solvents acetonitrile and N,N-dimethylformamide.

The lower value of the stability constant for $CoCl_2(PPh_3)_2$ in 1-butanol to acetonitrile can be explained by the strong interaction of 1-butanol molecules (Butanol DN=29 [5]) with Co ions and therefore weakening the bond between the cobalt ion and the phosphor atom. The formation of the complex in 1-butanol is negligible. Figure 2.7(a) ($CoCl_2(PPh_3)_2$ in 1-butanol) shows that almost all metal is in its free form. Acetonitrile as a dipolar aprotic solvent has a weaker interaction with cobalt and therefore cobalt binds stronger with triphenylphosphine as shown in Figure 2.4(a).
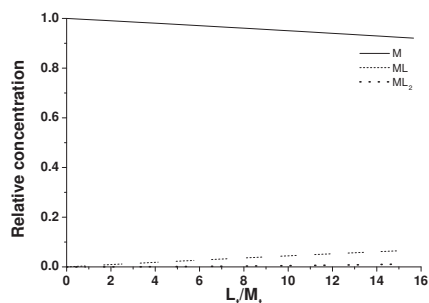
29

(a)   (b)
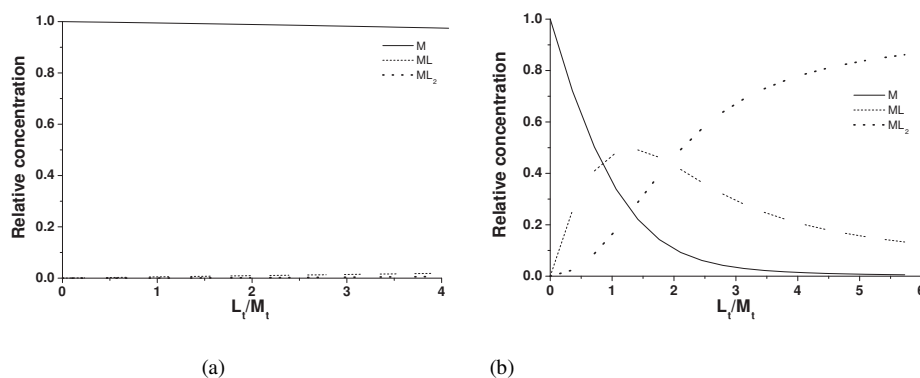
Figure 2.7. Relative amount of free metal and the complex forms as a function of the total ligand to metal ratio for
(a) $CoCl_2(PPh_3)_2$ in 1-butanol and (b) $PdCl_2(PPh_3)_2$ in DMF

The same effect was observed with $PdCl_2(PPh_3)_2$ in acetonitrile and N,N-dimethylformamide. DMF is excellent electron donor, while on the other hand acetonitrile is a medium an electron donor (acetonitrile DN= 14.1; DMF DN=26.6) [5]. Therefore acetonitrile interacts less with the palladium which results in a stronger bond between palladium and triphenylphosphine than in the case of DMF as a solvent. At the ratio metal to ligand 1:2 there is still around 10% of the total metal amount in its free form with DMF as a solvent (Figure 2.7(b)) compared to less then 0.001% of free metal salt with acetonitrile as a solvent (Figure 2.4(b)).

2.5.5   Influence of the concentration

As expected the concentration of the complex does not influence the value of the stability constant. This is proven by titration experiments with three different $PdCl_2(PPh_3)_2$ concentration levels of 0.04, 0.08 and 0.1 mM (Table 2.2, No: 5-1, 5-2 and 5-3). The Pd-P bond is very strong and to obtain linearity on UV-Visible the lower concentration levels are chosen compared to cobalt or nickel. Experiment 5-3 is also done on a different UV-Vis spectrometer. In Figure 2.8 it is shown that the relative amount of the free $PdCl_2$ and the complex $PdCl_2(PPh_3)_2$ is equal in all three situation. The fitted values of the stability constants for cases 5-1, 5-2 compared to 5-3 do not show any significant difference. The range of 2.5 in the concentration is sufficient to show that the same stability constants values apply for all concentration ranges of the complex. This conclusion can be extended to other homogeneous complexes as well.

(a)   (b)

Figure 2.8. Relative amount of (a) the free $PdCl_2$ and (b) the complex $PdCl_2(PPh_3)_2$ in acetonitrile as a function of the total ligand to metal ratio for three different titration experiments
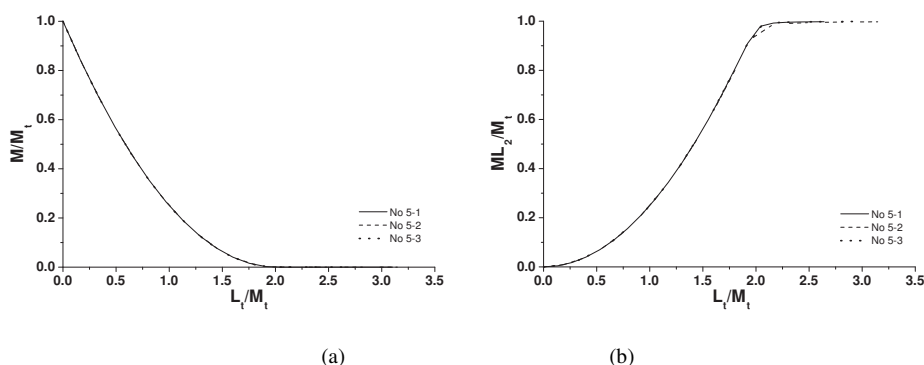
2.5.6   Modelling of the stability constant

The sensitivity of the fitting results increases by decreasing values of the stability constants. The results of the fit for the more stable complexes ($\beta_2 > 10^3$ [M^{-2}]) appeared to be independent of the starting values of the fitting parameters K_{S1}, K_{S2}, ε_{ml2} and ε_{ml}. For different starting values the determined optimal values for K_{S1}, K_{S2}, ε_{ml2} and ε_{ml} varies less than 1% in the case of $PdCl_2(PPh_3)_2$ in acetonitrile and increasing up to 5-10% in case of cobalt complexes in acetonitrile. For the stability constants measurements, where we are talking of orders of magnitude this sensitivity is acceptable. However this was not the case for the very low stability constants ($\beta_2 <\approx 10^1$ [M^{-2}]), for which different starting values resulted in different sets of K_{S1}, K_{S2}, ε_{ml2} and ε_{ml} with approximately the same minimum of the objective function. This problem is noticed in the titration experiments of $CoCl_2$ with PPh_3 in 1-butanol and $PdCl_2$ with OPP_3 in acetonitrile. It is caused by negligible changes in A_{obs} during the titration experiment because the bond between cobalt and phosphorus and palladium and oxygen is very weak and formation of the complex is negligible. The values of the stability constants for $CoCl_2(PPh_3)_2$ in 1-butanol and $PdCl_2(OPPh_3)_2$ in acetonitrile are approximated and only give a range for the stability constants. The determined values for K_{S1}, K_{S2}, ε_{ml2} and ε_{ml} are varying more then 100% with the same value of the minimized objective function.

The minimum in objective function reached for lower stability constant (cobalt and nickel) was in the range 10^{-5}, and for the higher values in the range of 10^{-2} (palladium). Although the minimum of the objective function gives lower values in a case of cobalt or nickel compared to palladium, it does not say that stability constant values are more accurate. This is also explained by smaller differences in A_{obs} during cobalt and nickel titration experiments compared to palladium. Figure 2.9 compares the measured and

calculated absorption for $PdCl_2(PPh_3)_2$ and $CoCl_2(PPh_3)_2$ in acetonitrile and show an excellent fit for both systems.

(a)

(b)
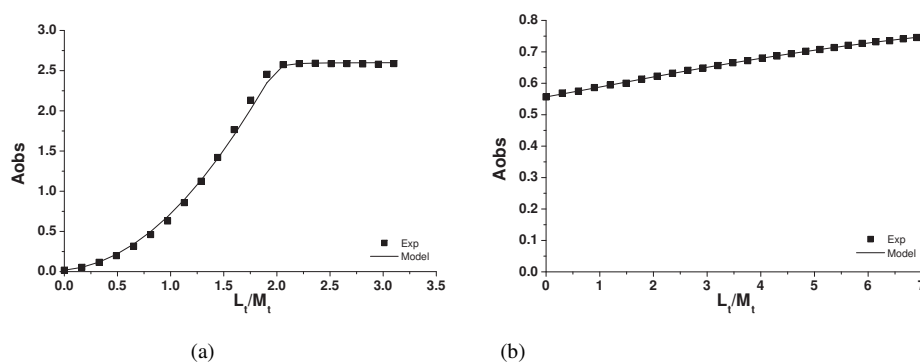
Figure 2.9. Comparison of Aobs from experiments and the model for (a) $PdCl_2(PPh_3)_2$ and (b) $CoCl_2(PPh_3)_2$ in acetonitrile

2.6   Conclusion

The stability constants of the complex systems that were selected increase in order:$[PdCl_2(OPPh_3)_2]_{acetonitrile} \approx [CoCl_2(PPh_3)_2]_{butanol} < [CoBr_2(PPh_3)_2]_{acetonitrile} < [CoCl_2(PPh_3)_2]_{acetonitrile} < [NiBr_2(PPh_3)_2]_{acetonitrile} < [PdCl_2(PPh_3)_2]_{DMF} < [PdCl_2(PPh_3)_2]_{acetonitrile}$. The obtained results for the stability constants can be explained with the Hard and Soft Acid Base theory in combination with the natural order of different species theory. Simultaneously the concentration of each species present in the solution is calculated. This is needed for the modelling and design of the reverse flow adsorption (RFA) technology. The results show that the sensitivity of the model is decreasing by increasing the values of the stability constants.

2.7   List of symbols

A_L-	Observed absorbance of the free ligand	[-]
A_M-	Observed absorbance of the free metal	[-]
A_{ML}-	Observed absorbance of the 1:1 complex	[-]
A_{ML2}-	Observed absorbance of the 1:2 complex	[-]
A_{obs}-	Total observed absorbance	[-]
$A_{obs,exp}$-	Total observed absorbance by experiment	[-]
$A_{obs,mod}$-	Total observed absorbance by model	[-]
β_2 -	Overall stability constant	$[M^{-n}]$
ε_L -	Molar absorptivity of the ligand	$[M^{-1}]$
ε_M -	Molar absorptivity of the metal	$[M^{-1}]$
ε_{ML} -	Molar absorptivity of the 1:1 complex	$[M^{-1}]$

32

ε_{ML2}-	Molar absorptivity of the 1:2 complex	$[M^{-1}]$
i,n-	Number of ligands present in the complex	[-]
K_{s1}-	Stability constant for the first complexation step	$[M^{-1}]$
K_{s2}-	Stability constant for the second complexation step	$[M^{-1}]$
K_{sn}-	Stability constant for the nth complexation step	$[M^{-1}]$
L-	Free ligand	[mol]
$[L]$-	Concentration of free ligand	[M]
$[L_t]$-	Concentration of the total amount of ligand	[M]
M-	Free metal	[mol]
$[M]$-	Concentration of the free metal	[M]
ML-	Complex of one metal and one ligand (1:1 complex)	[mol]
$[ML_i]$-	Concentration of the complex of one metal and i ligand	[M]
ML_2-	Complex of one metal and two ligands (1:2 complex)	[mol]
ML_n-	Complex of one metal and n ligands (1:n complex)	[mol]
$[M_t]$-	Concentration of the total amount of metal	[M]
$[L_t]$-	Concentration of the total amount of ligand	[M]

2.8   Reference:

[1]   J. Dunnewijk, H. Bosch, A.B. de Haan, Sep. and Purif. Technol. 40 (3), (2004) 317-320.

[2]   P.W.N.M van Leeuwen, Homogeneous Catalysis- Understanding the Art, Kluwer Academic Publishers, Dordrecht, 2004, pp.6-8.

[3]   J. Dunnewijk, H. Bosch, A.B. de Haan, Adsorption 11 (2005) 521-526.

[4]   S. F. A. Kettle, Coordination Compounds, Thomas Nelson and Sons Ltd, London, 1969, pp. 42-50.

[5]   V.Gutmann, Coordination chemistry in Non-Aqueous Solutions, Springer-Verlag, Wien, 1968, pp. 19.

[6]   K. Hirose, J. Inclusion Phenomena Macrocyclic Chem 39 (2001) 193-209.

[7]   D.J. Leggett, Computational Methods for the Determination of Formation Constants, Plenum press, NY, 1985, pp.39.

[8]   A.E. Martell, R.J. Motekaitis, Determination and Use of Stability constants, Wiley-VCH, NY, 1988, pp.14.

[9]   J. Huskens, H. van Bekkum, J.A. Peters, Computers Chem. 19 (4), (1995) 409-416.

[10]   M.J. Hynes, J.Chem. Soc., Dalton Trans., (1993) 311-312.

[11]   A.P. Bisson, C.A. Hunter, J. C. Morales, K. Young, Chem. Eur. J. 4 (5), (1998) 845-851.

[12]   P. Heimbach, H. Schenkluhn, Top. Current Chem. 92 (1980) 45-108.

[13]   Goggin, Comprehensive coordination chemistry, Pergamon Press, Oxford, 2, 1987, pp. 497-503.

[14]   http://mathworld.wolfram.com/CubicFormula.html, 2005.

2.9   Appendix

A.1 Stability constant model

The model that we developed is applied for complexes where the ratio of metal to ligand is 1:2 using a titration method with UV spectroscopy. It is also applicable for all complexes where the host to guest ratio is 1:2. For convenience we will rewrite all equations here.

Stability constants equations:

$$K_{s1} = \frac{[ML]}{[M]\cdot[L]} \tag{A.2.1}$$

$$K_{s2} = \frac{[ML_2]}{[ML]\cdot[L]} \tag{A.2.2}$$

$$\beta_2 = K_{s1}\cdot K_{s2} \tag{A.2.3}$$

Mass balance equations:

$$[M_t] = [M] + [ML] + [ML_2] \tag{A.2.4}$$

$$[L_t] = [L] + [ML] + 2\cdot[ML_2] \tag{A.2.5}$$

Observed absorbance according to the Beer's law:

$$Aobs,\mathrm{mod} = \varepsilon_{ml_2}\cdot[ML_2] + \varepsilon_{ml}\cdot[ML] + \varepsilon_m\cdot[M] + \varepsilon_l\cdot[L] \tag{A.2.6}$$

Substituting equations (A.2.4) and (A.2.5) in (A.2.1) and (A.2.2):

$$K_{s1} = \frac{[ML]}{([M_t]-[ML]-[ML_2])\cdot([L_t]-[ML]-2\cdot[ML_2])} \tag{A.2.7}$$

$$K_{s2} = \frac{[ML_2]}{[ML]\cdot([L_t]-[ML]-2\cdot[ML_2])} \tag{A.2.8}$$

Rewriting (A.2.8):

$$[ML_2] = K_{s2}\cdot[ML]\cdot\frac{[L_t]-[ML]}{2\cdot K_{s2}\cdot[ML]+1} \tag{A.2.9}$$

We can substitute it in (A.2.7), and then rewrite (A.2.7) as:

$$A_3 \cdot [ML]^3 + A_2 \cdot [ML]^2 + A_1 \cdot [ML] + A_0 = 0 \qquad (A.2.10)$$

Where

$$A_3 = K_{s1} \cdot K_{s2} - 4 \cdot K_{s2}^{2}$$

$$A_2 = -2 \cdot K_{s1} \cdot [M_t] \cdot K_{s2} - 4 \cdot K_{s2} + K_{s1}$$

$$A_1 = 2 \cdot K_{s1} \cdot [M_t] \cdot K_{s2} \cdot [L_t] - K_{s1} \cdot [L_t] - K_{s1} \cdot [M_t] - 1 - K_{s1} \cdot K_{s2} \cdot [L_t]^2$$

$$A_0 = K_{s1} \cdot [M_t] \cdot [L_t]$$

Dividing (A.2.10) by A$_3$, we get:

$$[ML]^3 + a_2 \cdot [ML]^2 + a_1 \cdot [ML] + a_0 = 0 \qquad (A.2.11)$$

Where:

$$a_2 = \frac{A_2}{A_3} \; ; \quad a_1 = \frac{A_1}{A_3} \; ; \quad a_0 = \frac{A_0}{A_3} \; ;$$

Solving the cubic equation (A.2.11) is further done by substitutions [14], resulting in:

$$Q = \frac{3 \cdot a_1 - a_2^2}{9}$$

$$R = \frac{9 \cdot a_2 \cdot a_1 - 27 \cdot a_0 - 2 \cdot a_2^3}{54}$$

$$D = Q^3 + R^2$$

If the D>0 then one solution is real and two are imaginary. The real solution is described by:

$$[ML] = -\frac{a_2}{3} + (S + T) \qquad (A.2.12)$$

Where

$$S = \sqrt[3]{R + \sqrt{D}}$$

35

$$T = \sqrt[3]{R - \sqrt{D}}$$

If the D≤0 then all three solutions are real solutions and are calculated from:

$$[ML]_1 = 2 \cdot \sqrt{-Q} \cdot \cos\left(\frac{\Theta}{3}\right) - \frac{a_2}{3} \qquad \text{(A.2.13-1)}$$

$$[ML]_2 = 2 \cdot \sqrt{-Q} \cdot \cos\left(\frac{\Theta + 2\pi}{3}\right) - \frac{a_2}{3} \qquad \text{(A.2.13-2)}$$

$$[ML]_3 = 2 \cdot \sqrt{-Q} \cdot \cos\left(\frac{\Theta + 4\pi}{3}\right) - \frac{a_2}{3} \,, \qquad \text{(A.2.13-3)}$$

where

$$\Theta = \cos^{-1}\left(\frac{R}{\sqrt{-Q^3}}\right).$$

Only one of those three solutions has a real physical meaning. Results that are negative or have a higher value than $[M_t]$ are dismissed. For high values of the stability constants, e.g. the palladium titration experiments, the determinant was always negative (D≤0). For the lower values the determinant was always positive (D>0).

The solution for [ML] from (A.2.12) or (A.2.13s) can be used in (A.2.9) and (A.2.4) to calculate $[M]$ and $[ML_2]$ and therefore $A_{obs,\,mod}$ and the objective function defined as $\Sigma(\Delta = (Aobs, \text{mod} - Aobs, \exp)^2)$ .By adjusting the values of K_{S1}, K_{S2}, ε_{ml} and ε_{ml2} the objective function was minimized.

Evaluation of functionalized silica's for the two-step recovery of homogenous catalysts by affinity adsorption through the metal centre and the ligand

Abstract

The goal of this chapter is the evaluation of functionalized silica's for the two-step recovery of homogeneous complexes by affinity adsorption through its metal centre and ligand. Bis(triphenylphosphine)cobalt(II)dichloride $(CoCl_2(PPh_3)_2)$, bis(triphenylphosphine)-palladium(II)dichloride $(PdCl_2(PPh_3)_2)$ and tris(triphenylphosphine)rhodium(I)chloride $(RhCl(PPh_3)_3)$ are selected as coordination complexes often found as catalyst precursors. Twelve functionalized groups selected from four classes containing one or more N-, O-, P- or S- atoms were evaluated for adsorption of metal centres and five functionalized groups are selected for adsorption of ligand. A preliminary selection of the adsorbents was done by investigating the adsorption of the metal salts for the cobalt and the palladium complex. The results could be explained by the Hard and Soft Acid Base (HSAB) theory. For the most suitable functionalized adsorbents these experiments were extended by introducing the ligand in the system which promoted the competition of the functionalized groups on adsorbent and the ligands present in solution. These experiments demonstrated that different complex species are adsorbed. 2-(2pyridyl)ethyl- functionalized silica is selected as a promising affinity adsorbent for adsorption of the $CoCl_2(PPh_3)_2$ from acetonitrile, while 3-(mercapto)propyl- functionalized silica is selected as a promising affinity adsorbent for adsorption of the $PdCl_2(PPh_3)_2$ and $RhCl(PPh_3)_3$ from DMF. Propyl-sulphonic acid containing functionalized silica is selected as the suitable affinity adsorbent for adsorption of the triphenylphosphine.

3.1 Introduction

Recently chemists refer to homogeneous catalysts as organometallic complexes [1]. Coordination complexes are often catalyst precursor forms of organometallic catalysts. In this work we study coordination complexes where metal centre is surrounded with monodenate ligands. Those complexes are always in equilibrium with their free metal salt, ligands and other complex forms (3.1).

$$M + nL \xrightarrow{\;\;K_{S1}\;\;} ML + (n-1)L \xrightarrow{\;\;K_{S2}\;\;} ... \xrightarrow{\;\;K_{Sn}\;\;} ML_n \qquad (3.1)$$
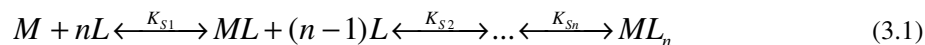
where M, L, ML and ML_n represent the free metal salt, the free ligand, and different forms of the complex respectively. n represents the maximum number of ligands in the complex and K_{S1}, K_{S2} and K_{Sn} are the stability constants for the different equilibriums. Therefore our main strategy is to develop a reverse flow adsorption concept based on a two step adsorption approach [2]. In the first bed the complex is adsorbed via an interaction of the metal centre with the functionalized adsorbent where different complex forms can be adsorbed, and in the second bed the excess of ligands is adsorbed from the reactor effluent (Figure 3.1). The binding strength between the functionalized adsorbent and adsorbate should be balanced to obtain a suitable adsorption and desorption behaviour. The suitable adsorbent was selected by excluding too strong and too weak adsorbents. Very strong adsorption was excluded due corresponding difficult desorption, and weak adsorption was excluded because of low capacity.
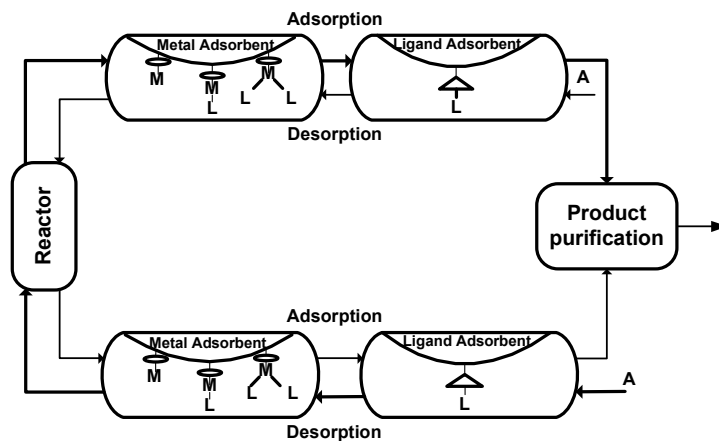

Figure 3.1. Two step strategy for reversible catalyst adsorption

In the work of Dunnewijk et al. [2] different polymer based adsorbents were selected for adsorption of bis(triphenylphosphine)cobalt(II)dichloride ($CoCl_2(PPh_3)_2$) in 1-

butanol. Their adsorbent selection was based on the Hard and Soft Acid Base theory (HSAB theory) [3] by which he could predict and explain the interactions between adsorbents and metal/ ligand species. These results were the basis for our present research.

We directed our investigation to more industrial applicable systems. As a coordination complexes bis(triphenylphosphine)cobalt(II)dichloride $(CoCl_2(PPh_3)_2)$ dissolved in acetonitrile is selected where the bonding between the metal and ligands is stronger compared to 1-butanol [4]. Bis(triphenylphosphine)palladium(II) dichloride $(PdCl_2(PPh_3)_2)$ and tris(triphenylphosphine)rhodium(I)dichloride $(RhCl(PPh_3)_3)$ in DMF, were also selected due to their broad use in industry [5,6]. Silica gel was selected as the carrier of the functionalized groups because it has a more stable structure (no swelling) and contains relatively large pore (60 Å) allowing the bulky homogeneous catalyst complexes to diffuse into the particle. The types of solvent and operating temperature are also two important parameters that influence the overall process [7-10]. The type of solvent can change both the reaction [7], and the adsorption mechanism. Depending on the solvent properties this interaction can vary in strength depending on its donor properties and the acidity of the metal salts [8]. The temperature is the second parameter that also influences the adsorption mechanism by changing the adsorbate-adsorbent [9] and the solute(adsorbate)-solvent bond [10]. Therefore both the solvent and the temperature effect require further attention in this research.

The goal of this chapter is to determine the promising functionalized silica adsorbents for the reversible affinity adsorption of our coordination complexes by binding via:

- the metal centre
- the ligand.

This chapter starts by using the Hard and Soft Acid Base (HSAB) theory for prediction of the adsorbate-adsorbent strength and pre-selection of potential functionalized silica adsorbents for affinity adsorption of the metal centre. A preliminary evaluation of the functionalized silica is done by investigating the adsorption of the metal salts ($CoCl_2$ or $PdCl_2$). The results will be explained by the HSAB theory. For the promising adsorbents these experiments are extended by adding the ligand to the system. With these equilibrium experiments the competition of the ligands in solution and the functionalized groups on the silica carrier is investigated. The influence of different solvents and temperature on the adsorption isotherms of metal salts is also studied. Finally the selection of the suitable functionalized silica adsorbents for the rhodium complex will be discussed.

After selection of suitable affinity adsorbents for the adsorption of the complex by binding via the metal centre, we focus our research on the selection of a suitable affinity adsorbent for ligand adsorption. Two types of bonding are included:
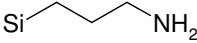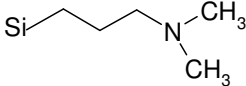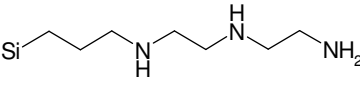
- covalent bond between the P atom of the triphenylphosphine and a proton of the functionalized acidic silica forming $HPPh_3^+$ which bonds with then present anionic group on the silica;
- π-interaction between benzene rings of the triphenylphosphine and phenyl-functionalized silica.

Based on the experimental evaluation results a selection of the most suitable adsorbent for the reversible adsorption of triphenylphosphine will be made.

3.2   Material

Chemicals palladium(II)chloride (99.9%), cobalt(II)chloride (anhydrous), tris(triphenylphosphine)rhodium(I)dichloride (99.99%), triphenylphosphine, acetonitrile (99.9%) and N,N-dimethylformamide, DMF, (99.9%) used for the adsorption experiments were obtained by Sigma-Aldrich. Functionalized silica (f.s) (Table 3.1 and Table 3.2) (except P-1, P-2 and boronic acid-polymer supported) were products of Silicycle and obtained through via either Sigma-Aldrich or Screening Devices. P-1 and P-2 were synthesized according to a literature procedure [11-13]. The silica carrier for these functionalized groups had the same properties as the commercially available. Boronic acid-polymer supported is ordered via Sigma-Aldrich. Solvents were degassed before the use, and all experiments in which triphenylphosphine was used were performed in argon atmosphere. The commercially available silica adsorbents (200-400 mesh, 60 Å, 500 m^2/g) were applied without pre-treatment.

Table 3.1. List of functionalized silica (f.s) adsorbents for adsorption of metal centre

Structure	Name	Abbreviation
N-containing functionalized groups		
	3-amino-f.s ($q_{f.g}$=1.02 mmol/g)	N-1
	3-(dimethylamino)propyl-f.s ($q_{f.g}$=1.50 mmol/g)	N-2
	3-(diethylentriamino)propyl-f.s ($q_{f.g}$=1.29 mmol/g)	N-3
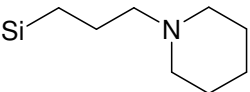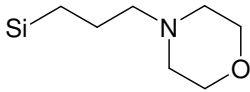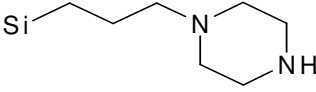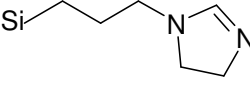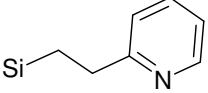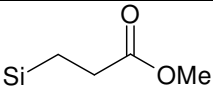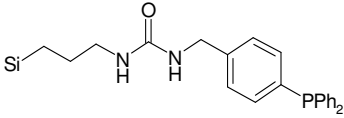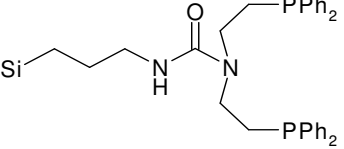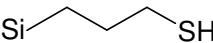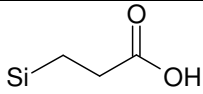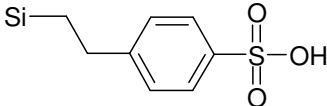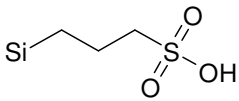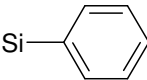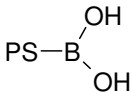
3-(1-piperidino)propyl-f.s	N-4	
$(q_{f.g}=1.11$ mmol/g)		
3-(1-morpholino)propyl-f.s	N-5	
$(q_{f.g}=1.33$ mmol/g)		
3-(1-piperazino)propyl-f.s	N-6	
$(q_{f.g}=0.85$ mmol/g)		
3-(1-imidazol-1-yl)propyl-f.s	N-7	
$(q_{f.g}=0.99$ mmol/g)		
2-(2pyridyl)ethyl-f.s	N-8	
$(q_{f.g}=1.09$ mmol/g)		

O-containing functionalized groups

2-(carbomethoxy)ethyl-f.s	O-1	
$(q_{f.g}=2.18$ mmol/g)		

P-containing functionalized groups

1-(4-(diphenylphosphino) benzyl)-3-(3-(triethoxysilyl)propyl)urea- f.s	P-1	
N-N-bis(2-(diphenylphosphino)ethyl) -urea-n-propyl –f.s	P-2	

S-containing functionalized groups

3-(mercapto)propyl- f.s	S-1	
$(q_{f.g}=0.98$ mmol/g)		

41

Table 3.2. List of functionalized silica (f.s) adsorbents for adsorption of the ligand

Structure	Name	Abbreviation
Si—CH$_2$CH$_2$—C(=O)OH	Carboxylic acid-f.s ($q_{f.g}$=1.02 mmol/g)	L-1
Si—CH$_2$CH$_2$—C$_6$H$_4$—S(=O)$_2$—OH	Tosic acid-f.s ($q_{f.g}$=1.50 mmol/g)	L-2
Si—CH$_2$CH$_2$CH$_2$—S(=O)$_2$—OH	Propylsulphonic acid-f.s ($q_{f.g}$=1.1 mmol/g)	L-3
Si—C$_6$H$_5$	Phenyl-f.s ($q_{f.g}$=9%carbon)	L-4
PS—B(OH)$_2$	Boronic acid-polymer supported ($q_{f.g}$=0.85 mmol/g)	L-5

3.3 Experimental

All adsorption equilibrium experiments were conducted batch wise and performed in a shaking bath at a constant temperature of 30ºC and 50 ºC. Each isotherm consists of four to five points with the initial concentration of the solutions in the range of 0-8 mmol/l for the metal salts and a triphenylphosphine and 0-4 mmol/l for the complexes. The lower concentration range for the complexes was necessary due to its limited solubility. The solvent volume is 10 ml for all experiments and approximately 0.15 g of adsorbent was added. Although the preliminary experiments indicated very fast kinetics, 16 hours were chosen to assume the equilibrium was reached. The equilibrium metal concentration in the solution was measured with an Atomic Absorbance Spectrometer, SpectrAA 110, from Varian. The experiments were repeated including all experimental steps and reproducibility was within 2%.

Each adsorption isotherm is presented as $q_e = f(C_e)$ where q_e is the equilibrium concentration of the total amount of the metal on the adsorbent [mmol/g$_{adsorbent}$], and C_e is the equilibrium concentration of the total amount of the metal in the solution [mmol/l]. q_e is calculated according to the equation

$$q_e = \frac{(C_o - C_e) \cdot V}{m} \tag{3.2}$$

where C_o is the initial concentration of the total amount of metal in solution [mmol/l], V is a volume of the solution [l] and m is the mass of adsorbent [g].

3.4   Results and discussion

3.4.1   Selection of adsorbents for the adsorption of the metal centre

Our first step was to select functional groups for which promising adsorption via the metal atom in the catalyst complex can be expected. The HSAB theory gives the first qualitative indication of the adsorbent - adsorbate interaction [3]. Figure 3.2 illustrates that cobalt and rhodium belong to the borderline acids, and palladium to the soft acids. However cobalt is nearer to the hard acids, and rhodium to the soft. On the other hand amines and their derivates belong to the hard bases, while pyridine belongs to the borderline bases. Oxygen containing groups are mostly located in the hard bases group. Phosphine and sulphur groups belong to the soft bases. According to the empirical generalization that the strongest binding is obtained by combining hard acids and hard bases, or soft acids and soft bases [3] we can predict that cobalt will bind stronger to the amines than to the phosphor or sulphur containing groups, while in the case of palladium it will be the opposite. Rhodium will have intermediate properties. With these bases but now functionalized on a silica carrier selection of a suitable adsorbent should be possible (Table 1).

$$Mo^{3+} < Mn < Fe < Co < Ni < Cu < Zn < Ru < Rh < M(0)\ Pd < Ag < Cd$$

<div align="center">
Hard Acids   Borderline   Soft Acids
</div>

$$RNH_2,\ OR^- < py < RSH,\ R_3P$$

<div align="center">
Hard Bases   Borderline   Soft Bases
</div>
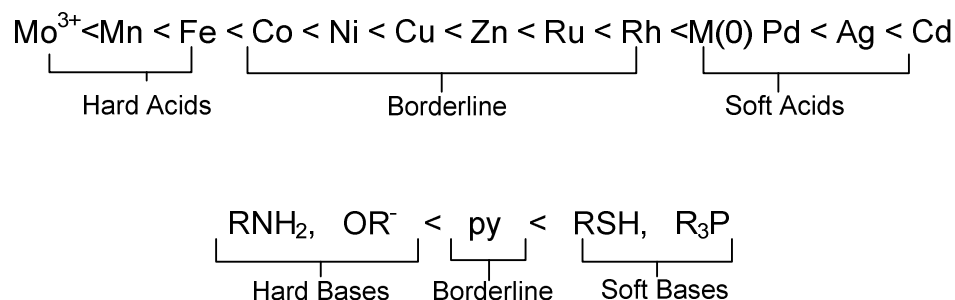
Figure 3.2. Acids and bases according to the HSAB theory [8]

Twelve adsorbents from four classes of groups were selected containing one or more N-, O-, P- or S- atom. All functionalized silica's is commercially available, with the exceptions of P-1 and P-2 (see Table 3.1), which were synthesized according to the

literature procedure [11-13]. Functionalized silica's have the highest diversity in N-containing groups, and therefore this class of groups is the most studied in this paper. There are two types of N-containing groups: alkyl (N-1 – N-3) and cyclo (N-4 – N-8). From the alkyl group we selected the amine group (N-1), the amine group with two methyl groups (N-2) and functionalized group comprised of three amines (N-3). Comparing the N-1 and the N-2 we can evaluate the effect of the alkyl side groups, and by comparing N-1 and N-3 the influence of multiple nitrogen atoms in one functional group is obtained. From the cyclo-group we selected: rings with single-bonded N atoms (N-4 – N-6) and double bonded N atoms (N-7 and N-8). The idea behind selecting the cyclic nitrogen groups was to compare the influence of the ring structure with the chain (alkyl) structure for the adsorption properties. Inside the cyclic group, the influence of one double bond (N-7), an aromatic structure (N-8), multiple N-atoms (N-6), and a combination of two different basic atoms (N-5) were investigated. The mono- dentate (P-1) and the bi-dentate (P-2) P-containing functionalized silica's were selected to investigate the influence of the diverse number of P atoms inside one functional group. It is expected that the bi-dentate will have a stronger binding with the metal centre since the two phosphorus atoms are within the same functional group. Due to the limited availability only one type of O- and S- containing functional group was chosen (O-1 and S-1).

3.4.2   *CoCl$_2$ adsorption*

CoCl$_2$ dissolved in acetonitrile was adsorbed on different functionalized silica materials (see Table 3.1) at a temperature of 30ºC. Figure 3.3 shows the measured adsorption isotherms for different adsorbents. Three regions are observed in Figure 3.3.: strong, intermediate and weak adsorption. Adsorbents in the strong adsorption region are functionalized with N- containing groups: amine derivatives (N-1, N-2) or cyclic groups containing one or more N atoms (N-4 – N-7). Amine derivatives belong to the hard bases because they easily share their electron pair to make a strong bond with cobalt. The presence of multiple N-atoms in one group (N-6) shows the extremely strong binding with cobalt. For this reason N-3 is expected to adsorb cobalt even stronger and therefore it was not investigated. N-5 and N-7 are the weakest N-functionalized adsorbents in the strong adsorption area because N-5 contains also an oxygen atom which is withdrawing the electrons from nitrogen, and therefore makes nitrogen a softer base, and N-7 has a double bond which distributes the electrons more evenly over the ring, but it has two nitrogen atom which still makes it a strong base.

As expected cobalt(II)chloride is weakly adsorbed to P-1 and S-1 adsorbents. This is expected because phosphor and sulphur type ligands belong to the soft bases, which are

not attracted to the borderline cobalt. With P-2 the $CoCl_2$ bond is stronger than with P-1, since it contains two phosphorus atoms inside the same group and therefore the basic character becomes more pronounced. Maximum loading of this material was insufficient for practical use. Adsorption of $CoCl_2$ was not observed for the adsorbent functionalized with an O-containing group (O-1).
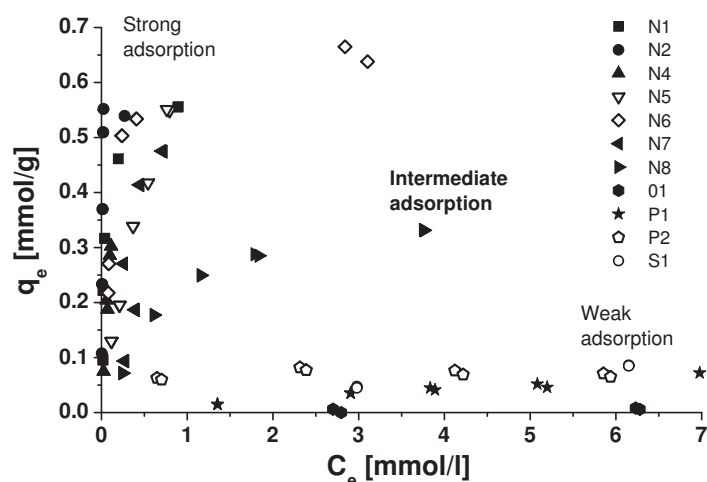
Figure 3.3. $CoCl_2$ adsorption from acetonitrile on different functionalized silicas at 30ºC

The most suitable region for adsorption of $CoCl_2$ is obtained on 2-(2-pyridyl)ethyl- functionalized silica (N-8). Now, the nitrogen atom is part of the aromatic ring which pulls the lone electron pair more inside the ring and makes the binding with cobalt weaker than with the other N-containing functional groups. The results are in agreement with the HSAB theory where cobalt belongs to the "harder" borderline group of the acids and therefore the strongest binding will be with strong bases (N1-N7), weaker with the pyridine, and the weakest with soft bases (P- and S- containing groups).

3.4.3   Desorption of $CoCl_2$

After selection of 2-(2-pyridyl)ethyl- functionalized silica (N-8) as an intermediate adsorbent for the reversible recovery of $CoCl_2$ from acetonitrile, the next step is to demonstrate reversibility of the adsorption process. This is shown in Figure 3.4 where equilibrium isotherms are given for $CoCl_2$ adsorption and desorption experiments. Since

both isotherms have a same trend CoCl$_2$ can be reversible recovered by adsorption on 2-(2-pyridyl)ethyl- functionalized silica.
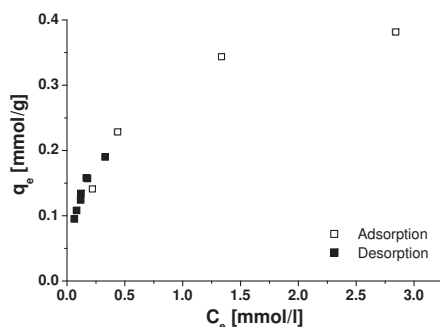
Figure 3.4. CoCl$_2$ adsorption and desorption from acetonitrile on 2-(2-pyridyl)ethyl- functionalized silica at 30ºC

3.4.4   *PdCl$_2$ adsorption*

The adsorption of PdCl$_2$ dissolved in DMF on different functionalized silica gels was investigated and the results are presented in Figure 3.5. Three regions, strong, intermediate and weak adsorption, are also observed in this case. Since palladium(II)chloride is a soft acid it is strongly adsorbed on S-1. Also the interaction with P-1 is very strong, but the loading of this material is low and therefore it is excluded from further research. N-3 till N-8 were tested and as expected from the HSAB theory its interaction with PdCl$_2$ is weaker than with the sulphur group, but still sufficiently strong. N-1 and N-2 were not investigated because of their similar binding properties as N-4 (see cobalt experiments). N-3 is the strongest of the N-containing adsorbents since it contains three nitrogen atoms per functionalized group. Adsorption on O-1 was not noticeable which can be explained by the high valence state for both Co^{2+} and Pd^{2+} [14]. The behaviour of the adsorbents with N-, S- and P- containing functional groups is in agreement with the HSAB theory.

Based on the experimental results 3-(1-morpholino)propyl-f.s (N-5), 3-(1-piperidino)propyl-f.s (N-4) and 2-(2-pyridyl)ethyl-f.s (N-8) were selected as the most suitable affinity adsorbents for PdCl$_2$.

46
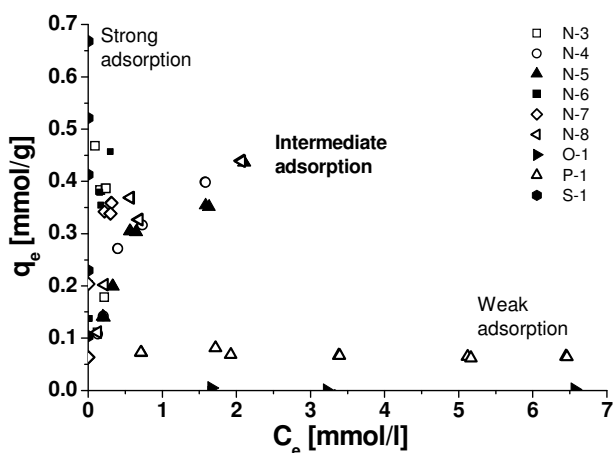
Figure 3.5. PdCl$_2$ adsorption from DMF on different functionalized silicas at 30ºC

3.4.5   *Influence of the solvent*

The adsorption of CoCl$_2$ and PdCl$_2$ from two solvents, acetonitrile and DMF was investigated. Cobalt(II)chloride was adsorbed on two adsorbents N-5 and N-8. Beside the N-8 which was selected as the most suitable adsorbent, also the strong binding N-5 is selected since we expected a reduction of the CoCl$_2$ adsorption in DMF. The same reason was behind selection of the adsorbents for PdCl$_2$ adsorption. The influence of the solvent is very pronounced as shown in Figure 3.6. Adsorption of CoCl$_2$ in acetonitrile is either strong (N-5) or suitable (N-8), but in DMF the adsorption of the cobalt salt is very weak for both adsorbents. This can be explained with the donor number. Since DMF has a higher donor number than acetonitrile [8] it interacts more strongly with the cobalt salt preventing the adsorption of CoCl$_2$.

Adsorption of PdCl$_2$ on the S-1 and N-5 adsorbents was studied for the same solvents DMF and acetonitrile. For the adsorbent S-1 the solvent effect is negligible due to the very strong interaction between the palladium and the functional group. Some minor effect of the solvent can be seen in the adsorption of palladium(II)chloride on the N-5 adsorbent. In general the influence of the solvent is less pronounced compared to cobalt because palladium is softer [6], and therefore interacts less with the solvent molecules.
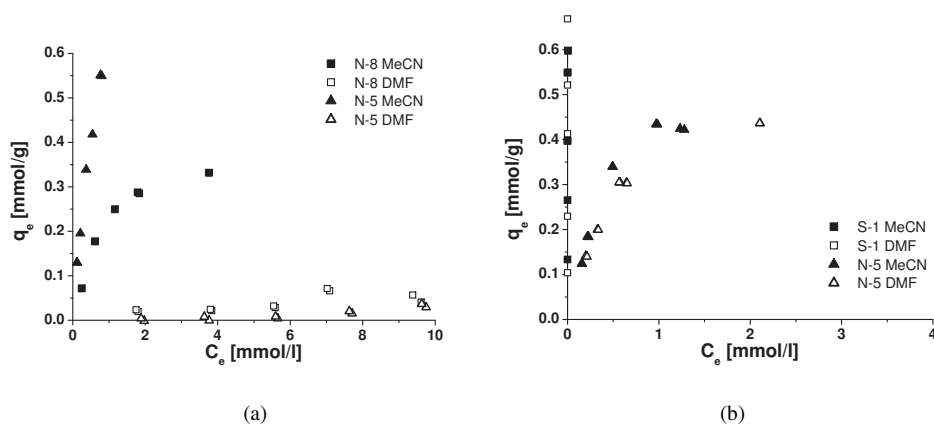
Figure 3.6. (a) CoCl$_2$ adsorption from acetonitrile and DMF on N-5 and N-8 and (b) PdCl$_2$ adsorption from acetonitrile and DMF on S-1 and N-5 at 30ºC

3.4.6   Influence of the temperature

The temperature effect is investigated by adsorbing CoCl$_2$ in acetonitrile on N-8 and PdCl$_2$ in DMF on N-5 at two different temperatures, 30ºC and 50ºC (Figure 3.7). N-8 and N-5 adsorbents are selected since they are already identified as the promising adsorbents for CoCl$_2$ and PdCl$_2$ respectively. In both situations it can be seen from the initial slope that the binding strength decreases with increasing temperature, while the maximum loading remains constant. There is a combined effect of the adsorbate-adsorbent interaction and the solvent-solute interaction where the solute and the adsorbate are CoCl$_2$ and PdCl$_2$. The experimental results describe the combined effect of both interactions. Since the adsorption strength decreases by temperature increase they can be explained with the theoretically well-known temperature effect on the adsorbate-adsorbent strength [9] by neglecting the solvent-solute interaction.
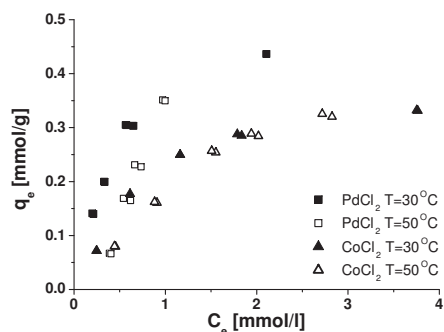
Figure 3.7. Influence of the temperature on the adsorption of CoCl$_2$ in MeCN on N-8, and PdCl$_2$ in DMF on N-5

48

3.4.7   Influence of the ligand

After selecting the most suitable adsorbents for the adsorption of $CoCl_2$ and $PdCl_2$ the next step was to investigate the ligand influence. Two equivalents of triphenylphosphine, PPh_3, were added to a solution of $CoCl_2$ and $PdCl_2$ since this is the ligand-metal ratio in the complex, ML_2. For this ratio, cobalt is present in all three forms, M, ML and ML_2, on the other hand palladium is dominantly present as the ML and ML_2 forms [6]. The results of the adsorption isotherms obtained for adsorption of $CoCl_2$ on adsorbent N-8 and $PdCl_2$ on adsorbents N-5 and S-1 are presented in Figure 3.8. The equilibrium concentration, Ce, measured for cobalt and palladium in the presence of ligands is the overall metal concentration, not taking into account which forms of the complexes are present. Also the loading is calculated for the total amount of adsorbed metal forms.

In the case of cobalt, Figure 3.8(a) illustrate that a slight decrease in initial slope of the isotherm on N-8 is noticed since the cobalt-triphenylphosphine bond is relatively weak [4]. In contrast, there was a very pronounced decrease in the initial slope of the adsorption isotherm for the palladium as shown in Figure 3.8(b). Morpholine functionalized silica (N-5), which was suitable for the adsorption of the palladium chloride, did not adsorb the palladium complex at all. Triphenylphosphine ligands strongly bind to palladium and therefore morpholine cannot compete with them. Therefore the adsorption of the palladium complex was tested with an adsorbent from the strong adsorption region, such as S-1. Since it is known that the amount of palladium salt is negligible compared to the other complex forms [4] we can also conclude that different complex species, M, ML and ML_2, are simultaneously adsorbed on S-1.

(a)   (b)
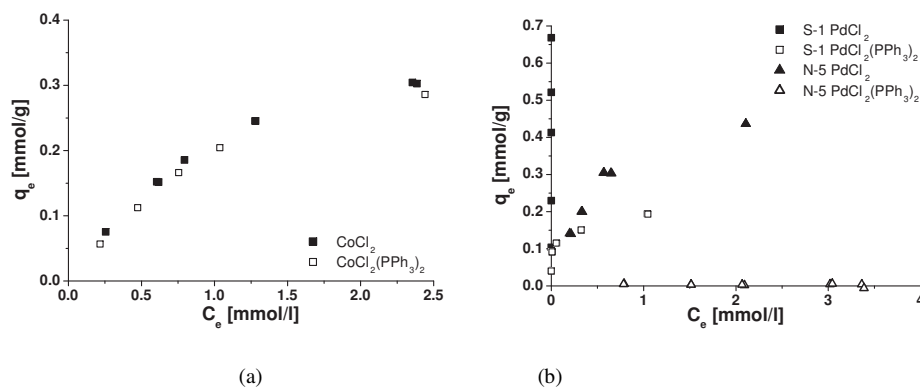
Figure 3.8. Influence of the ligand on the adsorption of the cobalt (a) and palladium complex (b) via the metal centre

Results of these experiments show a decrease in adsorption due to the ligand presence. This is explained with competition between the functionalized groups on the adsorbent and ligands in solution. This competition is in favour of the ligands if the complexation strength is sufficiently strong (e.g palladium complex).

3.4.8 RhCl(PPh₃)₃ adsorption

Selection of the promising adsorbent for the rhodium complex was done in the presence of the triphenylphosphine ligand since Rh^{1+} does not exist as a salt. Therefore the influence of the ligand will always be included. Two groups of results are presented in Figure 3.9:

- A group with the intermediate adsorbents (N-1, N-3, N-6, N-7, S-1)
- A group with the weak adsorbents (N-2, N-4, N-5, N-8, O-1)

In contrast to $CoCl_2$ and $PdCl_2$ a group of strong adsorbents is not found since there is a competition between triphenylphosphine in solution and functionalized groups on the silica which decreases the adsorption strength.
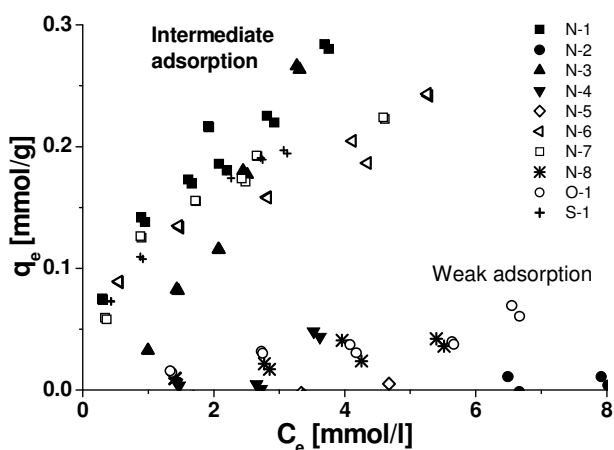
Figure 3.9. RhCl(PPh₃)₃ adsorption from DMF on different functionalized silicas at 30ºC

The difference in behaviour of the N-containing functionalized silica that belongs to the intermediate or to the weak adsorbents can be explained by the accessibility of the functional groups for the bulky rhodium complex. This is clearly shown by comparing the adsorption isotherms of N-1 and N-2. The difference between those two materials is the side groups attached to N-atom. N-1 has two hydrogen atoms, and N-2 two methyl groups. We assume that although the methyl groups are not very large they shield the nitrogen atom for the Rh-complex, and additionally also reduce the electro negativity of nitrogen. The

same effect is shown in the adsorption isotherms of N-4, N-5 and N-8. N-6 and N-7 belong to the intermediate group of adsorbents because the functionalized group (i) contains two nitrogen atoms that contribute to the higher electronegativity of the group and (ii) it contains one nitrogen atom that is outer orientated and therefore better accessible for the rhodium complex.

The intermediate adsorption on S-1 can be explained by the HSAB theory. Adsorption on O-1 is due to the low valance state of rhodium (Rh^{1+}) [14], but is not sufficiently strong which makes it a non-suitable adsorbent.

Based on the experimental results 3-amino-f.s (N-1), 3-(diethylentriamino)propyl-f.s (N-3), 3-(1-piperazino)propyl-f.s (N-6), 3-(1-imidazol-1-yl)propyl-f.s (N-7), 3-(mercapto)propyl- f.s (S-1) were selected as the suitable affinity adsorbents for adsorption of $RhCl(PPh_3)_3$ from DMF.

3.4.9 *Triphenylphosphine (PPh_3) adsorption*

Adsorption of PPh_3 from the acetonitrile is investigated and the results are presented in Figure 3.10. Four different functionalized silica containing acidic groups are selected for adsorption of PPh_3: carboxylic (L1), tosic (L2), propylsulphonic (L3) and boronic acid (L5). The bond is formed between the proton of the –OH group and the phosphor atom forming cationic group $HPPh_3^+$ which will form then acid/base interaction ($–O^- –(HPPh_3)^+$) with immobilized anionic group. In the previous work [15] it is shown that this type of interaction is reversible by means of concentration differences between solid and liquid phase. As shown in Figure 3.10, PPh_3 forms the strongest bond with tosic acid and a weak bond with carboxylic and boronic acids. Propylsulphonic acid belongs more to the intermediate region. This range is explained by the acidity of the functionalized groups. Tosic acid is the most acidic functionalized group. It means that H^+ is the most positively charged and therefore forms the strongest covalent bond with a lone electron pair of the phosphor atom. By decreasing the positive proton charge also the strength of the covalent binding is decreasing. Therefore, as a less acidic group compared to tosic acid, and a stronger than carboxylic or boronic acids, propylsulphonic acid shows suitable bonding for the reversible adsorption of PPh_3. Finally, in the case of phenyl-functionalized silica (L4) the bond via the π-electrons of the phenyl rings present on the silica and in triphenylphosphine is investigated. The conclusion of this experiment is that π-interaction is not sufficiently strong to recover triphenylphosphine from acetonitrile. Based on the obtained experimental results propylsulphonic acid functionalized silica (L3) is selected as a promising adsorbent for the recovery of triphenylphosphine.
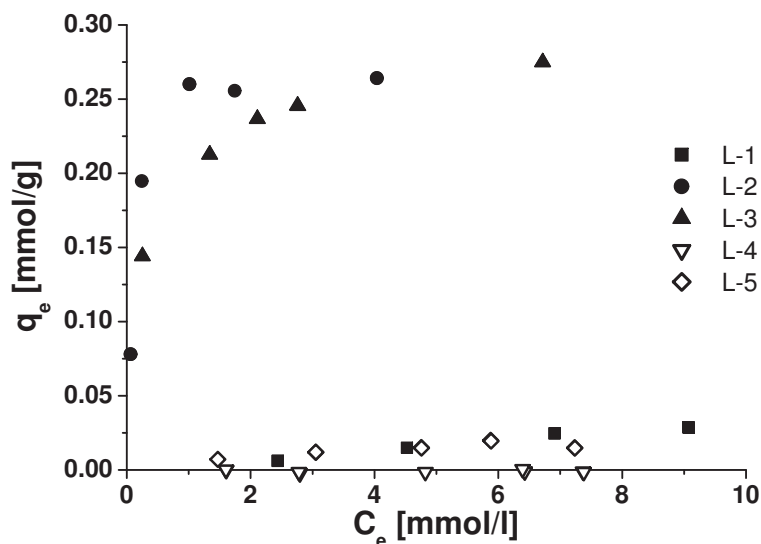
Figure 3.10. PPh$_3$ adsorption from MeCN on different functionalized silica at 30ºC

3.5   Conclusion

By screening a wide range of functionalized silica's the following promising affinity adsorbents were selected:

- 2-(2pyridyl)ethyl- functionalized silica (N-8) for recovery of CoCl$_2$(PPh$_3$)$_2$ from the acetonitrile;

- 3-(mercapto)propyl- functionalized silica (S-1) for recovery of PdCl$_2$(PPh$_3$)$_2$ from the DMF;

- 3-amino- functionalized silica (N-1), 3-(diethylentriamino)propyl- functionalized silica (N-3), 3-(1-piperazino)propyl- functionalized silica (N-6), 3-(1-imidazol-1-yl)propyl- functionalized silica (N-7), 3-(mercapto)propyl- functionalized silica (S-1) for recovery of RhCl(PPh$_3$)$_3$ from the DMF;

- Propylsulphonic acid functionalized silica (L-3) for recovery of PPh$_3$ from acetonitrile.

The presence of a ligand, an increase of the temperature and the presence of a solvent with the donor properties can decrease the adsorption equilibrium and need to be taken into account. Consequently it can render initially promising adsorbents into being unsuitable for a specific approach. The adsorption equilibrium results presented in this paper indicate that different forms of the complex that contain a metal centre are

simultaneously adsorbed. This supports the Reverse Flow Adsorption as a promising concept for the complete and reversible catalyst recovery.

3.6   Reference:

[1]   P.W.N.M van Leeuwen, Homogeneous Catalysis- Understanding the Art, Kluwer Academic Publishers, Dordrecht, The Netherlands, 2004, p.7-8.

[2]   J. Dunnewijk, H. Bosch, A.B. de Haan, Adsorption 11(2005) 521-526.

[3]   S. F. A. Kettle, Coordination Compounds, Thomas Neslon and Sons Ltd, London, 1969, p. 42-50.

[4]   T. Djekić, Z. Zivkovic, A.G.J. van der Ham, A.B. de Haan, J. Appl Catal A, 312 (2006) 144-152.

[5]   G. Zeni, D.Alves, A.L. Braga, H.A. Stefani, C.W. Nogueira, Tetrahedron Lett. 45, (2004) 4823-4826.

[6]   J. A. Osborn, F. H. Jardine, J. F. Young, G. Wilkinson, J. Chem. Soc. A. (1966) 1711.

[7]   F. Zhao, B.M. Bhanage, M. Shirai, M. Arai, J. Mol. Catal. A: Chem. 142 (1999) 383-388.

[8]   V.Gutmann, The Donor-Acceptor Approach to Molecular Interactions, Plenum Press, New York, 1978, p.20.

[9]   G. Guiochon, S.G. Shirazi, A.M. Katti, Fundamentals of Preparative and Nonlinear Chromatography, Academic Press, 2006, p.70-77.

[10]   A.M. Persky, J. A. Hughes, Solutions and Solubility, University of Florida, <http://www.cop.ufl.edu/safezone/prokai/pha5100/solubility.htm >, 2006.

[11]   D. de Groot, B.F.M. de Waal, J. N.H. Reek, A.P.H.J. Schenning, P.C.J.Kamer, E.W. Meijer, P.W.N.M. van Leeuwen, J. Am. Chem. Soc., 123 (2001) 8453-8458.

[12]   B. Sandee, Tailor-made catalysts immobilized on silica, "theses", University of Amsterdam, 2001, p.39-40,105.

[13]   R.G. Nuzzo, S.L.Haynie, M.E.Wilson, G.M. Whitesides, J. Org. Chem. 46 (1981) 2861-2867.

[14]   Silicycle, Silicycle catalog, Silia Bond TAAcOH, <http://www.silicycle.com/html/english/products/produit_detail.php?pro_id=7>, (2006).

[15]   Dunnewijk J., Reverse Flow Adsorption Technology for Homogeneous Catalyst Recycling, thesis, University of Twente, (2006)

Competitive adsorption isotherm modelling for the adsorption of homogeneous complexes by functionalized silica adsorbents

Abstract

For the modelling of the RFA process it is important to have a good description of the adsorption of various complex species present in the solution. Therefore the goal of this chapter is to develop an adequate model which can describe the adsorption of coordination complexes. In this research bis(triphenylphosphine) cobalt(II)dichloride ($CoCl_2(PPh_3)_2$) was selected as a model catalyst and 2-(2-pyridyl)ethyl-functionalized silica and 3-(1-morpholino)propyl-functionalized silica were selected as suitable adsorbents. Since in a solution $CoCl_2(PPh_3)_2$ is always in equilibrium with its free metal centre $CoCl_2$ (M), free ligand PPh_3 (L) and other complex forms, $CoCl_2(PPh_3)$ and $CoCl_2(PPh_3)_2$ (ML and ML_2), three models were evaluated (M, M-ML and M-ML-ML_2) that combine the equilibrium of the complex forms present in the solvent with its competitive adsorption on the functionalized silica. Comparison of the model results with the experimental adsorption data shows that the model which takes all three forms M, ML and ML_2, into account describes the results most consistently.

4.1 Introduction

Nowadays homogeneous catalysts are refered to organometallic complexes [1] that are mostly found in equilibrium with their free metal centre, ligands and other complex forms (Figure 4.1). Coordination complexes are often catalyst precursor forms of organometallic catalysts. In this work we study coordination complexes where metal centre is surrounded with monodenate ligands. Since they are as complex compounds in solution present in different forms, it is important to adsorb all forms to prevent their leaching. Therefore the *Two Step Adsorption* approach was selected as a strategy for their complete and reversible recovery of homogeneous catalysts (Figure 4.2) [2]. By this approach the catalyst is adsorbed on two different adsorbent beds. The first bed adsorbs all the metal containing forms by binding via the metal centre, and the second bed adsorbs the excess of ligand. The binding strength between the adsorbate (catalyst) and adsorbent should be balanced to obtain the optimal adsorption/desorption equilibrium necessary for the recycling of the catalyst.
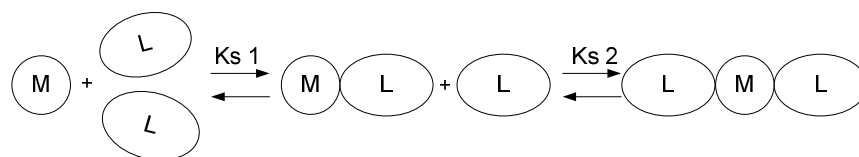
Figure 4.1. Homogeneous catalyst equilibrium
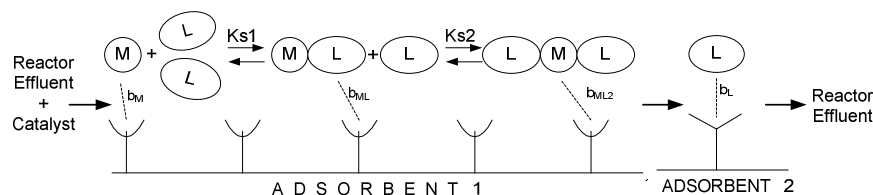
Figure 4.2. Strategy for reversible catalyst adsorption and schematic representation of the competitive adsorption of the catalysts species to the functional groups on two adsorption beds (M is a metal centre, L is a ligand, b_M, b_{ML}, b_{ML2} and b_L are adsorption constants)

For the modelling of the RFA process it is essential to have a good description of the adsorption isotherm for the model catalyst, in our case. Since the coordination compound is a complex compound found in solution in different forms (Figure 4.1), it is crucial to be acquainted with the amount of each complex species both in the solution and on the adsorbent. The concentration of different forms present in solution is calculated from the stability constants for the specific model catalyst. In our previous work stability constants for different complex systems were reported [3]. Introducing an adsorbent to a solution

which contains the model catalyst, the result will be a competition between: (i) the ligand in solution and the functionalized groups on the adsorbent for the metal containing compounds and (ii) the adsorbing species for the free sites on the adsorbent (Figure 4.2). Therefore to describe the adsorption mechanism of the complex compounds both the competitive adsorption and the equilibrium between the species present in solution should be considered. In literature a wide range of models were reported for describing the competitive adsorption isotherms between different compounds [4]. The common competitive adsorption models previously reported are the multicomponent Langmuir model [4,5], the multicomponent Freundlich model [6] and the Polanyi-Dubinin isotherm for chemical mixtures [7]. These models are used for fitting experimental adsorption equilibrium data, where different compounds are competing for the same site on an adsorbent. Modelling of the multicomponent adsorption of metal complexes is also reported by Guaus et al. [8], they adsorbed the complexes on the electrode surface. Since their model is applied in the field of electrochemistry it was not applicable in our research.

The goal of this paper is to develop an adequate model that describes the competitive adsorption of the homogeneous complexes taking into account the equilibrium in the liquid phase. In this research bis(triphenylphosphine) cobalt(II)dichloride $(CoCl_2(PPh_3)_2)$ was selected as a model coordination complex, while 2-(2pyridyl)ethyl-functionalized silica and 3-(1-morpholino)propyl-functionalized silica were selected as two suitable adsorbents. Cobalt(II)chloride represents the metal centre of the complex, while triphenylphosphine the ligand. This paper starts with an approach in which just three models were developed that cover the following possibilities: (i) adsorption of the free metal centre (*M*) only; (ii) adsorption of the free metal centre (*M*) and the complex containing free metal centre and one ligand (*ML*); (iii) adsorption of all species that contain metal (*M*, *ML* and *ML$_2$*). These models consist of mass balances for each species, the competitive adsorption isotherm and the stability constant equations. In this paper the competitive Langmuir isotherm is selected since the adsorption of the free metal centre $(CoCl_2)$ is described well by the Langmuir isotherm (see experimental part). To show the influence of the ligand the experimental results of the adsorption for the model complexes at different metal-ligand ratios are presented. The initial 1:0 metal/ligand ratio is increased up to 1:20 which is sufficiently large to clearly show the contribution of each complex form present. With these data the three models were evaluated and their results are given and discussed. Finally the best model is selected.

4.2 Model for competitive adsorption of homogeneous complexes

To select the adequate model for describing the adsorption of the coordination complexes three models were developed: (i) M, (ii) M-ML and (iii) M-ML-ML$_2$ model.

The first model (M model) assumes that only the free metal centre is adsorbed; the second model (M-ML model) assumes that both the free metal centre, M, and the complex form ML are adsorbed, while the third model (M-ML-ML$_2$ model) includes the adsorption of all forms that contain metal. Adsorption of the ligand was not taken into account since it shows no interaction with the functionalized groups on the adsorbent [9,10]. All models consist of mass balance equations, stability constant equations and competitive adsorption isotherms.

4.2.1 Stability constants

Since our model complex consists of a metal centre and two ligands, the equilibrium between the forms present in the solution can be written as:

$$M + 2L \underset{\longleftarrow}{\overset{K_{S1}}{\longrightarrow}} ML + L \underset{\longleftarrow}{\overset{K_{S2}}{\longrightarrow}} ML_2 \, .$$

This equilibrium is described by stability constants defined as the ratio between the concentration of the reacting species, see equation (4.1-4.2):

$$K_{S1} = \frac{[ML]}{[M] \cdot [L]} \tag{4.1}$$

$$K_{S2} = \frac{[ML_2]}{[ML] \cdot [L]} \, . \tag{4.2}$$

K_{s1} and K_{s2} are stability constants of the first and the second complexation step respectively. [ML_i], [M] and [L] represent the concentration of the complex forms, the free metal centre and the free ligand respectively.

4.2.2 Mass balances

Mass balances are applied for the metal (equations 4.3-4.4), the ligand (equations 4.5-4.6) and the adsorbent phase (equation 4.7). Due to the low concentrations of the model complexes the mass balance is expressed in concentrations assuming no volume change due to adsorption.

$$\left[M_{t0}\right] = \left[M_{te}\right] + \frac{q_{t,e} \cdot m}{V} \tag{4.3}$$

$$[M_{te}] = [M] + [ML] + [ML_2] \tag{4.4}$$

$$[L_{t0}] = [L_{te}] + \frac{(q_{ML,e} + 2 \cdot q_{ML_2,e}) \cdot m}{V} \qquad (4.5)$$

$$[L_{te}] = [L] + [ML] + 2 \cdot [ML_2] \qquad (4.6)$$

$$q_{t,e} = q_{M,e} + q_{ML,e} + q_{ML_2,e} \qquad (4.7)$$

where $[M]$, $[L]$, $[ML]$ and $[ML_2]$ represents the concentrations of free metal centre, free ligand, and different forms of the complexes respectively. $[M_{t0}]$ is the initial total metal concentration, $[M_{te}]$ is the total metal concentration at equilibrium, and $[L_{t0}]$ is the initial total ligand concentration and $[L_{te}]$ is the total ligand concentration at equilibrium. $q_{t,e}$ is the total loading of adsorbent at equilibrium with $q_{M,e}$, $q_{ML,e}$ and $q_{ML2,e}$ representing the loadings of the free metal centre, M, and different forms of the complex, ML and ML_2, respectively. m is the amount of adsorbent and V is the volume of solution applied. It is experimentally shown that there is no ligand adsoprtion.

4.2.3   Competitive adsorption isotherm

A multicomponent Langmuir isotherm is selected to describe the competitive binding of the free metal centre, M, and the complex forms, ML and ML_2. This isotherm assumes that each adsorbed specie occupies one adsorption site [4]. The general form of the competitive Langmuir isotherm is given as:

$$q_{i,e} = \frac{C_{ei} \cdot b_i \cdot q_s}{1 + \sum_{j}^{n} b_j \cdot C_{ej}}; i, j = 1..n \qquad (4.8)$$

where n can be either 1, 2 or 3. If n=1 then the competitive Langmuir isotherm becomes a Langmuir isotherm for the single component and it is used in the M model. If n=2, then adsorbing species are M and ML, and this form of the isotherm is used in the M-ML model. At last, if n=3 then all three species, M, ML and ML_2, are adsorbing and this form of the competitive Langmuir isotherm is used in the M-ML-ML$_2$ model. $q_{i,e}$ is the adsorbed amount of component i at equilibrium [mmol/g], i refers to the metal containing species that are adsorbed (M, ML or ML_2), $C_{e,i}$ is the equilibrium concentration of the component i in solution [mmol/l], b_i is the Langmuir constant [l/mmol] of component i, q_s is the maximum capacity of the adsorbent [mmol/g] and i refers to the metal containing species that are adsorbed (M, ML or ML_2).   Since M is found in individual form, b_M is experimentally determined for single component, as well as q_s. On the other hand ML and ML_2 are not present in solution in individual form since they dissociate as shown in Figure

4.2. Therefore b_{ML} and b_{ML2} are obtained from the model by fitting it to the experimental data.

The total amount adsorbed, $q_{t,e,exp}$, can be experimentally determined from the initial and equilibrium concentration of the total amount of metal, $[M_{t0}]$ and $[M_{te}]$, respectively:

$$q_{t,e,\exp} = q_{M,e} + q_{ML,e} + q_{ML_2,e} = \frac{([M_{t0}] - [M_{te}])V}{m} \qquad (4.9)$$

Using a competitive Langmuir model $q_{t,e,mod}$ is calculated as:

$$q_{t,e,\mathrm{mod}} = q_{M,e} + q_{ML,e} + q_{ML_2,e} = \frac{(b_M \cdot [M] + b_{ML} \cdot [ML] + b_{ML_2} \cdot [ML_2]) \cdot q_s}{1 + b_M \cdot [M] + b_{ML} \cdot [ML] + b_{ML_2} \cdot [ML_2]} . \qquad (4.10)$$
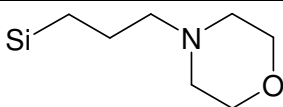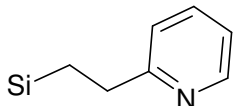
Combining the equations (4.1-4.10) parameters b_{ML} is adjusted for the M-ML model, and additionally b_{ML2} is adjusted for the M-ML-ML2 model to minimize the objective function as shown in equation (4.11):

$$\Delta = \sum (q_{t,e,\exp} - q_{t,e,\mathrm{mod}})^2 \rightarrow \min . \qquad (4.11)$$

4.3   Materials

Chemicals cobalt(II)chloride (anhydrous), triphenylphophshine, acetonitrile (MeCN) (99.9%) used for the adsorption experiments were obtained from Sigma-Aldrich. 2-(2pyridyl)ethyl functionalized silica and 3-(1-morpholino)propyl functionalized silica were produced by Silicycle and obtained via Screening Devices Solvents were degassed before use, and all experiments in which triphenylphosphine was used were performed in an argon atmosphere. No preliminary treatment of the silica adsorbents (200-400 mesh, 60 Å, 500 m^2/g) was performed. The chemical structures of adsorbents, their names and the amount of functionalized groups per gram of silica are presented in Table 4.1.

Table 4.1. Investigated functionalized silica (f.s) adsorbents

Structure	Name
	3-(1-morpholino)propyl-f.s ($q_{f.g}$=1.33 mmol/g)
	2-(2pyridyl)ethyl-f.s ($q_{f.g}$=1.09 mmol/g)

4.4 Experimental

All adsorption equilibrium experiments were conducted batchwise and performed in a shaking bath at a constant temperature of 30ºC. Each isotherm consists of four to five points with the initial concentration of the solutions in the range of 0-8 mmol/l of total metal amount for $CoCl_2$ and $CoCl_2(PPh_3)_2$ + ligands in excess (Co:PPh_3=1:0, 1:2, 1:5, 1:10 and 1:20). The solvent volume is 10 ml for all experiments and approximately 0.15 g of adsorbent was accurately weighted and added. Although preliminary experiments indicated very fast kinetics, 16 hours were chosen to assure equilibrium was reached. The final metal concentration in the solution [M_{te}] was measured with an Atomic Absorbance Spectrometer, SpectrAA 110 (Varian). Each adsorption isotherm is presented as: $q_{t,e,\exp} = f\left([M_{te}]\right)$ where $q_{t,e,exp}$ is calculated by equation (4.9). Duplication of a number of experiments showed reproducibility better than 2%.

4.5 Results and discussion

To describe the adsorption of $CoCl_2(PPh_3)_2$ from acetonitrile by the previously discussed models following parameters should be determined: b_M, b_{ML}, b_{ML2} and q_S. The binding constant b_M and the maximum loading q_S can be calculated from the adsorption experiments where only the metals salt (M) $CoCl_2$ is adsorbed (Co:PPh_3=1:0). The other constants, b_{ML} and b_{ML2}, are fitted from the models. The values of the stability constants are determined in the previous work [3], and their values are: K_{S1}=0.0236 [l/mmol] and K_{S2}=0.106 [l/mmol].

4.5.1 CoCl₂ adsorption

In our previous work 2-(2pyridyl)ethyl-functionalized silica was already selected as a suitable adsorbent for the adsorption of $CoCl_2$ from acetonitrile. 3-(1-morpholino)propyl-functionalized silica was selected as an adsorbent from the strong

adsorption region [9]. Fitting the experimental adsorption isotherms of $CoCl_2$ with the Langmuir isotherm (see Figure 4.3 and Table 4.2) shows that the binding strength (b_M) is approximately the same but the maximum loading differs.

Table 4.2 also shows that the ratio $q_{f.g}/q_s$ is approximately 2 for 2-(2pyridyl)ethyl – functionalized silica which means that two functionalized groups act as one site, while in the case of the 3-(1-morpholino)propyl- functionalized silica one group acts as one site.
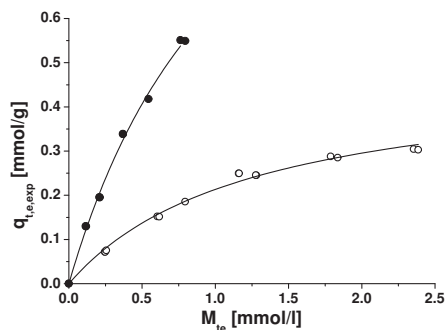
Figure 4.3. Adsorption isotherms for 2-(2pyridyl)ethyl-functionalized silica (empty circles) and 3-(1-morpholino)propyl-functionalized silica (full circles), with the Langmuir isotherm fit (solid lines)

Table 4.2. Langmuir isotherm parameters fitted for $CoCl_2$ adsorption experiments from acetonitrile on 2-(2pyridyl)ethyl-functionalized silica and 3-(1-morpholino)propyl-functionalized silica

Name	b_M [l/mmol]	q_s [mmol/g]	$q_{f.g}/q_s$
2-(2pyridyl)ethyl-functionalized silica	0.798	0.48	2.27≈2
3-(1-morpholino)propyl-functionalized silica	0.822	1.40	0.95≈1

4.5.2 $CoCl_2$ with PPh_3 adsorption

The adsorption equilibrium experiments were extended by adding approximately 2, 5, 10 and 20 equivalents of the triphenylphosphine ligand, PPh_3 to the initial solution of $CoCl_2$ in acetonitrile. The results are shown in Figure 4.4 where the equilibrium loading of the adsorbent, expressed as the total amount of metal species adsorbed, as a function of the equilibrium concentration of the total amount of metal species in the solution are presented for both adsorbents. A decrease in the slope of the isotherm with increasing amount of ligand is noticed. This can be explained by two effects:

(i)   The competition between the ligands present in solution and the functionalized groups on the silica adsorbent which is in favour of the increasing amount of ligands.

(ii) The competitive adsorption of different species present in solution.

The first effect applies in all situations and is not discriminating between M, $M+ML$ and $M+ML+ML_2$ adsorption. However, the second effect applies only if next to M also ML and ML_2 are adsorbed.

(a)   (b)
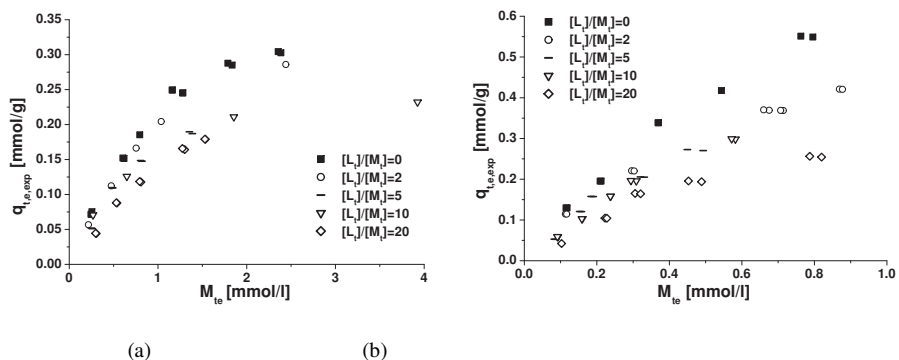
Figure 4.4. Adsorption of the species containing $CoCl_2$ from acetonitrile in the presence of triphenylphosphine ligand (a) on the 2-(2pyridyl)ethyl-functionalized silica adsorbent (b) on the 3-(1-morpholino)propyl-functionalized silica adsorbent

4.5.3   Modeling

Two criteria were used to select the adequate model for describing the competitive adsorption of the different forms of complexes (M, ML and ML_2) present in solution:

- R^2 of the parity line $q_{t,e,exp}$ vs. $q_{t,e,mod}$
- The distribution of the points over the parity line for different ratios of $[ML_2]$ over $[M_{te}]$

Table 4.3 shows the results of R^2 and the parameters fitted from the experimental adsorption data of 2-(2pyridyl)ethyl-functionalized silica and 3-(1-morpholino)propyl-functionalized silica. Graphical presentation of all parity graphs for the adsorption of the model catalyst over the 2-(2pyridyl)ethyl-functionalized silica (Figures 4.5 (a)-(c)) are presented with three sets of data that show the relative amount of the complex form, ML_2, compared to the total amount of metal present in solution at equilibrium:

- $[ML_2]/[M_{te}]<20\%$
- $20\%<[ML_2]/[M_{te}]<65\%$
- $[ML_2]/[M_{te}]>65\%$.

These sets are selected to show the distribution of the points along the parity line for the ranges of low, medium and high relative amount of catalyst complex. Since ML and ML_2 are bulkier forms compared to the M form, there is a possibility that they occupy more space than M. It means that the maximum loading of an adsorbent is not the same for each specie and therefore the multi-component Langmuir model can not be applied. Since it is

63

assumed that each form is occupying one adsorption site by presenting the experimental data in three ranges we can check the validity of the model description. If the model describes the adsorption of the complex species well, the points along the parity line should be equally distributed for each range. It means that the model describes both the adsorption at the low range where the free metal centre is mostly present as well as the adsorption at the higher ranges where mainly the ML_2 complex form is present well.

The results in Table 4.3 are used to select the best of the three models. If a model is eliminated it is based on the parameter value marked grey in this table. Model M was eliminated since the R^2 value differ significantly from 1 (Table 4.3). This gives a clear indication that other complex forms beside the free metal salt are adsorbed. Modelling was extended to the M-ML model which includes adsorption of free metal salt, M, and the complex which contains only one ligand, ML. This model was also excluded since Figure 5(b) clearly shows that the data points are too scattered along the parity line which results in a too low R^2 value. Also the points are not equally distributed along the parity line for all three relative concentration ranges $[ML_2]/[M_{te}]$.

Table 4.3. Results of the competitive adsorption modelling for the complex forms M, ML and ML_2 for both functionalized silica's

Model	M	M-ML	M-ML-ML$_2$
2-(2pyridyl)ethyl-functionalized silica			
R^2	0.37	0.7747	0.9743
b_{ML}	-	1.72	0.15
b_{ML2}	-	-	0.35
3-(1-morpholino)propyl- functionalized silica			
R^2	0.568	0.7803	0.8902
b_{ML}	-	1.61	0.67
b_{ML2}	-	-	0.29

The M-ML-ML$_2$ model gives the best description of the adsorption data of our model catalyst on 2-(2pyridyl)ethyl-functionalized silica (Table 4.3 and Figure 4.5(c)). This model assumes adsorption of all species that contain a metal atom. Compared to the previously discussed two models, the M-ML-ML$_2$ model also gives the best fitting results with the R^2 value close to 1 (see Table 4.3). ML and ML_2 forms contain next to the metal centre also one or two ligands respectively. Therefore there is a competition between ligands and adsorption sites for the metal centre, and, consequently, the adsorption strength should decrease. This is in line with the values of the Langmuir constants b_{ML} and b_{ML2} as found in our M-ML-ML$_2$ model which are both lower than the value of b_M. Furthermore,

the M-ML-ML$_2$ model shows in Figure 4.5(c) a good distribution of the points along the parity line for all ranges of $[ML_2]/[M_{te}]$. Therefore we believe that in spite of introducing extra degrees of freedom the multicomponent Langmuir isotherm which assumes that each component is competing for the same site on the adsorbent is valid to describe the adsorption of our model complex.

(a)

(b)

(c)
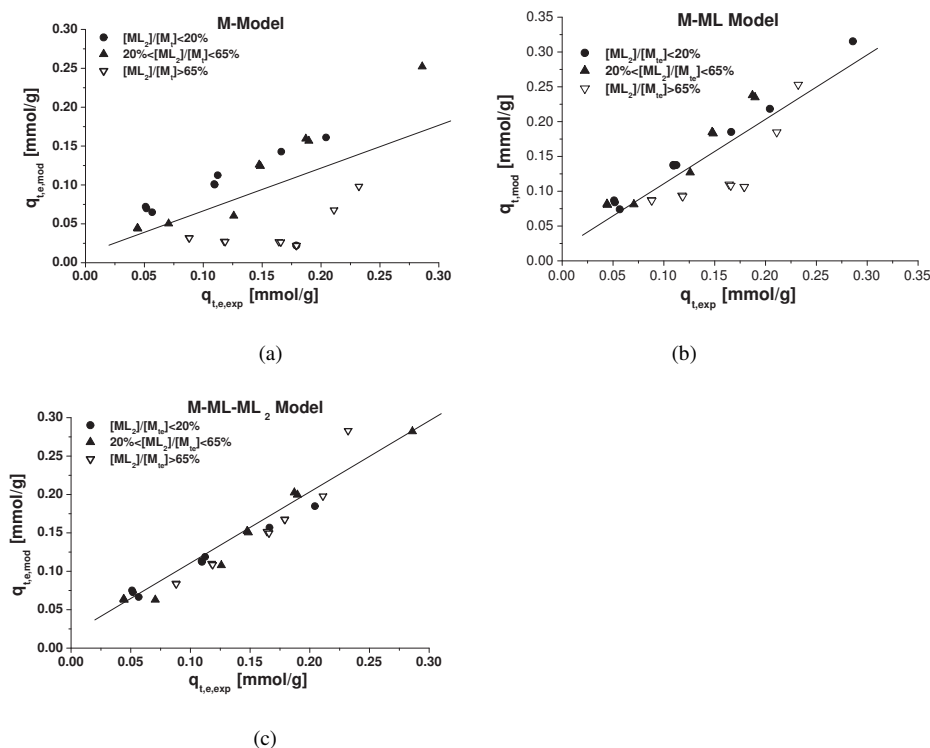
Figure 4.5. Parity graphs for the modelling results of the adsorption of the species containing CoCl$_2$ from acetonitrile on 2-(2pyridyl)ethyl-functionalized silica (a) the M model, (b) the M-ML model, (c) the M-ML-ML$_2$ model

The equilibrium data for the cobalt complex adsorption on 3-(1-morpholino)propyl-functionalized silica is also modelled to check the applicability of the developed model. The results of the fitted parameters are also given in Table 4.3 and Figure 4.6. The same conclusion can be drawn. Both the M and the M-ML model have poor values for R^2. The M-ML-ML$_2$ model gives also the best description of the competitive adsorption for the complex species present in solution.
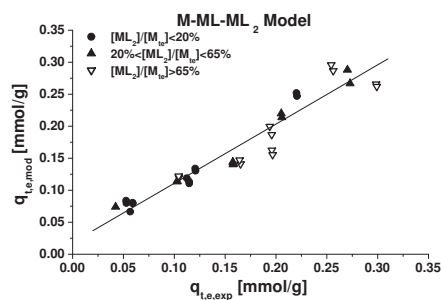
Figure 4.6. Parity graphs for the modelling results of the adsorption of the species containing $CoCl_2$ from acetonitrile on -(1-morpholino)propyl-functionalized silica- M-ML-ML_2 model

4.6   Conclusion

Three models were evaluated to describe the adsorption of coordination complexes: M, M-ML and M-ML-ML_2 model. Results show that the M-ML-ML_2 model is the best model to describe the adsorption of bis(triphenylphosphine) cobalt(II)dichloride ($CoCl_2(PPh_3)_2$) on 2-(2pyridyl)ethyl-functionalized silica and 3-(1-morpholino)propyl-functionalized silica. The M-ML-ML_2 model gives the best parity lines and a statistical distribution of the results along the line. It means that adsorption of all metal containing forms present in solution should be taken into account. Integrating the M-ML-ML_2 model in the Reverse Flow Adsorption gives possibility to design a process where the leaching of the metal is prevented. Therefore this work supports the Reverse Flow Adsorption as a promising concept for the complete and reversible catalyst recovery.

4.7   List of symbols

Δ-	Objective function	$[(mmol/g)^2]$
b_i-	Adsorption binding strength for a component I	[l/mmol]
b_M-	Adsorption binding strength for component M	[l/mmol]
b_{ML}-	Adsorption binding strength for component ML	[l/mmol]
b_{ML2}-	Adsorption binding strength for component	[l/mmol]
C_e-	Equilibrium concentration	[mmol/l]
i-	Counter	[-]
j-	Counter	[-]
K_{S1}-	Stability constant of the first complexation step	[l/mmol]
K_{S2}-	Stability constant of the second complexation step	[l/mmol]
L-	Free ligand	[-]
$[L]$-	Concentration of the free ligand	[mmol/l]

$[L_{t0}]$-	Initial total concentration of the ligand	[mmol/l]
$[L_{te}]$-	Equilibrium total concentration of the ligand	[mmol/l]
m-	Mass of the adsorbent	[g]
M-	Free metal centre	[-]
ML-	Complex that contain metal centre and one ligand	[-]
ML_2-	Complex that contain metal centre and two ligands	[-]
$[M]$-	Concentration of the free metal centre	[mmol/l]
$[ML]$-	Concentration of the ML complex	[mmol/l]
$[ML_2]$-	Concentration of the ML$_2$ complex	[mmol/l]
$[M_{t0}]$-	Initial total concentration of the all metal containing forms	[mmol/l]
$[M_{te}]$-	Equilibrium total concentration of the all metal containing forms	[mmol/l]
n-	Number of the compounds	[-]
R-	Correlation coefficient	[-]
q-	Loading on the adsorbent	[mmol/g]
$q_{i,e}$-	Loading on the adsorbent for the component i	[mmol/g]
$q_{M,e}$-	Loading on the adsorbent for the component M	[mmol/g]
$q_{ML,e}$-	Loading on the adsorbent for the component ML	[mmol/g]
$q_{ML2,e}$-	Loading on the adsorbent for the component ML$_2$	[mmol/g]
q_s-	Maximum loading on the adsorbent	[mmol/g]
$q_{t,e,exp}$-	Total loading on the adsorbent determined experimentally	[mmol/g]
$q_{t,e,mod}$-	Total loading on the adsorbent determined by model	[mmol/g]
V-	Volume of the solvent	[l]

4.8 Reference:

[1]   P.W.N.M van Leeuwen, Homogeneous Catalysis- Understanding the Art, Kluwer
        Academic Publishers, Dordrecht, 2004, p.7-8

[2]   J. Dunnewijk, H. Bosch, A.B. de Haan, Adsorption 11(2005) 521-526

[3]   T. Djekić, Z. Zivkovic, A.G.J. van der Ham, A.B. de Haan, Appl Catal A, 312 (2006) p.
        144-152

[4]   G. Guiochon, S.G. Shirazi, A.M. Katti, Fundamentals of Preparative and Nonlinear
        Chromatography, Academic Press, 2006,p.151-219

[5]   A.Felinger, A.Cavazzini, G. Guiochon, J Chrom A, 986 (2003), p. 207-225

[6]   Y.Sag, B. Akcael, T. Kutsal, Chem.Eng.Comm., 190 (2003) p. 797-812

[7]   J.Li, C.J.Werth, Environ Toxicol Chem 21(7), (2002), p. 1377-1383

[8]   E.Guaus, F. Sanz, M. Sluyters-Rehbach, J.H. Sluyters, J. Electroanal Chem, 385 (1995), p.
        121-134

[9]   T.Djekić, A.G.J. van der Ham, A.B. de Haan, J Chrom A, 11420(2007), p.32-38

[10]   S. F. A. Kettle, Coordination Compounds, Thomas Neslon and Sons Ltd, London, 1969, p. 42-50

Effective intraparticle diffusion coefficients of $CoCl_2$ in mesoporous functionalized silica adsorbents

 Abstract

The scope of this work is to determine the effective intraparticle diffusion coefficient of $CoCl_2$ over mesoporous functionalized silica. Silica is selected as a carrier of the functionalized groups for its rigid structure that excludes troublesome swelling, often found in polymeric adsorbents. 2-(2-pyridyl)ethyl-functionalized silica is selected as a promising affinity adsorbent for the reversible adsorption of $CoCl_2$. The adsorption kinetics is investigated with the Zero Length Column (ZLC) method. Initially, experiments were performed at different flow rates to eliminate the effect of external mass transfer. The effect of pore size (60Å and 90Å), particle size ($40 \cdot 10^{-6}$m-$1000 \cdot 10^{-6}$m) and initial $CoCl_2$ concentration (1 mol/m^3-2 mol/m^3) on the mass transfer was investigated. A model was developed to determine the effective diffusion coefficient of $CoCl_2$ by fitting the experimental data to the model. The effective diffusion coefficients determined for two different pore sizes of silica are $D_{eff}(60Å)=1.17 \cdot 10^{-10}$ [m^2/s] and $D_{eff}(90Å)=5.8 \cdot 10^{-10}$ [m^2/s]. The particle size and the initial $CoCl_2$ concentration do not have an influence on the value of diffusion coefficient. However, particle size has an influence on the diffusion time constant. In comparison with polymer adsorbents, silica based adsorbents have higher values of diffusion coefficients, as well as a more uniform and stable pore structure.

5.1.   Introduction

Dunnewijk et al., [1], who initially proposed Reverse Flow Adsorption (RFA) as a novel concept for the recovery and recycling of homogeneous catalysts, selected polymer adsorbents: Amberlyst A 21 and Polymerbound PPh_3 for adsorption of $CoCl_2$, and Ag^+ loadeded Amberlyst 15 for adsorption of triphenylphosphine [2]. They studied mass transfer properties of these adsorbents [3]. Amberlyst A 21 and Ag^+ loadeded Amberlyst 15 are bi-dispersed particles consisted of the macro- and micropores, while polymerbound PPh_3 is mono-dispersed microporous polymer material. The major drawback of these adsorbents for application in the RFA concept appeared the swelling of the adsorbent and the presence of micropores that caused a high mass transfer resistance. The slow diffusion in the particles and unstable particle properties due to swelling require longer residence times to prevent leaching from the adsorption bed and consequently larger bed volumes [4].

To overcome these limitations silica is selected as a carrier for different functionalized groups. A large surface area, a wide range of pore sizes and a stable structure make silica a potentially ideal carrier. Silica is widely used for adsorption purposes as non-functionalized adsorbent [5], carrier for the immobilization of functional groups [6], or as an already functionalized adsorbent [7]. In our previous work (Chapter 3) [8] a wide range of functionalized silica adsorbents was evaluated, and 2-(2-pyridyl)ethyl-functionalized silica was selected as a promising adsorbent for the reversible adsorption of cobalt (II) chloride. The goal of this chapter is to determine the effective intraparticle diffusion coefficients of cobalt (II) chloride inside the 2-(2-pyridyl)ethyl-functionalized silica by using the Zero Length Column (ZLC) method and compare these results with results obtained in a work of Dunnewijk et al., [3]. Comparison of these adsorbents, selection of the more suitable one and the determined effective diffusion coefficients are essential for further development and design of the RFA concept for the recovery of homogeneous catalysts.

The Zero Length Column (ZLC) method is commonly used to measure the effective intraparticle diffusion of an adsorbate. This technique applies a differential bed where axial dispersion can be neglected. Furthermore ZLC can be operated at such high flow rates that the external mass transfer resistance is eliminated [9] and calculation of the effective intraparticle diffusion becomes straightforward. The ZLC method was developed by Eic and Ruthven to study desorption of strongly adsorbed species such as the aromatic and polyaromatic hydrocarbons over zeolites [10]. This technique is applied both for gaseous [10,11] and liquid systems [9,11]. Several models to determine diffusivity by the ZLC method have been developed. Ruthven and Stapleton applied the linear driving force assumption to describe mass transfer inside particles [12]. This model is extended by more realistic models where the effective intraparticle diffusion is rate controlling [13]. Recently

Dunnewijk et al. [3] developed two models for macroreticular and gel particles where they combine practical advantages of the ZLC method with advantages of a more generalized dynamic model over the column.

This chapter starts first by describing the mathematical model that takes into account the effective intraparticle diffusion as the rate limiting step and is used to determine the effective intraparticle diffusion coefficients. Afterwards, the used materials and the ZLC set-up are discussed. To achieve our objectives ZLC experiments are performed at high flow rates to eliminate both external mass transfer and axial dispersion. The effective diffusion coefficients are calculated from the experimental data by fitting the developed model to the experimental data to determine the effective diffusivity and to investigate the effects of pore size, particle size and concentration of the adsorbate. Temperature effect is excluded in this study, and its investigation will be performed in the continuation of the project. The chapter is concluded with a comparison between polymeric adsorbents and silica adsorbents and final conclusions are drawn on the suitability of adsorbents.

5.2.   Mathematical model

To determine the effective diffusion coefficient of the sorbate inside the particle several assumptions are made:

- 2-(2-pyridyl)ethyl-functionalized silica has a uniform pore size distribution.
- The length of the bed is sufficiently small that change of concentration in the axial direction can be neglected as well as axial dispersion;
- The flow of the sorbate is sufficiently high to neglect the film layer around the particle and therefore the external mass transfer resistance can be neglected (Figure 5.1);
- Due to mezopore silica structure contribution of surface diffusion is significantly smaller compared to intraparticle diffusion [14]. However, both effects are lumped into one effective intraparticle diffusion coefficient;
- The equilibrium between the liquid and the solid phase is described by a Langmuir isotherm.

The mass balance of the adsorbate inside the particle is described by Eq. (5.1):

$$\varepsilon_p \frac{\partial C}{\partial t} + (1-\varepsilon_p)\rho_S \frac{\partial q}{\partial t} = D_{eff}(\frac{\partial^2 C}{\partial r^2} + \frac{2}{r}\frac{\partial C}{\partial r}) \qquad (5.1)$$

where ε_P is porosity of the particle, C is concentration of the solute inside the particle, ρ_S a density of the solid phase, D_{eff} is the effective intraparticle diffusion coefficient, r is radial distance in the particle, and t is time.

The Langmuir isotherm is described by Eq. (5.2):

$$q = \frac{C \cdot b \cdot q_s}{1 + C \cdot b} \tag{5.2}$$

where b is the Langmuir binding constant and q_S is the maximum loading on the adsorbent.
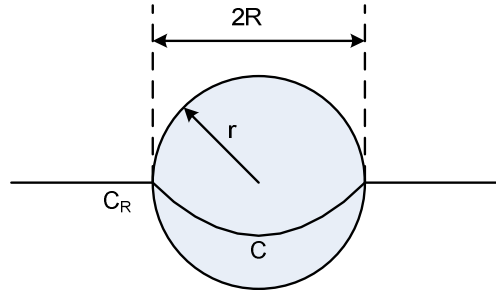
Figure 5.1. Concentration profile inside the silica particle

The initial conditions are:

For $t=0$ and $r=R$: $C=C_0$ and   (5.3)

For $t=0$ and $r<R$: $C=0$ (5.4)

where R is the radius of the particle and C_0 is the initial concentration of the solute.

The boundary conditions are:

For $t \neq 0$ and $r=R$: $C=C(R)$ and due to symmetry   (5.5)

For $t \neq 0$ and $r=0$: $\left(\dfrac{\partial C}{\partial r} \right) = 0$.   (5.6)

The concentration of the solute at the surface of the particle is assumed to be equal to the bulk concentration since the external mass transfer resistance is neglected. This concentration is given by the overall mass balance:

$$\frac{dC(R)}{dt} + \frac{m}{V} \frac{d\overline{q}}{dt} = 0 \tag{5.7}$$

$$\overline{q} = \frac{3}{R^3} \int_0^R r^2 \cdot q \cdot dr \qquad (5.8)$$

where $\overline{q}$ is the averaged loading of the adsorbent, m is the total mass of the adsorbent and V is the total volume of solution in the system.

The effective intraparticle diffusion coefficient is determined by fitting the model to the measured solute concentration profile over time. During fitting the following objective function is minimized:

$$\sum_{t=0}^{n} \left(C_{exp} - C(R) \right)^2 \rightarrow \min \qquad (5.9)$$

where *n* presents the total amount of time needed for the experiment. In parallel the diffusion time constant, K_i [1/s], is calculated as:

$$K_i = \frac{D_{eff}}{R^2} \qquad (5.10)$$

The calculations were performed with the software package MATLAB.

5.3.   Materials

Cobalt(II)chloride (anhydrous) and acetonitrile (MeCN) (99.9%) were obtained from Sigma-Aldrich. 2-(2pyridyl)ethyl-functionalized silica was produced by Silicycle and obtained via Screening Devices. No preliminary treatment of acetonitrile or the silica adsorbent was performed. Three batches of silica were used and their properties are presented in Table 5.1. Batches 2 and 3 are sieved and three fractions are obtained as shown in Table 5.1.

Table 5.1. Properties of functionalized silica

Batch	Pore size [A]	Porosity [-]	Surface area [m²/g]	Particle size [10⁻⁶m]	Sieved fractions [10⁻⁶m]		
					I	II	III
1	60	0.6	500	40-63	-	-	-
2	60	0.6	500	500-1000	500-700	700-810	810-1000
3	90	0.63	500	500-1000	500-700	700-810	810-1000

5.4.   Experimental

5.4.1.   Adsorption equilibrium experiments

All adsorption equilibrium experiments were conducted batch-wise and performed in a shaking bath at a constant temperature of 30ºC. Each isotherm consists of four to five points with the initial concentration of the solutions in the range of 0-8 mol/m^3 of CoCl$_2$. The solvent volume is $40 \cdot 10^{-6}$ m^3 for all experiments and approximately $0.2 \cdot 10^{-3}$ kg of adsorbent was accurately weighted and added. Although preliminary experiments indicated very fast kinetics, 16 hours were chosen to assure equilibrium was reached. The final CoCl$_2$ concentration in the solution was measured with UV-Visible Spectrometer (Cary 300 Conc,Varian). Each adsorption isotherm is presented as: $q = f(C)$ where q_{exp} is calculated by Eq. (5.11). Duplication of a number of experiments showed reproducibility better than 2%.

$$q_{\exp} = \frac{(C_0 - C_e) \cdot V}{m} \qquad (5.11)$$

5.4.2   ZLC set-up

The ZLC set-up was built to investigate the mass transfer properties necessary to determine the intraparticle diffusivity (see Figure 5.2). The set-up consists of a pump (Knauer K-1001), an UV/Vis detector (Knauer K-2600), two heat exchangers (H.E. I and H.E. II), a column (Omnifit), an oven, two thermocouples and two vessels. The pump flows applied were 10, 20, 30, 40 and 50 ml/min. The UV/Vis detector was set at 656 nm to detect cobalt(II)chloride. Heat exchanger H.E.I was used to heat the flow to 30°C which was also the temperature of the oven in which the column was placed. Heat exchanger H.E. II was used to cool the liquid flow to the room temperature. This operating procedure assures that the measurements by the UV/Vis detector were not effected by temperature fluctuations. During the experimental work, the ZLC set-up was used in two modes: non-recycling and recycling. In the non-recycle mode the inlet and the outlet tubes are in two separate vessels. This mode is used for cleaning the set-up and reaching an equilibrium state. In the recycling mode the inlet and the outlet tube of the set-up are placed in the same vessel equipped with a stirrer to assure ideal mixing. This mode is used for all kinetic experiments. The internal column diameter was $15 \cdot 10^{-3}$ m, and the length of the bed was not exceeding $2 \cdot 10^{-3}$ m.
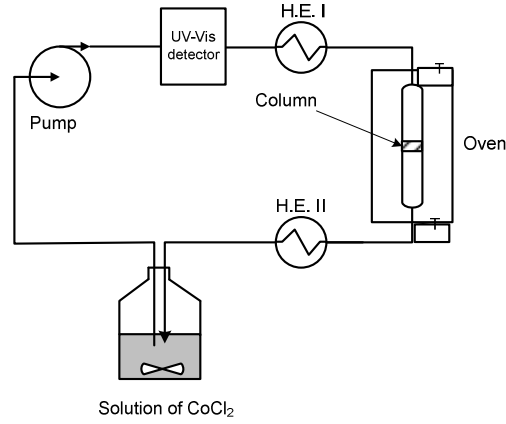
Figure 5.2. Schematic representation of the ZLC set-up in recycle mode

All kinetic experiments are performed according to the same procedure. First the column is loaded with $0.2 \cdot 10^{-3}$ kg of the 2-(2pyridyl)ethyl-functionalized silica. Then the set-up is equilibrated with the pure solvent in the non recycle mode. Afterwards, the pure solvent is replaced with the $40 \cdot 10^{-6}$ m^3 of CoCl$_2$ solution and the set-up is changed to the recycle mode. The UV-Vis signal over time is monitored online and recorded by a PC. Fresh silica is used for each experiment. Regeneration of silica was avoided due to time consumption. Some experiments are repeated including all experimental steps and reproducibility appeared to be within 2.5%.

5.4.2.1 Extra volume

The volume of the ZLC set-up, V_{extra}, is determined prior to start any experiment since the pure residual solvent found in the set-up dilutes the initial concentration of the solute. This volume is determined as a contribution of two volumes: the first, V^*_{extra}, which is the volume of all tubings, a pump cell and UV-Vis detector cell and the second, V_{bed}, porous part of the bed. V^*_{extra} is determined from the difference in CoCl$_2$ concentration measured in the set-up with an empty bed for both recycle and non-recycle mode which is described by Eq. (5.12):

$$C_{NRM} \cdot V = C_{RM} (V + V^*_{extra}) \qquad (5.12)$$

where C_{NRM} is a concentration of solution in the non-recycle mode and C_{RM} is a concentration of solution in the recycle mode (Figure 5.3). The volume of the bed, V_{bed}, is calculated from the Eq. (5.13):

$$V_{bed} = V_{column} - m \cdot \rho_S . \qquad (5.13)$$

The extra volume is determined for four different initial concentrations (0.5, 1, 1.5 and 2 [mol/m^3]) and the averaged extra volume, $V_{extra,}$ is calculated to be $3.48\pm0.06 \cdot 10^{-6}$ m^3.
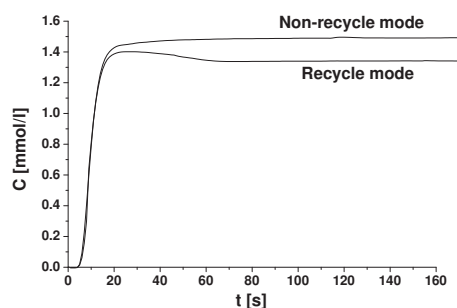
Figure 5.3. Change in concentration caused by the volume of ZLC set-up

5.5   Results and Discussion

5.5.1   *Adsorption isotherms*

In this work we used three batches of 2-(2-pyridyl)ethyl-functionalized silica adsorbents. The number of active sites on each silica is different. Therefore the adsorption isotherm was measured and modelled by the Langmuir isotherm for each batch (Figure 5.4). The coefficients of the Langmuir isotherm (Eq. (5.2)), b and q_S, are given in Table 2. As shown, the bonding strength, b, for each batch is the same within the experimental error and the fitting. This is expected since there is always the same interaction between the adsorbate, CoCl$_2$, and the pyridine group on the silica surface. However, the number of sites differs for each batch. To minimize error in the fitted diffusion coefficient for each batch the corresponding b and q_S values are used.
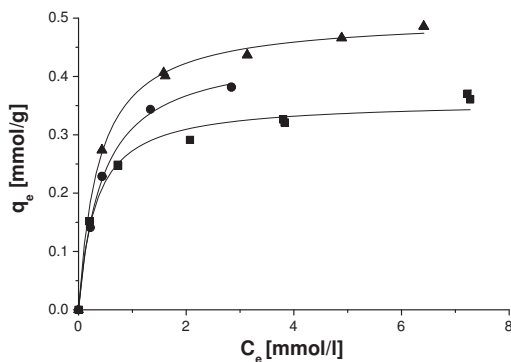
Figure 5.4. Equilibrium isotherms of CoCl2 on 2-(2-pyridyl)-functionalized silica at 30ºC for three different batches: full squares (■): Batch 1; full circles (●): Batch 2; full triangles(▲): Batch 3

Table 5.2. Coefficients of the Langmuir isotherms used to model the adsorption equilibrium of three different functionalized silica batches

	b [m^3/mol]	q_S [mol/kg]
Batch 1	3.20	0.357
Batch 2	2.28	0.447
Batch 3	2.68	0.501

5.5.2 Influence of the liquid flow

The adsorption mass transfer is a function of the external and the internal mass transfer resistance. At sufficiently high flow rates contribution of the external mass transfer resistance can be neglected, and the change of concentration over time is determined only by effective intraparticle diffusion. Therefore, the first step was to monitor the change of the cobalt(II) chloride concentration over time as a function of the volumetric flow rate. Figure 5.5 shows the results for three batches: Batch 1, Batch 2/Fraction I and Batch 3/Fraction I.

(a) (b)

(c)
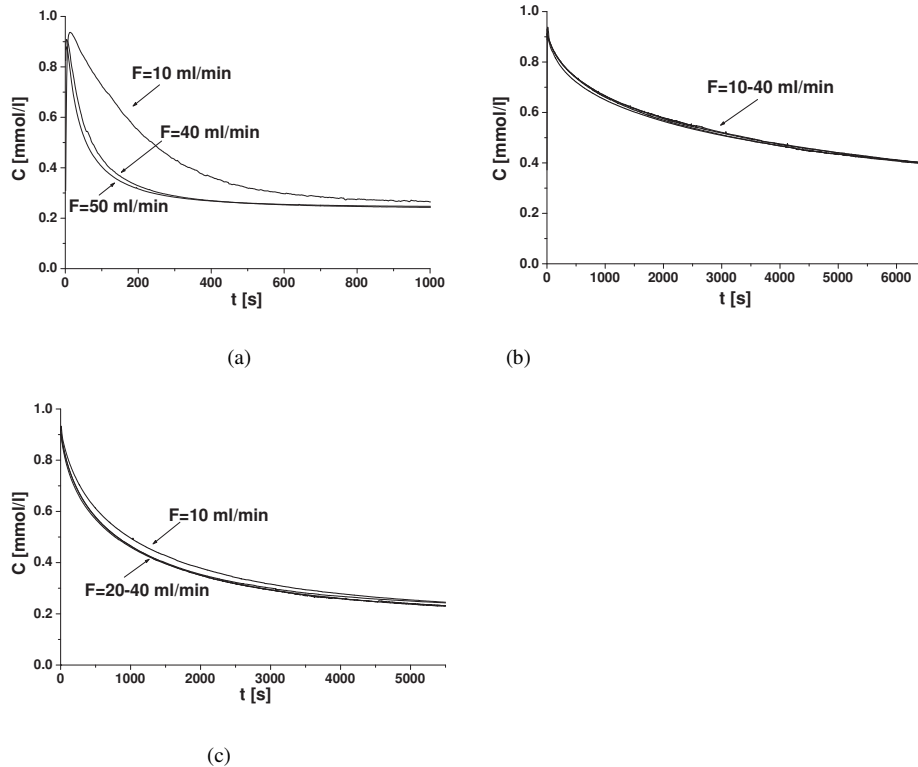
Figure 5.5. Cobalt(II)chloride's concentration in the liquid phase at 30ºC as a function of time during adsorption on: (a) Batch 1 (b)Batch 2/Fraction I (c) Batch 3/Fraction I at different volumetric flows

77

Since the external mass transfer is also inversely proportional to the particle size [14], the influence of the external mass transfer is best shown for Batch 1 since it contains the smallest particles. Figure 5.5a clearly shows that the difference between 40 and 50 ml/min is negligible. Since the maximum volumetric flow of the pump is 50 [ml/min], this flow rate was selected to determine the effective intraparticle diffusion coefficient for Batch 1. For, Batch 2/Fraction I (Figure 5.5b) and Batch 3/Fraction I (Figure 5.5c), the influence of external mass transfer at flow rate of 40 ml/min is negligible. The fitted effective intraparticle diffusivity was based on these data. Fractions II and III of Batch 2 were also tested (see the influence of the particle size), and also in these experiments influence of the external mass transfer is not noticed for volumetric flows of 10 and 40 [ml/min].

5.5.3   Influence of the particle size

The influence of particle size on the internal mass transfer rate is shown by adsorbing cobalt(II)chloride on four different ranges of silica's particle sizes: 40-63, 500-710, 710-800 and 800-1000 [10^{-6} m]. Figure 5.6 shows both experimental and model results of the CoCl$_2$ concentration change over time. Table 5.3 gives both the fitted pore diffusion coefficients and diffusion time constants for all four particle sizes. As expected particle size does not have any influence on the effective pore diffusion coefficient, in contrast to the diffusion time constant, K_i, used to describe the internal mass transfer rate. The smaller particle sizes are preferable since they increase the internal mass transfer rate. On the other hand, handling of the smaller particles, such as particles with 40-63 [10^{-6} m] diameter, will certainly lead to high pressure drops inside the adsorption columns. Therefore a balance between required pressure drop within an adsorption bed and mass transfer rate in a bed is needed.
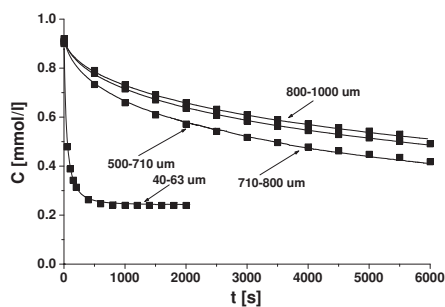
Figure 5.6. The experimental (solid line) and the model (full square) results of CoCl$_2$'s concentration changes over time at 30ºC during its adsorption on four different particle ranges of 2-(2-pyridyl)-functionalized silica

Table 5.3. The pore diffusion coefficient and the reciprocal time constant for four different particle sizes and two pore sizes

Batch	1		2		3
Pore size [Å]	60		60		90
Particle size [10^{-6} m]	40-63	500-710	710-800	800-1000	500-710
D_{eff} [m^2/s]	$1.05 \cdot 10^{-10}$	$1.17 \cdot 10^{-10}$	$1.15 \cdot 10^{-10}$	$1.22 \cdot 10^{-10}$	$3.48 \cdot 10^{-10}$
K_i [1/s]	$2.63 \cdot 10^{-1}$	$2.13 \cdot 10^{-3}$	$1.35 \cdot 10^{-3}$	$1.03 \cdot 10^{-3}$	$6.34 \cdot 10^{-3}$

5.5.4 Influence of the pore size

To investigate the effect of pore size on diffusivity two silica adsorbents with different pore sizes with a mean diameter of 60Å and 90Å (respectively Batch 2 and 3) are selected. Figure 5.7 shows experimental data and model results of $CoCl_2$ concentration change over time for the selected silica. Results clearly show the faster concentration change of $CoCl_2$ for a larger pore diameter. The results of the fitted effective intraparticle diffusion coefficients and the diffusion time constants are shown in Table 5.3. The differences in the effective intraparticle diffusion coefficients can be partially originate from different intraparticle porosity and better accessibility inside the pores.
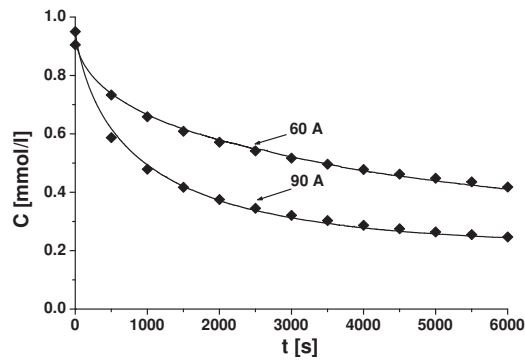
Figure 5.7. The experimental (solid line) and the model (full diamonds) results of the $CoCl_2$ concentration change over time at 30ºC for silica with a 60Å and 90Å pore size

5.5.5 Influence of the adsorbate initial concentration

Since it is reported in the literature [15] that concentration can have an influence on the kinetic properties, it is decided to check the influence of the initial $CoCl_2$ concentration. The selected concentration range is 1-2 [mol/m^3]. This very narrow range is of our interest. The experimental data and model results are shown in Figure 5.8. The pore diffusion coefficients are given in Table 5.4. As it is observed concentration of the $CoCl_2$

solution in acetonitrile does not have an effect on the value of effective pore diffusion coefficient. Therefore this effect can be disregarded in further modelling of the adsorption process.
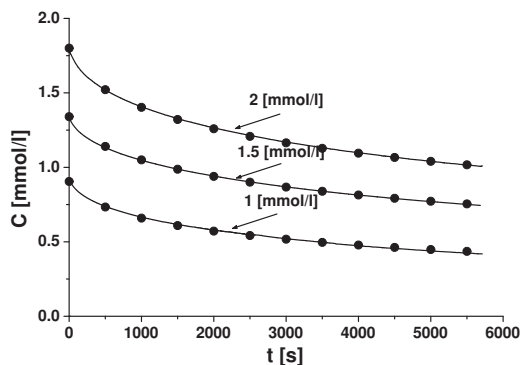
Figure 5.8. The experimental (solid line) and the model (full circles) results of the CoCl$_2$ concentration changes over the time at 30ºC for three different initial concentrations

Table 5.4. The pore diffusion coefficients for three different initial concentrations

C_0 [mol/m^3]	1	1.5	2
D_{eff} [m^2/s]	$1.17 \cdot 10^{-10}$	$0.95 \cdot 10^{-10}$	$1.2 \cdot 10^{-10}$

5.5.6 Comparison between polymeric and silica based adsorbents

Diffusion coefficients for the polymeric adsorbents used in the work of Dunnewijk et al. [3] and for functionalized silica adsorbents studied in this work are given in Table 5.5. Nomenclature for bi-dispersed Amberlyst A 21 diffusion coefficients is D_a and D_i corresponding to the macro- and micro- pore intraparticle diffusivity respectively, while for mono-dispersed particles D_{eff} is kept. Diffusion coefficients for both pore diameters (60 Å and 90 Å) of mesoporous silica are in the same range as diffusion coefficient for macropores, D_a, of the polymeric adsorbent Amberlyst A 21. Micropore diffusion coefficient present in Amberlyst A 21 and Polymerbound PPh3 are significantly lower compared to silica's diffusion coefficients. These very low diffusion coefficients lead to slow mass transfer and longer residence time in the adsorption column. Swelling of Amberlyst A 21 and Polymerbound PPh3 caused by solvent penetration is also reported by Dunnewijk et al [3]. Therefore it is evident that silica based adsorbents have preferred structure and mass transfer properties compared to polymer ones. In our previous work [8] it is shown that 2-(2-pyridyl)-functionalized silica has intermediate binding strength for recovery of CoCl$_2$ which is essential for the RFA application. Amberlyst A21 has a very

strong and Polymerbound PPh3 a very weak binding strength [2] for recovery of $CoCl_2$. Therefore they cannot be considered as an optional type of adsorbents for implementation in the RFA.

Table 5.5. Comparison of intraparticle diffusion coefficients between polymeric [5] and silica based adsorbents

Amberlyst A 21 [5]		Polymerbound PPh₃ [5]	2-(2-pyridyl)ethyl-functionalized silica	
D_a [m²/s]	D_i [m²/s]	D_P [m²/s]	D_{eff} (60Å) [m²/s]	D_{eff} (90Å) [m²/s]
$1.25 \cdot 10^{-10}$	$8.22 \cdot 10^{-20}$	$7.14 \cdot 10^{-16}$	$1.17 \cdot 10^{-10}$	$3.48 \cdot 10^{-10}$

5.6 Conclusion

In this paper the effective intraparticle diffusion coefficient of $CoCl_2$ in mesoporous 2-(2-pyridyl)-functionalized silica is determined by using the Zero Length Column method. At sufficiently high flow rates contribution of the external mass transfer resistance is neglected. A mathematical model which is developed to calculate the effective intraparticle diffusivity for uniform pore distribution silica describes well the adsorption of $CoCl_2$ over time. The values of the effective diffusion coefficient do not depend on the particle size but only on pore size:

- pore size of 60Å: D_{eff}=$1.17 \cdot 10^{-10}$m²/s,
- pore size of 90Å: D_{eff}=$3.48 \cdot 10^{-10}$m²/s.

Particles with 90Å pore size should be selected for further research because they provide faster diffusion inside particles, and still have equivalent surface area as the one with 60 Å pore size. Since the effective pore diffusion coefficient does not depend on the particle size, but the internal mass transfer rate does, it is recommended to use smaller particle sizes for the adsorption bed. It was also shown that the effective pore diffusion coefficient does not depend on the concentration range (1-2 [mol/m³]). Due to uniform pore structure and high effective intraparticle diffusion coefficients silica adsorbents are promising adsorbents for the Reverse Flow Adsorption application.

5.7 List of symbols

b-	Langmuir adsorption constant	[m³/mol]
C-	Adsorbate concentration	[mol/ m³]
C_0-	Initial adsorbate concentration	[mol/ m³]
C_e-	Equilibrium adsorbate concentration	[mol/ m³]
C_{NRM}-	Adsorbate concentration with a non-recycle mode	[mol/ m³]
C_{RM}-	Adsorbate concentration with a recycle mode	[mol/ m³]
C_{exp}-	Experimental adsorbate concentration	[mol/ m³]
D_a-	Macropore diffusion coefficient	[m²/s]

D_i-	Micropore diffusion coefficient	[m^2/s]
D_{eff}-	Effective intraparticle diffusion coefficient	[m^2/s]
F-	Volumetric flow	[ml/min]
K_i-	Diffusion time constant	[1/s]
m-	Mass of adsorbent	[kg]
q-	Loading of the adsorbent	[mol/kg]
$\overline{q}$ -	Averaged loading of the adsorbent	[mol/kg]
q_{exp}-	Experimentally determined loading of the adsorbent	[mol/kg]
q_s-	Maximal loading of the adsorbent	[mol/kg]
r-	Radial position in the particle	[m]
R-	Radius of the particle	[m]
ρ_S-	Density of the solid	[kg/m^3]
t-	Time	[s]
V-	Volume of solution	[m^3]
V_{bed}-	Volume of the bed in the ZLC set-up	[m^3]
V_{extra}-	Volume of the ZLC set-up	[m^3]
V^*_{extra}-	Volume of the ZLC set-up with empty bed	[m^3]

5.8   Reference:

[1]   Dunnewijk J., H. Bosch, A.B. de Haan, Sep. Purif. Technol. 40 (3), (2004) 317-320

[2]   Dunnewijk J., H. Bosch, A.B. de Haan, Adsorption, 11, (2005) 521-526

[3]   Dunnewijk J., H. Bosch, A.B. de Haan, Chem. Eng. Sci. 61, (2006) 4813-4826

[4]   Dunnewijk J., Reverse Flow Adsorption Technology for Homogeneous Catalyst Recycling, thesis, University of Twente, (2006)

[5]   Aristov Y. I., M. M. Tokarev, A. Freni, I. S. Glaznev, G. Restuccia, Micropor Mesopor Mat, 96, (2006) 65–71

[6]   Li F., P. Du, W. Chen, S. Zhang, Anal Chim Acta, 585, (2007) 211–218

[7]   Qu R., Y. Niu, C. Sun, C. Ji, C. Wang, G. Cheng, Micropor Mesopor Mat, 97, (2006) 58–65

[8]   Djekić T., A.G.J. van der Ham, A.B. de Haan, J Chrom A, 11420, (2007) 32-38

[9]   Rodriguez J.F., J.L. Valverde, A.E. Rodrigues, Ind. Eng.Chem. Res., 37, (1998) 2020-2028

[10]   Eic M., D.M. Ruthven, Zeolites, 8, 41 (1988)

[11]   Silva J.A.C., A.E. Rodrigues, Ind. Eng.Chem. Res., 36, (1997) 493-500

[12]   Ruthven D.M., P. Stapleton, Chem. Eng. Sci., 48,(1), (1993) 89-98

[13]   Brandani S., D.M.Ruthven, Chem. Eng. Sci., 50, (13), (1995) 2055-2059

[14]   Guiochon, G., Shirazi, S.G., Katti, A.M., Academic Press, Elsevier, Amsterdam, 2006, p.295-301

[15]   Serarols J., J. Poch, I. Villaescusa, React. Funct. Polym. **48**, (2001) 53-63

[16]   D. Nicholls, Complexes and First –Row Transition Elements, The Whitefriars press Ltd., London and Tonbridge,1974

5.9   Appendix

The good fit of experimental and model data, previously discussed, could not be achieved by using Langmuir isotherm coefficients obtained in Chapter 4. To understand and solve the problem, $CoCl_2$ adsorption equilibrium experiments were performed on 2-(2-pyridyl)-ethyl functionalized silica with two different volume to mass (V/m) ratios as given in Experimental parts of Chapters 4 and 5. In the equilibrium adsorption experiments discussed in part Experimental (Chapter 4) the volume to mass ratio was 50 ml/g, while in Experimental (Chapter 5) this ratio was 200 ml/g. By comparing the equilibrium data for these two ratios (Figure A.5.1) we have noticed a difference in the shape of the adsorption isotherms. $CoCl_2$ adsorption where V/m ratio is 200 ml/g has slightly stronger adsorption behaviour compared to $CoCl_2$ adsorption where V/m ratio was 50 ml/g. This can be explained with Figure A.5.2 where UV-Vis spectra are given for:

- $CoCl_2$ solution in acetonitrile before adsorption,
- $CoCl_2$ solution in acetonitrile after adsorption where V/m ratio was 200 ml/g,
- $CoCl_2$ solution in acetonitrile after adsorption where V/m ratio was 50 ml/g.

The shape of $CoCl_2$'s UV-Vis spectra before adsorption and after adsorption with a V/m ratio of 200 ml/g are matching: the number and the shape of peaks are equivalent. On the other hand, spectrum of $CoCl_2$ after adsorption with a V/m ratio of 50 ml/g differs from the previous two by shape and number of peaks. Possible explanation is that $CoCl_2$ in solution forms diverse species [16] with the certain equilibria between them. There is as well competitive adsorption of these forms where the adsorption strength of these forms is different. This results in distinct profiles of the adsorption isotherms. This effect is not noticed for the same V/m ratio and different initial $CoCl_2$ concentration.
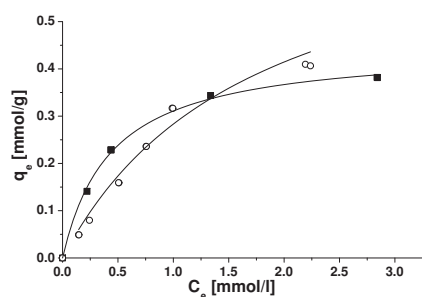
Figure A.5.1. Adsorption equilibrium data for $CoCl_2$ adsorption on 2-(2-pyridyl)ethyl-functionalized silica where full squares (▪) are for V/m ratio of 200 ml/g and empty circles (○)are for V/m ratio of 50 ml/g
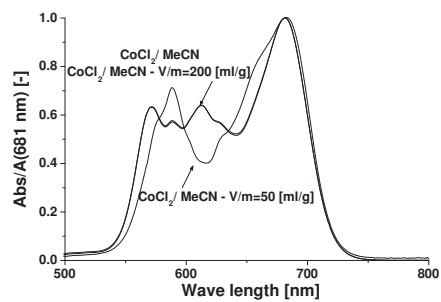
Figure A.5.2. UV-Vis spectra for CoCl$_2$ solution in acetonitrile before adsorption and after adsorption for two different V/m ratios

Silica adsorbent design and process evaluation for recovery of homogeneous catalysts by Reverse Flow Adsorption

Abstract

The goal of this work is to demonstrate the stability of the reverse flow adsorption process for recovery of homogeneous catalysts and to study the influence of catalyst and adsorbent parameters for optimizing the RFA process operation. Data used in simulations were obtained from our previous work. Two models are developed to describe the reversible adsorption. One which describes the adsorption of the metal containing species and second model that describes adsorption of the free ligand. It is shown that a stable operation is reached without leaching of metal. The RFA process can be applied for wide ranges of catalyst stability constants (10^0-10^{12} $(dm^3/mol)^2$) and it is specially applicable for the recovery of homogeneous catalysts that have a lower metal concentration. Characteristics of the adsorbent (β_M=0.8, α=1850, Pe_P=376.4, d_p=100 μm and ε_b=0.5)) and the column (Bo=1.74·10^4 and N=6.6·10^4) necessary for a sharp concentration profile inside the bed are determined. Simulation of the recovery of rhodium catalyst in the BASF hydroformylation process required a total adsorption bed volume for the recovery of metal specie of 6% of the reactor volume.

6.1 Introduction

The reverse flow concept is mainly used in the field of reactor engineering, where Boreskov and Matros [1,2] were among the first researchers working on reverse flow reactors. Since then many scientists contributed to this field [3-5]. Beside its use in reactor design, the reverse flow concept was also used in electrokinetic chromatography [6] and nano- and ultra-filtration [7,8].

Reverse flow adsorption (RFA) is a novel concept for the recovery of homogenous catalysts that combines separation by adsorption with reverse flow technology [9]. In reverse flow adsorption, the feed (reactants, homogeneous catalyst and solvent) periodically changes its flow direction in the process. The homogeneous catalyst is separated from the reaction mixture by adsorption downstream from the reactor (Figure 6.1). In the subsequent desorption step the homogenous catalyst is recovered and recycled to the reactor. This approach should overcome drawbacks of present recovery methods, such as leaching and deactivation of the catalyst [10]. Leaching can be prevented by designing the RFA process in a way that all catalyst species are kept inside the beds. Due to mild adsorption and desorption conditions deactivation of the catalyst is likely to be prevented.
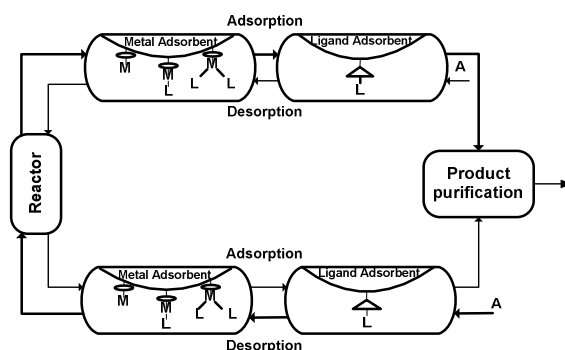
Figure 6.1. Reverse Flow Adsorption concept

Since a homogeneous catalyst is found in different complex forms [11] we propose to recover the catalyst using a two-step adsorption approach: separately adsorbing the metal containing species from the excess of ligand. The metal containing catalyst species are adsorbed from the reactor effluent in the first adsorption bed, whereas the remaining free ligand is adsorbed in the second adsorption bed. For this reason four adsorption beds are needed to adsorb homogenous catalysts by the two step approach (Figure 6.1). Dunnewijk et al, who worked on the RFA concept [12], also applied the two-step adsorption approach. Their focus was on separate adsorption of the free metal centre

and the free ligand by neglecting any interaction between them. Bidispersed polymer type and gel type adsorbents were selected to recover the free metal and the free ligand, but this material was prone to swelling and showed a very slow mass transfer [13]. Additionally, the selected adsorbents were mostly either very strong or rather weak for reversible adsorption of the homogeneous catalysts species [14]. Dunnewijk [12] also developed a model to simulate the RFA process which consisted of two adsorption columns and a CIST reactor. He showed stability of the RFA process with the data obtained from ion-exchange experiments neglecting micropore diffusion. The drawbacks of polymeric adsorbents directed our research to functionalized silica adsorbents which have a mesoporous and rigid structure. In our previous work we showed promising adsorbents [15, 16] with intermediate binding strength and with sufficiently high mass transfer coefficients [17].

The objective of this work is to demonstrate that stable operation of the reverse flow adsorption process with the data obtained from functionalized silica adsorbents [15-17] and to study the influence of adsorbent and process parameters to improve reverse flow adsorption operation. Design and study of the reactor is not included in this study. This paper proceeds with the mathematical models developed to describe reversible adsorption of the complex species. One model describes the reversible adsorption of the metal containing species and other model describes adsorption of the free ligand. The first model is more complex because it contains competitive adsorption of different complex forms which are interconnected via a chemical equilibrium in solution [11]. Therefore, stability of the process is initially shown by monitoring the total metal concentration (sum of all metal containing species) profile during continuous adsorption and desorption for 500 cycles. Furthermore, the influences of the adsorbent and process parameters are discussed as well as the influence of different catalyst characteristics such as concentration, stability constants or ligand to metal ratio. These effects are studied with our first model that describes the adsorption of the metal containing species. Their optimized values are afterwards applied for the ligand bed. Finally, the application of the RFA is evaluated for the BASF hydroformylation process [18]. Several adsorption bed designs are evaluated to obtain the maximal operation time.

6.2 Dynamic models for the reversible adsorption of the catalyst species

To simulate the Reverse Flow Adsorption process two models are developed: one for adsorption of the metal containing species, and the other for adsorption of the free ligand. Similarities and differences between those two models are listed in Table 6.1. Both models are written in their dimensionless forms and the nomenclature is given in the Symbol section.

Table 6.1. Similarities and differences between the model for adsorption of the metal containing species and the model for adsorption of the free ligand

Model for adsorption of metal containing species	Model for adsorption of free ligand
Similarity	
Dimensionless	
Negligible external mass transfer resistance	
Internal mass transfer described by linear driving force model	
Diffusion of all species is the same	
Negligible radial concentration gradient	
Constant bed porosity (exclusion of channelling)	
Constant velocity across the cross-section	
Preloaded columns	
Same process parameters	
Difference	
Stability constants- equilibrium is infinitely fast	-
Competitive Langmuir isotherm	Langmuir isotherm for single component
Different adsorbent parameters	
Different bed parameters	

In the previous work of Dunnewijk [12] it is shown that half of the adsorption bed used in the RFA process should be preloaded with the adsorbing specie to allow broadening of the concentration front during its reversible adsorption and desorption. This prerequisite is obtained in our simulations by setting proper initial conditions (see Section 6.2.1.5.). Stability of the process and optimization of the adsorbent/ process parameters are shown by simulating reversible adsorption of the catalyst species in just one bed. A change of concentration in the bed is monitored over time and in axial direction.

6.2.1   Model for adsorption of the metal containing species
6.2.1.1   Stability constants

In this model it is assumed that the homogeneous catalyst is a complex compound consisting of one metal centre and two ligands. Dissolved in a solvent a homogenous catalyst forms different species:

$$M + 2L \underset{\longleftarrow}{\overset{K_{S1}}{\longrightarrow}} ML + L \underset{\longleftarrow}{\overset{K_{S2}}{\longrightarrow}} ML_2 . \tag{6.1}$$
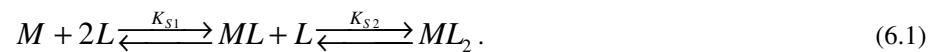
The ratio of different species at equilibrium is described by stability constants presented as:

$$\kappa_{S1} = \frac{x_{ML}(\chi,\tau)}{x_M(\chi,\tau) \cdot x_L(\chi,\tau)} \tag{6.2}$$

$$\kappa_{S2} = \frac{x_{ML_2}(\chi,\tau)}{x_{ML}(\chi,\tau) \cdot x_L(\chi,\tau)} . \tag{6.3}$$

6.2.1.2 Competitive adsorption isotherm

In our previous work [13] we have shown that all metal containing species (M, ML and ML$_2$) are adsorbing on one active site of the adsorbent and their adsorption can be described with the competitive Langmuir isotherm:

$$\Gamma_M(z,t) = \frac{\beta_M \cdot x_M(\chi,\tau)}{1 + \beta_M \cdot x_M(\chi,\tau) + \beta_{ML} \cdot x_{ML}(\chi,\tau) + \beta_{ML_2} \cdot x_{ML_2}(\chi,\tau)} \tag{6.4}$$

Equivalent equations can be written for ML and ML$_2$. The total amount of metal adsorbed is described as:

$$\Gamma_{M_t}(\chi,\tau) = \Gamma_M(\chi,\tau) + \Gamma_{ML}(\chi,\tau) + \Gamma_{ML_2}(\chi,\tau) \tag{6.5}$$

6.2.1.3 Mass balance for the liquid phase in adsorption bed

The dimensionless mass balance for the liquid phase is given for the total amounts of metal in the system, M$_t$:

$$\frac{1}{\varepsilon_b}\frac{\partial x_{M_t}(\chi,\tau)}{\partial \chi} + \frac{\partial x_{M_t}(\chi,\tau)}{\partial \tau} + \frac{1-\varepsilon_b}{\varepsilon_b}\alpha\frac{\partial \overline{\Gamma}_{M_t}(\chi,\tau)}{\partial \tau} = \frac{1}{Bo}\frac{\partial^2 x_{M_t}(\chi,\tau)}{\partial \chi^2} \tag{6.6}$$

$$x_{M_t}(\chi,\tau) = x_M(\chi,\tau) + x_{ML}(\chi,\tau) + x_{ML_2}(\chi,\tau) , \tag{6.7}$$

and ligand L$_t$:

$$\frac{1}{\varepsilon_b}\frac{\partial x_{L_t}(\chi,\tau)}{\partial \chi} + \frac{\partial x_{L_t}(\chi,\tau)}{\partial \tau} = \frac{1}{Bo}\frac{\partial^2 x_{L_t}(\chi,\tau)}{\partial \chi^2} \tag{6.8}$$

$$r \cdot x_{L_t}(\chi,\tau) = r \cdot x_L(\chi,\tau) + x_{ML}(\chi,\tau) + 2 \cdot x_{ML_2}(\chi,\tau) \tag{6.9}$$

which applies for every time unit and every axial position. Mass balances for the other complex forms are not necessary since they are already coupled with the previous equations (6.2) and (6.3).

r, α, and Bo are dimensionless parameters found in equations (6.6)-(6.9). r is the concentration ratio of total initial amount of ligand over total initial amount of metal:

$$r = \frac{[L_t]}{[M_t]},$$
(6.10)

α gives the ratio of the maximum adsorbent capacity and the initial total metal concentration in the liquid:

$$\alpha = \frac{\rho_S \cdot q_S}{[M_t]}$$
(6.11)

and Bo is the Bodenstein number which gives the ratio convection over axial diffusion:

$$Bo = \frac{u \cdot L}{D_{ax}}$$
(6.12)

6.2.1.4 Internal mass transfer

The internal mass transfer is described with the linear driving force model [19]. The dimensionless form of the internal mass transfer is given as:

$$\frac{\partial \bar{\Gamma}_M(\chi,\tau)}{\partial \tau} = \frac{60N}{Pe_p}(\Gamma_M(\chi,\tau) - \bar{\Gamma}_M(\chi,\tau))$$
(6.13)

for the M specie, and equivalent equation can be written as well for ML and ML$_2$. N is the number of particles over the axial direction:

$$N = \frac{L}{d_p},$$
(6.14)

and Pe_P is Peclet number for the particle [19]:

$$Pe_p = \frac{u \cdot d_p}{D_{eff}}.$$
(6.15)

The total loading for all adsorbed species can be written as:

$$\bar{\Gamma}_{M_t}(\chi,\tau) = \bar{\Gamma}_M(\chi,\tau) + \bar{\Gamma}_{ML}(\chi,\tau) + \bar{\Gamma}_{ML_2}(\chi,\tau).$$ (6.16)

6.2.1.5   Initial and boundary conditions

In our simulations half of the adsorption column is initially preloaded to allow broadening of the concentration front during reversible adsorption/desorption cycles. Therefore, the initial conditions used in the model for the first half of column that is preloaded with the catalyst are:

For $\chi = 0\ldots0.5^{-}$ and τ=0 : $x_{M_t}(\chi,\tau) = 1$

$$x_{L_t}(\chi,\tau) = 1$$

$$\bar{\Gamma}_M(\chi,\tau) = \Gamma_M(\chi,\tau)$$

$$\bar{\Gamma}_{ML}(\chi,\tau) = \Gamma_{ML}(\chi,\tau)$$

$$\bar{\Gamma}_{ML_2}(\chi,\tau) = \Gamma_{ML_2}(\chi,\tau).$$ (6.17)

Since the second half of the bed is set to be empty, the initial conditions for this part are:

For $\chi = 0.5\ldots1$ and τ=0: $x_{M_t}(\chi,\tau) = 0$

$$x_{L_t}(\chi,\tau) = 0$$

$$\bar{\Gamma}_M(\chi,\tau) = 0$$

$$\bar{\Gamma}_{ML}(\chi,\tau) = 0$$

$$\bar{\Gamma}_{ML_2}(\chi,\tau) = 0.$$ (6.18)

Boundary conditions of the bed are set due to symmetry as:

For χ=0 and χ=1:
$$\frac{\partial x_{M_t}(\chi,\tau)}{\partial \chi} = 0$$ (6.19)

$$\frac{\partial x_{L_t}(\chi,\tau)}{\partial \chi} = 0$$ (6.20)

6.2.2   Model for adsorption of the free ligand

In the second adsorption bed only the free ligand is adsorbed. Therefore the stability constant equations are not needed here. Equations used in this model are just listed and no additional explanations are added except that L is the index for the ligand.

6.2.2.1 Langmuir adsorption isotherm for single component

$$\Gamma_L(\chi,\tau) = \frac{\beta_L \cdot x_L(\chi,\tau)}{1 + \beta_L \cdot x_L(\chi,\tau)}$$ (6.21)

6.2.2.2 Mass balance for the liquid phase in adsorption bed

$$\frac{1}{\varepsilon_b}\frac{\partial x_L(\chi,\tau)}{\partial \chi} + \frac{\partial x_L(\chi,\tau)}{\partial \tau} + \frac{1-\varepsilon_b}{\varepsilon_b}\alpha\frac{\partial \overline{\Gamma}_L(\chi,\tau)}{\partial \tau} = \frac{1}{Bo}\frac{\partial^2 x_L(\chi,\tau)}{\partial \chi^2}$$ (6.22)

6.2.2.3 Internal mass transfer

$$\frac{\partial \overline{\Gamma}_L(\chi,\tau)}{\partial \tau} = \frac{60N}{Pe_p}(\Gamma_L(\chi,\tau) - \overline{\Gamma}_L(\chi,\tau))$$ (6.23)

6.2.2.4 Initial and boundary conditions

Initial and boundary conditions are the same as for the metal adsorption column, except that in this case only the free ligand is adsorbing.

6.3 Results and Discussion

6.3.1 Stability of the metal adsorbing column

Data selected to show the stability of the reversible adsorption and desorption are given in Table 6.2. The half time cycle constant is set as well as the ligand/metal ratio and bed porosities. Catalyst and adsorbent parameters values in the range that are obtained from our experimental research for $CoCl_2$ adsorption on 2-(2-pyridyl)-ethyl functionalized silica and stability constant measurements [11, 15, 17]. Solvent parameters necessary to estimate Reynolds and Bodestein numbers are taken for acetonitrile. 90 m^3 is taken as the reactor volume, and the adsorption bed is selected to be 10% of the reactor volume with the length to diameter ratio of 5. Therefore length of the column L is set to be 6.6 m and column diameter of D_C=1.32 m. N is calculated from equation (6.14) where the particle diameter, d_p, is set to be 10^{-4} m. The Peclet number is calculated from equation (6.15) where D_{eff} is taken from our previous research D_{eff}=1.95·10^{-10}m^2/s [17], and the velocity is recalculated for a given flow of F= 5·10^{-3} m^3/s and column diameter, D_C. In our previous work [17] we have shown that for a Reynold number larger than 0.1 the external mass transfer resistance can be neglected. The Bodenstein number is calculated as [19]:

$$Bo = 0.2 \frac{N}{\varepsilon_b}. \tag{6.24}$$

In our initial simulations it is shown that for Bodenstein numbers larger than $1.74 \cdot 10^4$ axial dispersion can be neglected.

Table 6.2. Input base case parameters for the reversible adsorption/desorption of the metal containing species

Parameter	Value	Ref
Catalyst parameters		
R	2	[-]
K_1	1	[10]
κ_2	1	[10]
Adsorbent parameters		
β_M	0.8	[14]
β_{ML}	0.4	[14]
β_{ML2}	0.3	[14]
A	925	[14]
Pe_P	1882	[16]
Process parameters		
$\tau_{1/2}$	5	[-]
ε_b	0.76	[-]
N	$6.6 \cdot 10^4$	[-]
Re	0.44	[-]
Bo	$1.74 \cdot 10^4$	[-]

Reversible adsorption/desorption inside one bed is simulated to show stability of the process as well as no concentration gradient at the entry (z/L=0) and the exit (z/L=1) of the column. Initially, half of the column (z/L=0..0.5) is preloaded with catalyst species. Then, the flow through the column is simulated and complex species are adsorbed for a period of $\tau_{1/2}$. Afterwards, the flow direction is reversed and desorption occurs for the same period, $\tau_{1/2}$. The first cycle is ended. This process is repeated and monitored for 500 cycles.

The total metal concentration profiles in the liquid phase are given after adsorption (Figure 6.2a) and subsequently desorption (Figure 6.2b) for a selection of cycles (1, 100, 200, 300, 400 and 500). The figures show that the concentration profile broadens over time due to unfavourable desorption, and the limiting uptake rate during the adsorption. However, the broadening of the concentration profile decreases over time which finally results in a stable profile. The concentration profile of all metal species in the liquid phase,

x_{Mt}, at the entry and the exit of the column are given correspondingly in Figures 6.3a and 6.3b. No decrease of the metal concentration is observed at the entry ($z/L=0$) (Figure 6.3a), as well as no leaching at the end of the column ($z/L=1$) (Figure 6.3b). Both are essential for application of the RFA process.

(a)   (b)
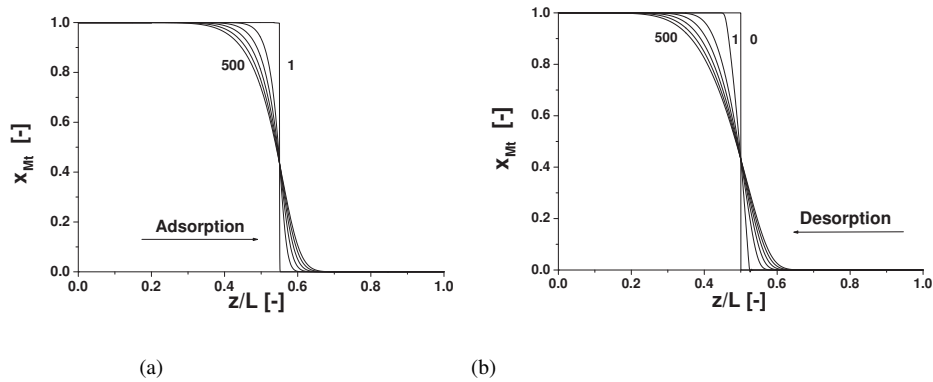
Figure 6.**2.** The total metal concentration profile in the liquid phase after the selected number of cycles (1, 100, 200, 300, 400 and 500) for: (a) adsorption and (b) desorption

(a)   (b)
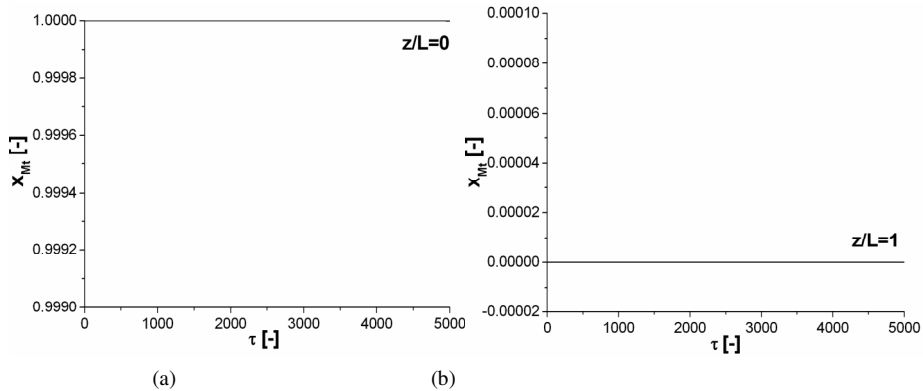
Figure 6.3. The total metal concentration profile in the liquid phase over time at: (a) $z/L=0$ and (b) $z/L=1$

6.3.2   Influence of catalyst parameters

The first step in designing a RFA process is defining the catalyst properties such as catalyst concentration, stability constants and initial ligand/metal ratio. The catalyst concentration depends on each application. Therefore the range of catalyst concentrations for which RFA can be applied should be investigated as well as how the concentration influences the concentration profile. Also, depending on the type of metal, ligand, solvent and ligand-metal ratio different distributions of the complex species occurs. Since the complex species (e.g. M, ML, ML_2) have different binding constants it is important to

know the catalyst properties to be able to design an affinity adsorbent for the recovery of the catalyst species.

Catalyst properties are specific for each catalytic reaction and cannot be varied to assist a design of the adsorption columns used in the RFA. Therefore, in the following paragraphs we will discuss what kind of effects are observed by altering the above mentioned catalyst properties. These observations will help to design an affinity adsorbents and the corresponding adsorption column.

6.3.2.1   Metal inlet concentration

The concentration of the metal used in homogeneous catalysis depends on its application. For example, typical catalyst's concentrations in hydroformylation processes are between 0.1 mmol/l and 1.5 mmol/l [20].

Figure 6.4. Influence of the metal inlet concentration on the total metal concentration profile in the liquid phase after adsorption in the 500th cycle

The total metal concentration influences both the distribution of the complex forms, M, ML and ML_2 [11], and the value of α (Eq. 6.11). In Figure 6.4 the total metal concentration profiles are given after 500 cycles for three metal feed concentrations: base case M_t (M_t=1 mmol/l), *2M_t* and *0.5M_t*. The ligand to metal ratio is kept constant (Table 6.2). Figure 6.4 shows that at lower concentrations a sharper concentration front is obtained. Therefore, RFA becomes even more applicable for the recovery of low concentration homogeneous catalysts.

6.3.2.2   Stability constants

Depending on the type of metal, ligand or solvent [11], different values of stability constants are found to describe the ratio of complex species present. In Figure 6.5 concentration profiles of the total metal after 500 cycles are given for three values of the stability constants: base case κ_1, κ_2 (Table 6.2), $10^3\kappa_1$, $10^3\kappa_2$, and $10^6\kappa_1$, $10^6\kappa_2$. In our

95

previous work [11] we have shown that depending on the type of catalyst the stability constants can vary with 10^6. In Table 6.3 two sets of binding strengths are given (β_1's, β_2's), while in Table 6.4 the relative amounts of M, ML and ML_2 are given for the selected stability constants and different ligand/metal ratio. Figure 6.5 shows that an increase of the stability constants for constant set of binding constants results in broadening of the concentration front. This is expected because increasing the stability constant increases the contribution of the ML_2 form, which has the lowest binding strength value.

Table 6.3. Binding constants of M, ML and ML_2 forms for different values of stability constants

	x_M	x_{ML}	x_{ML2}
β_1	0.8	0.4	0.3
β_2	1.6	1.2	0.8

Table 6.4. Concentration distributions of M, ML and ML_2 forms for different values of stability constants and different ligand/metal ratio

	(a)	(b)	(c)	(d)
	κ_1, κ_2 $(r=2)$	$10^3\kappa_1, 10^3\kappa_2$ $(r=2)$	$10^3\kappa_1, 10^3\kappa_2$ $(r=10)$	$10^6\kappa_1, 10^6\kappa_2$ $(r=2)$
x_M	0.998	0.33	$1.33\cdot10^{-2}$	$9.4\cdot10^{-4}$
x_{ML}	$2\cdot10^{-2}$	0.33	0.108	$3.02\cdot10^{-2}$
x_{ML2}	$4\cdot10^{-6}$	0.33	0.878	0.968

Therefore the most favourable binding strength that will lead to the sharpest concentration profile should be selected for the form which is dominant (Table 6.4). This is illustrated in Figure 6.6. In this case the selected dimensionless stability constant values are $\kappa_{S1}=10^6$ and $\kappa_{S2}=10^6$ where the ML_2 specie is dominant (Table 6.4(d)). Two sets of binding constants are compared: binding constants for the base case, β_1's, and a new set of binding constants, β_2's, (Table 6.3). In the new set of binding constants we have increased values of binding constants for all forms. The concentration front with an increased β_{ML2} value of 0.8 shows now a significantly sharper profile compared to the concentration profile for the base case. This example also shows that RFA can be applied for a wide range of the stability constants providing that the optimal binding constants are selected.
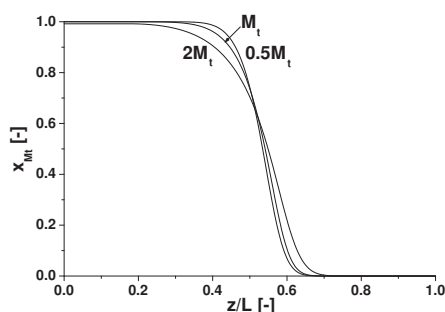
Figure 6.5. Influence of the stability constants on the total metal concentration profile in the liquid phase after adsorption in the 500th cycle
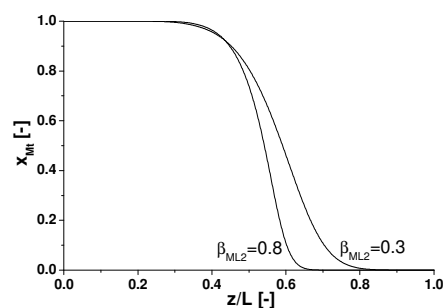
Figure 6.6. Influence of the binding strengths of M, ML and ML_2 for $\kappa_{S1}=10^6$ and $\kappa_{S2}=10^6$ on the total metal concentration profile in the liquid phase after adsorption in the 500th cycle

6.3.2.3 Ligand to metal ratio

Increasing the ligand/metal ratio will shift the equilibrium between the species in the direction of ML_2 (Equation (6.1) and Table 6.4(b) and (c)). Since the ML_2 contribution is increased, a similar effect on the concentration front of the total metal concentration can be noticed as for increasing the stability constants. Figure 6.7 shows the total metal concentration profile for two different ligand/metal ratios: *r* (see Table 6.2) and 5*r*. In both cases the stability constants were $10^3\kappa_1$ and $10^3\kappa_2$. The concentration profile is broadened by increasing the ligand/metal ratio, which is due to the increase of the amount of ML_2 which adsorbs weaker. This, again, supports that RFA can be applied for a wide range of catalysts, provided that the binding constant is selected for the dominant specie present.
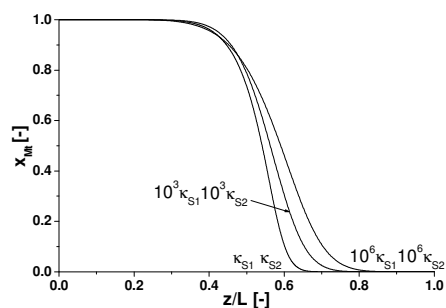
Figure 6.7. Influence of the ligand/metal ratio on the total metal concentration profile in the liquid phase after adsorption in the 500th cycle

6.3.3. *Influence of adsorbent parameters*

The concentration profile of the adsorbing species in the adsorption bed mainly depends on the adsorbent properties. The isotherm shape can either bring self-sharpening (favourable isotherm) or self-broadening (unfavourable isotherm) of the concentration front. External and internal mass transfer of the adsorbing species create the "S" shape of the concentration profile, and by reducing these effects sharpening of the concentration profile becomes more pronounced, and at the same time results in a more efficient utilisation of the column [21]. Therefore five characteristics are considered for improving the design of the affinity adsorbent:

- Binding strength of the adsorbent
- Capacity of the adsorbent
- Effective intraparticle diffusion coefficient
- Particle size of the adsorbent
- Bed porosity.

All five characteristics influence the mass transfer rate inside the particle, while binding strength and adsorbent capacity also influence the shape of the adsorption isotherm. The objective of the following text is to show how altering these four adsorbent characteristics can sharpen the concentration profile inside the bed, and consequently assist in design of a promising affinity adsorbent for the RFA concept.

6.3.3.1 Binding constants

The binding constant value influences both the shape of the adsorption isotherm and the driving force for mass transfer. Increasing the binding strength of the adsorbent slightly increases the mass transfer and sharpens the concentration front in the liquid phase. An increase of the binding strength also sharpens the adsorption isotherm profile which can

cause sharpening of the wave front during adsorption. On the other hand, desorption becomes more unfavourable: broadening of the concentration profile during desorption and a decrease of the driving force for mass transfer. Therefore the binding strength should be balanced to find an optimal adsorption/desorption behaviour.

These effects are shown in Figure 6.8 where we studied three binding strengths: the base case, (β_M=0.8), increased binding strength ([4·β_M]=3.2) and decreased binding strength ([0.25·β_M] =0.2). It was decided to change only the β_M value since in the base case the free metal specie is dominant (more than 99%) due to low values of stability constants. Compared to the base case, β_M, increased binding strength, 4·β_M, causes sharpening of the profile in the lower concentration range, while broadening in the higher concentration range. For the decreased binding strength, 0.25·β_M, broadening of the concentration front is noticed for the whole concentration range. These effects can be explained with a combination of continuous adsorption and desorption half-cycles and the presence of the linear part of the isotherm that causes broadening of the metal concentration profile.

It can be concluded that the binding strength between the adsorbing species and the functionalized groups of the promising affinity adsorbents should be in the range of β_M=0.8. This range of β_M values gives a sharp concentration profile in the adsorption bed where continuous adsorption and desorption are applied.
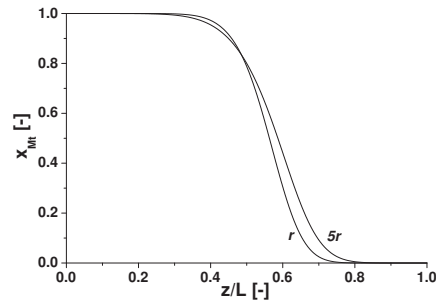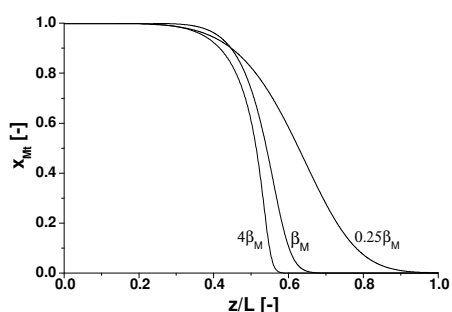

Figure 6.8. Influence of the bonding strength on the total metal concentration profile in the liquid phase after adsorption in the 500th cycle

6.3.3.2   Adsorbent capacity

Similar to the binding constant, varying the adsorbent capacity has also two effects: a change of the isotherm's shape and a change of the driving force for mass transfer. The sharpening speed of the concentration profile due to the isotherm profile will decrease by increasing the adsorption capacity. On the other hand, an increase of the adsorption capacity will lead to a larger driving force and larger bed capacity, and consequently self-sharpening of the concentration front. In case of the linear driving force

model, the mass transfer rate increase correlates linearly with the increase in the adsorption capacity. The clear influence of the adsorption capacity on the mass transfer resistance decrease is illustrated in Figure 6.9. The total metal concentration profiles are shown after 500 cycles for the reference adsorption capacity ($\alpha=925$), and for cases where the adsorption capacity is doubled ($\alpha=1850$) and halved ($\alpha=462.5$). As it can be seen the wave front is sharpening by increasing the value of α. This means that sharpening of the front due to the increase of the driving force for mass transfer is more pronounced than broadening due to change in isotherm shape. In conclusion, the value of $\alpha=1850$ gives the sharpest concentration profile. It is a realistic value for the maximum loading that a silica based affinity adsorbent can have.
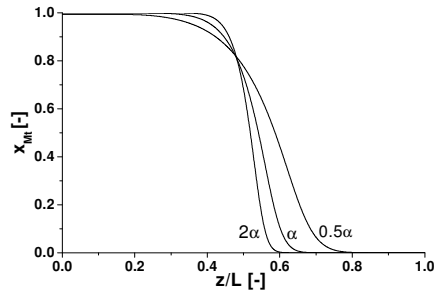
Figure 6.9. Influence of the adsorbent capacity on the total metal concentration profile in the liquid phase profile after adsorption in the 500th cycle

6.3.3.3 Effective diffusion coefficient

The mass transfer rate inside the adsorbent particle can be enhanced by increasing the value of the effective diffusion coefficient by designing an adsorbent with larger pores [17]. The effective diffusivity in our dimensionless model is described by the Peclet number for particles, Pe_P (Eq. 6.15). Figure 6.10 shows the total metal concentration profiles for three different Pe_P numbers: $Pe_P=1882$, $5 \cdot Pe_P=9410$ and $0.2 \cdot Pe_P=376.4$. As expected a decrease of Pe_P numbers (larger effective diffusion coefficients or a smaller particle diameter) enhances mass transfer. Since the dependence of the concentration change on Pe_P number is exponential (Eq. 6.13), it can explain the non-linear change of the concentration profile. Therefore it can be expected that at small Pe_P numbers the concentration profile will not change its shape any further.

The sharpest concentration profile is reached for the particle Peclet number $Pe_P=376.4$. This value is also a realistic value that can be reached by designing a silica based affinity adsorbent with large and uniform pores of e.g. 90 Å in diameter.

Figure 6.10. Influence of the effective diffusion coefficient on the total metal concentration profile in the liquid phase after adsorption in the 500th cycle

6.3.3.4 Particle size

Mass transfer between the liquid and solid phase can be increased by decreasing the particle size of the adsorbent (see Equations (6.13-6.15) and Figure 6.12). Change of the particle size influences the dimensionless numbers, Pe_P and N. The influence of Pe_P change is discussed in the previous part (Effective diffusion coefficient) where it was shown that for smaller Pe_P numbers a sharper profile can be reached. Figure 6.11 shows that increasing the N value (increasing column length or decreasing particle size) results in a sharper concentration profile. Figure 6.12 illustrates the sharpening of the concentration front by decreasing the particle size, where effects of changing two dimensionless numbers, Pe_P and N, are combined. As a result it is concluded that the smallest particle diameter should be selected for the best design of an affinity adsorbent.

The practical problem that arises by decreasing the particle size is an increase of the pressure drop across the column. In this work the pressure drop is estimated by the Ergun equation for a fixed bed:

$$\frac{\Delta P}{L} = \frac{150\mu(1-\varepsilon_b)^2 u}{\varepsilon_b^3 \cdot d_p^2} + \frac{1.75(1-\varepsilon_b)\rho \cdot u^2}{\varepsilon_b^3 \cdot d_p} \qquad (6.25)$$

Table 6.5 shows the calculated pressure drop for the base case (d_p =100 μm) and two cases with different particle sizes (d_p =50 μm and d_p =200 μm). The allowed pressure drop usually depends on each specific application. Since the commonly selected maximum allowable pressure drop inside a packed column for liquid bulk applications is around 0.5 bar, d_p=100 μm (N=6.6·10[4] and Pe_P=1882) is selected as a realistic particle size used in bulk operations. If an application allows higher pressure drops it is recommended to use smaller particles to enhance the mass transfer even further.

Table 6.5. Influence of the particle size on the pressure drop across the column

d_p [μm]	100	50	200
N [-]	$6.6 \cdot 10^4$	$1.32 \cdot 10^5$	$3.3 \cdot 10^4$
Pe_P [-]	1882	941	3764
ΔP [bar]	0.39	1.54	0.10

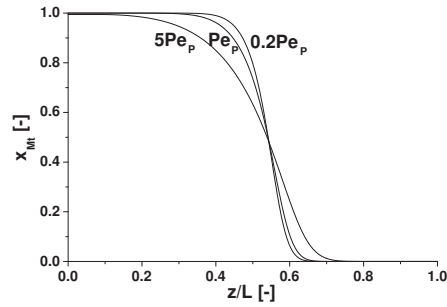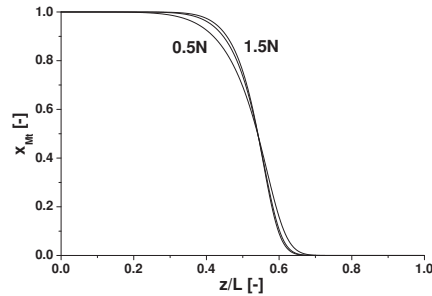**Figure 6.11.** Influence of the N value on the total metal concentration profile in the liquid phase after adsorption in the 500th cycle
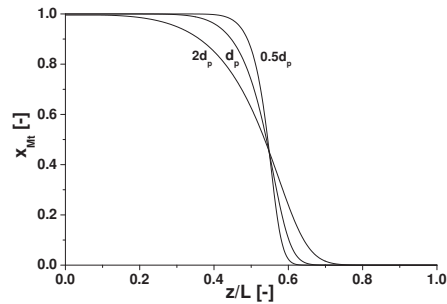
Figure 6.12. Influence of the particle diameter on the total metal concentration profile in the liquid phase after adsorption in the 500th cycle

<u>6.3.3.5   Bed porosity</u>

Porosity of the bed depends on the particle size and shape. Influence of the bed porosities on the concentration profile is studied for two values: 0.5 and 0.76, where particle size is kept constant (d_p=100μm). It is expected that by decreasing the bed porosity the concentration profile is sharpening since the contribution of the solid phase increases (Figure 6.13). On the other hand, pressure drop inside the bed increases by decreasing the bed porosity (Eq. 6.25). For these two porosities (ε_b=0.5 and ε_b=0.76) calculated pressure drop is respectively 5.8 bar and 0.39 bar. To avoid large pressure drops influences of bed

porosity and particle size have to be combined: smaller bed porosity asks for larger particle size and vice versa.

Therefore, we recommend that for a porosity of ε_b=0.5 a particle size of d_p=200μm is selected, and for a porosity of of ε_b=0.76 a particle size of d_p=100μm is selected.
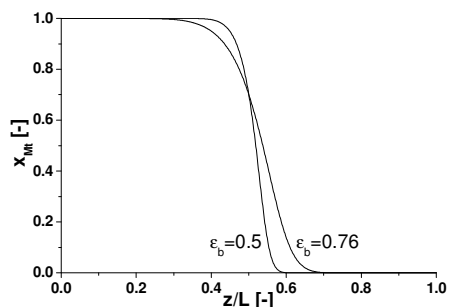
Figure 6.13. Influence of the bed porosity on the total metal concentration in the liquid phase after adsorption in the 500th cycles

6.3.3.6   Silica adsorbent design

Conclusions for silica based adsorbent design are given in Table 6.6. General conclusions and possible material or system limitations are given for the main five adsorbent characteristics. Table 6.6 should be a guideline for the design of adsorbents which will be applied in the RFA process. In the second column general conclusions drawn from the previous simulations are given, while in the third column material and system limitations are pointed. Designing an adsorbent for the RFA process, one should follow general conclusions, but in the same time comprise both material and process limitations.

Table 6.6. Overview of the adsorbent design

	General conclusions	Material/system limitation
Binding constants, b,	≈ 0.8 m^3/mol (β=0.8)	No
Adsorbent capacity, q_s,	Maximal	$\approx 10^{-3}$ mol/g (α=1850)
Effective diffusion coefficient, D_{eff},	Maximal	$\approx 6 \cdot 10^{-10}$ m^2/s (Pe_P=376.4) $D_{eff} \rightarrow D_m$
Particle size, d_p,	Minimal	Allowable pressure drop
Bed porosity, ε_b,	Minimal	Allowable pressure drop

6.3.4   Design of the ligand column

In the first column, the metal adsorbing bed, a part of the ligand is always adsorbed through adsorbing the ML and ML_2 species. In the second column only the free ligand is adsorbed. Therefore in this bed competitive adsorption of different forms, present in the first bed, is excluded. However, depending on each application the ligand can be in a large excess (ligand/metal ratio *r* can be as high as 100 [18]). Objective of the following work is to show stability of the ligand adsorbing column and to study up to which excess of ligand the RFA process can be applied.

6.3.4.1   Stability of the process

Parameters used in simulating the reversible adsorption and desorption of the free ligand are given in Table 6.7. These values are based on the conclusions drawn in the previous part of our study of adsorbent parameters. Figure 6.14 confirms that a stable operation is obtained also for the reversible adsorption and desorption of the free ligand. As well as in the metal column the broadening speed of the concentration profile due to unfavourable desorption isotherm, and a limited uptake rate decreases over time which finally results in a stable operation. Additionally, there was no decrease in the ligand concentration front at z/L=0, as well as no leaching at z/L=1 during adsorption (Figure 6.15).

Table 6.7. Input base case parameters for the reversible adsorption/desorption of the free ligand

Parameter	Value
Adsorbent parameters	
β_L	1.6
α	1850
Pe_P	376.4
Process parameters	
$\tau_{1/2}$	5
ε_b	0.5
N	$6.6 \cdot 10^4$
Bo	$1.74 \cdot 10^4$
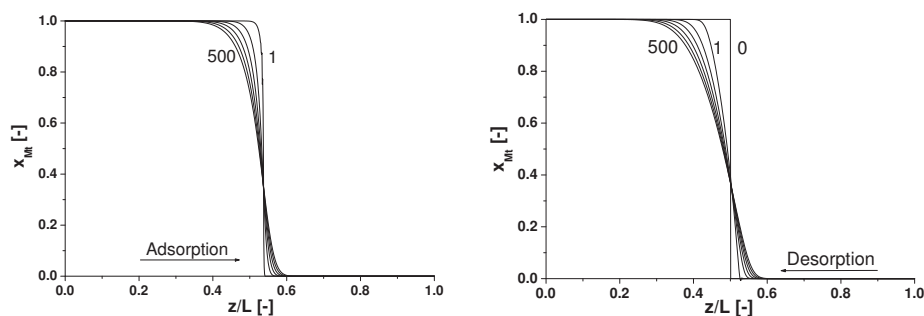
Figure 6.14. The ligand concentration profile in the liquid phase for the selected number of cycles (1, 100, 200, 300, 400 and 500) after: (a) adsorption and (b) desorption
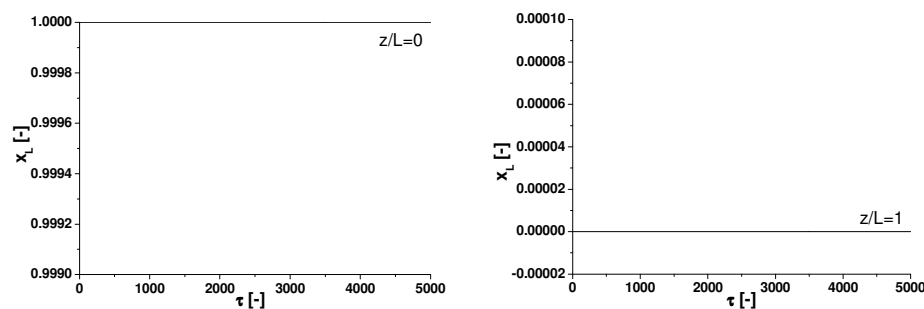
Figure 6.15. The ligand concentration profile in the liquid phase over time at: (a) z/L=0 and (b) z/L=1

6.3.4.2   Ligand concentration

In many homogeneous catalytic reactions the ligand is used in excess [20], and therefore the ligand concentration can vary depending on each specific application. In this simulation the maximal ligand concentration that can be recovered in an adsorption column based on parameters given in Table 6.7 is studied. Figure 6.16 shows ligand concentration profiles after 500 cycles for different initial concentrations ($2L_t$, L_t, $0.5L_t$ and $0.25L_t$). For all initial concentrations no leaching of the ligand was detected. However for $2L_t$ a decrease in the ligand concentration at z/L=0 was found (Figure 6.16b). At low ligand concentrations the profile is very sharp, while in the higher region profile is broadening. Therefore, we preloaded 70% of column and with this condition ligand with $2L_t$ concentration could be kept inside the column, while already at $3L_t$ decrease in the ligand concentration at z/L=0 were as well found (Figure 6.17). In conclusion, ligand concentrations of L_t=4 mmol/l or lower can be recovered by RFA using adsorbent properties given in this simulation. Otherwise, if the ligand concentration is higher than $3L_t$

either the column parameters should be changed (e.g. increasing the preloading part or column size) or other technique for the recovery of the free ligand might be needed.

(a)   (b)
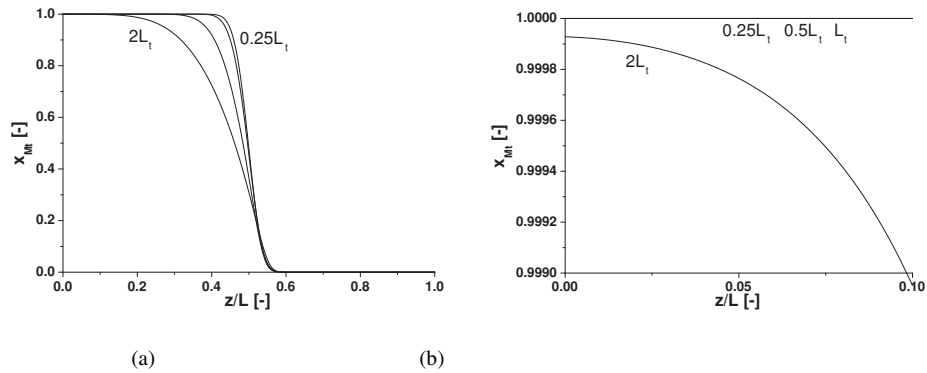
Figure 6.16. (a)Influence of the ligand inlet concentration on ligand concentration in the liquid phase after desorption in the 500th cycle (b) enlarged for the entry of a column
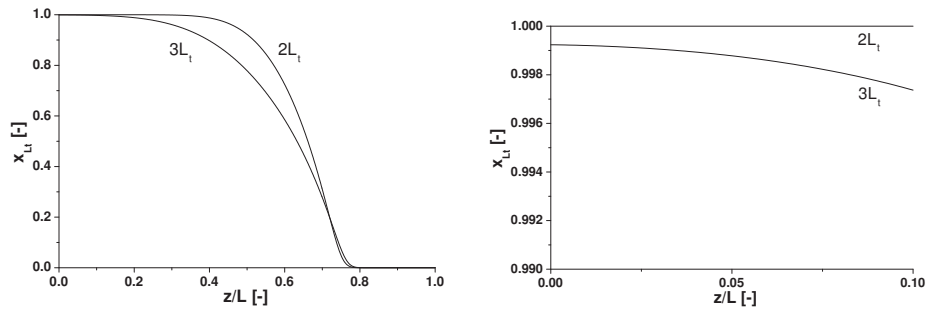
Figure 6.17. (a)Influence of the ligand inlet concentration on ligand concentration in the liquid phase after desorption in the 500th cycle with a 70% preloaded column (b) enlarged for the entry of a column

6.3.5   *Example: Hydroformylation process*

The BASF hydroformylation process was selected as a demo-process to design an adsorption column for the recovery of the metal species. In this process rhodium is used as a metal centre while PPh_3 as a ligand. Reactor volume ($V_{reactor}$), flow rate (F), and concentration of rhodium (C_{Rh}) are taken from Cornils et al. [18] (Table 6.8). Adsorbent parameters are taken from the conclusions drawn in the previous part of the paper. Since stability constants of this catalyst are unknown it is chosen to simulate a process where the catalyst complex is present in only one form, ML_3.

Table 6.9 shows different combinations of maximal operating times for different volumes of adsorption bed as well as for different designs (L/Dc ratio). Three bed volumes are studied: 10% (column (a)), 3% (column (b)) and 1% (column (f)) of the reactor volume. By increasing the bed volume a longer maximum operating time is obtained. For the bed

volume of $1.35 m^3$ after approximately 51 day of RFA operation a breakthrough of the catalyst at the entry of the bed occurs. This time is changed to 1190 days by increasing the bed volume 10 times. On the other hand, increasing the bed volume will result in larger investments both in the equipment and preloading of the adsorbent by catalyst.

Table 6.8. BASF hydroformylation data [18] and parameters selected

$V_{reactor}$ [m³]	135
F [m3/s]	$2.3 \cdot 10^{-3}$
C_{Rh} [mol/ m³]	0.8
β_M	0.8
α	1850
ε_b	0.5

Table 6.9. Maximal operation time for metal adsorbing column

	(a)	(b)	(c)	(d)	(e)	(f)
$V_{reactor}$ [m³]	135	135	135	135	135	135
V_{bed} [%$V_{reactor}$]	**10**	**3**	3	3	3	**1**
$C_{catalyst}$ [mmol/l]	0.8	0.8	0.8	**0.4**	**0.4**	0.8
L/Dc [-]	5	5	**10**	5	**10**	5
N^o cycles [-]	500	500	500	500	500	500
$\tau_{1/2, max}$ [-]	35	25	35	35	50	15
$t_{total,max}$ [days]	**1190**	**254**	**355**	**356**	**507**	**50.8**
ΔP [bar]	0.54	0.85	2.2	0.85	2.2	1.27

One way to extend the maximal operation time is by keeping the same bed volume and changing the bed design. This is shown in Table 6.9 (columns (b) and (c)) where the maximum operation times are given for constant bed volumes (4.05 m3) but in the first case the ratio of bed length over bed diameter is 5 and in the second 10. The maximal operating time is extended from 254 days to 355 days due to decrease in axial dispersion. This has its penalty by increasing the pressure drop in the system from 0.85 bar to 2.2 bar.

The operating time would also increase if the process would be changed by introducing a new, more effective catalyst which has a higher TON (turnover number) (less

of catalyst concentration is needed). For the bed volume equal to 3% of thereactor volume and an initial catalyst concentration of 0.8 mmol/l (column (b)) the estimated maximal half cycle time, $\tau_{1/2, \, max}$, is 25 and maximal operation time is 254 days. If the initial metal concentration decreases with 50% (column (d)), the half cycle time increases to 35 and the maximum operating time is now 356 days. At the end, an increase in L/Dc and a decrease in catalyst concentration are applied. The results show that the maximum operating time is extended to approximately 507 days (column (e)).

It can be concluded that an adsorption column with a volume of 3% of the reactor volume is sufficient for full recovery of the metal containing species in the BASF hydroformulation process. Therefore the total bed volume for two adsorption beds applied in the RFA should be 6% for recovery of metal containing species. The maximum operating time can be increased by increasing the L/Dc ratio and by introducing more efficient catalysts. Since in this process ratio L/M is around 100, another separation technique, e.g. extraction, is required for recovery of ligands.

6.4 Conclusions

Silica adsorbent design and modelling of the reversible adsorption/desoprtion process for the recovery of homogeneous catalysts are studied in this work. The following major conclusions are drawn:

- Stable operation for 500 cycles can be reached for the reversible adsorption/desorption process without leaching of the catalyst species;
- Silica based adsorbent which will provide a sharpening of the concentration profile inside the bed should have binding constant of around 0.8 m^3/mol (β=0.8), adsorbent capacity of 10^{-3} mol/g (α=1850), effective diffusion coefficient in the range of $6 \cdot 10^{-10}$ m^2/s (Pe_P=376.4), and a minimal particle size and bed porosity with the limitation of an acceptable pressure drop.
- For Bodenstein numbers larger than $1.74 \cdot 10^4$ axial dispersion can be neglected;
- The RFA process can be applied for a wide range of the stability constants and becomes even more applicable for the recovery of homogeneous catalysts that have a lower metal concentration;
- Simulation of the recovery of the rhodium catalyst in the BASF hydroformylation process required a total adsorption bed volume for recovery of the metal species of 6% of the reactor volume.

6.5   List of symbols

b_L-   Adsorption binding strength for component L   [m³/mol]

b_M-   Adsorption binding strength for component M   [m³/mol]

b_{ML}-   Adsorption binding strength for component ML   [m³/mol]

b_{ML2}-   Adsorption binding strength for component ML_2 [m³/mol]

Bo-   Bodenstein number $(= \dfrac{u \cdot d_p}{D_{ax}})$ [-]

$C_{catalyst}$- Concentration of the catalyst   [mol/m³]

C_{Rh}-   Rhodium concentration   [mol/m³]

Dax-   Axial dispersion coefficient   [m²/s]

Dc-   Column diameter   [m]

$Deff$-   Effective diffusion coefficient   [m²/s]

d_P-   Particle diameter   [m]

F-   Flow   [m³/s]

i-   Index for L, M, ML and ML_2 [-]

K_{s1}-   Stability constant for the first complexation step   [m³/mol]

K_{s2}-   Stability constant for the second complexation step   [m³/mol]

L-   Length of the column   [m]

$[L_t]$-   Total concentration of the free ligand   [mol/m³]

$[M]$-   Concentration of the free metal   [mol/m³]

$[ML]$-   Concentration of the ML complex   [mol/m³]

$[ML_2]$-   Concentration of the ML_2 complex   [mol/m³]

$[M_t]$-   Total concentration of all metal containing forms   [mol/m³]

N-   Number of particle over the axial distance $(= \dfrac{L}{d_p})$ [-]

ΔP-   Pressure drop   [bar]

Pe_P-   Peclet number for particle $(= \dfrac{u \cdot d_p}{D_{eff}})$ [-]

q_i-   Loading of free ligand, free metal, ML and ML_2 on the
        adsorbent at the interface   [mol/kg]

$\overline{q}_i$ -   Averaged loading of free ligand, free metal, ML and ML_2
        on the adsorbent   [mol/kg]

q_S-   Maximum loading on the adsorbent   [mol/kg]

109

r-	Ratio between total ligand and total metal concentration $(= \dfrac{[L_t]}{[M_t]})$	[-]	

$t_{1/2}$-   Half cycle time   [s]

$t_{total,max}$-   Maximal total operation time   [days]

u-   Superficial velocity $(= \dfrac{F \cdot 4}{D_C^2 \cdot \pi})$ [m/s]

x_L-   Dimensionless concentration of the free ligand $(= \dfrac{[L]}{[L_t]} = \dfrac{[L]}{[M_t] \cdot r})$ [-]

x_M-   Dimensionless concentration of the free metal $(= \dfrac{[M]}{[M_t]})$ [-]

x_{ML}-   Dimensionless concentration of the ML complex $(= \dfrac{[ML]}{[M_t]})$ [-]

x_{ML2}-   Dimensionless   concentration of the ML_2 complex $(= \dfrac{[ML_2]}{[M_t]})$ [-]

V_{bed}-   Bed volume   [m³]

$V_{reactor}$-   Reactor volume   [m³]

z-   Axial distance   [m]

β_L-   Dimensionless adsorption binding constant for L $(= b_L \cdot [L_t])$ [-]

β_M-   Dimensionless adsorption binding constant for M $(= b_M \cdot [M_t])$ [-]

β_{ML}-   Dimensionless adsorption binding constant for ML $(= b_{ML} \cdot [M_t])$ [-]

β_{ML2}-   Dimensionless adsorption binding constant for ML_2 $(= b_{ML_2} \cdot [M_t])$ [-]

Γ_i-   Dimensionless loading of free ligand, free metal, ML and ML_2

             on the adsorbent at the particle interface $(= \dfrac{q_i}{q_S})$ [-]

$\overline{\Gamma}_i$-   Dimensionless averaged loading of free ligand, free metal, ML

             and ML_2 on the adsorbent $(= \dfrac{\overline{q}_i}{q_S})$ [-]

ε_b-   Porosity of the bed   [-]

κ_1-   Dimensionless stability constant, K_{s1}, $(= K_{S1} \cdot r \cdot [M_t])$ [-]

κ_2-	Dimensionless stability constant, K_{s2}, ($= K_{S2} \cdot [L_t]$)	[-]
μ-	viscosity	[Pa·s]
ρ_S-	Density of the adsorbent	[kg/m^3]
$\tau_{1/2}$-	Dimensionless time ($= \dfrac{t \cdot u_{sup}}{L}$)	[-]
$\tau_{1/2,\,max}$-	Dimensionless maximal half cycle time	[-]
χ-	Dimensionless axial distance ($= \dfrac{z}{L}$)	[-]

6.6 References

[1] Boreskov G.K., Matros Yu.Sh., Appl. Catal., 5 (1983) p. 337-343

[2] Matros Yu.Sh., Noskov A.S., Chumachenko V.A., Goldman O.V., Chem. Eng. Sci., 43, 8, (1988), p. 2061-2066

[3] Chan F.L., Keith J.M., J. Environ. Manag. 78 (2006) p. 223-231

[4] Smit J., Bekink G.J., van Sint Annaland M., Kuipers J.A.M., 62 (2007) p. 1239-1250

[5] Gosiewski K., Chem. Eng. Proc., 32 (1993) p.233-244

[6] Dubber M.J., Kanfer I., J. Chrom. A, 1122 (2006) p.266-274

[7] Gilron J., Waisman M., Daltrophe N., Pomerantz N., Milman M., Ladizhansky I., Korin E., Desalination 199 (2006) p.29-30

[8] Govender S., Jacobs E.P., Leukes W.D., Odhav B., Pillay V.L., 238 (2004) p. 83-92

[9] J. Dunnewijk, H. Bosch, A.B. de Haan, Sep. Purif. Technol. 40 (3), (2004) 317-320

[10] J.T. Scarpello, Nair D., et al., J. Membr. Sci. 5180 (2002) p. 1-15

[11] T. Djekić, Z. Zivkovic, A.G.J. van der Ham, A.B. de Haan, J. Appl Catal A, 312 (2006) 144-152

[12] J. Dunnewijk, *Reverse Flow Adsorption Technology for Homogeneous Catalyst Recycling,* thesis, University of Twente, (2006)

[13] Dunnewijk J., Bosch H., de Haan A.B., Chem. Eng. Sci. 61, (2006) p. 4813-4826

[14] Dunnewijk J., Bosch H., de Haan A.B., Adsorption, 11, (2005) p.521-526

[15] T. Djekić, A.G.J. van der Ham, H. Bosch, A.B. de Haan, J. Chem. Eng. Sci.,62, (2007) p. 2032-2039

[16] T.Djekić, A.G.J. van der Ham, A.B. de Haan, J Chrom A, 11420 (2007), p.32-38

[17] T.Djekić, V. Tripkovic, A.G.J. van der Ham, A.B. de Haan, Adsorption, (submitted)

[18] B. Cornils and W. A. Hermann (Eds.), Applied homogeneous catalysis with organometallic compounds : a comprehensive handbook , Weinheim, Wiley-VCH, 2002 p. 82-83

[19] G. Guiochon, S.G. Shirazi, A.M. Katti, Fundamentals of Preparative and Nonlinear Chromatography, Academic Press, 2006,p.151-219

[20]   P.W.N.M van Leeuwen, Homogeneous Catalysis- Understanding the Art, Kluwer Academic Publishers, Dordrecht, The Netherlands, 2004, p.7-8

[21]   Bosch H, de Haan AB. Fundamentals of Industrial Separations (2nd edition). ISBN 978-90-810973-2-1, 2007: 6-1-6-23.

Activity of palladium catalysts in the Heck reaction during its recovery by Reverse Flow Adsorption technology

Abstract

Difficult recovery of homogeneous catalysts is the main drawback for their broader application. Leaching of the very expensive metals as well as deactivation of the homogeneous catalyst are two main drawbacks of present recovery methods. Therefore Reverse Flow Adsorption is proposed as a novel concept for the recovery and recycling of homogeneous catalyst. In this work the stability of the reverse flow adsorption concept and the activity of the catalyst after several cycles of the reversible adsorption/desorption of the catalyst precursor are studied. The Heck reaction is selected as a test reaction to measure the catalytic activity of $PdCl_2(PPh_3)_2$ in acetonitrile at very low concentrations. The RFA set-up is built to continuously adsorb and desorb $PdCl_2$ and the Heck reaction is used in the subsequent step to test the activity. The results show that after several cycles of continuous adsorption and desorption of $PdCl_2$, the activity of the homogeneous catalyst is constant.

7.1 Introduction

Although homogeneous catalysts offer a number of advantages compared to heterogeneous catalysts [1], they have a major problem: recovery. Many techniques such as distillation, extraction, filtration, membrane separation or biphasic catalysis are developed to separate a homogeneous catalyst from a reaction mixture [2]. Often found limitations of these techniques are incomplete recovery and deactivation of the catalyst caused by the recovery process. In our previous chapters (Chapter 3 and Chapter 4) [3,4] we have shown separate adsorption of metal containing species and free ligands. In Chapter 4 [4] we have shown that all cobalt complex species are adsorbed. Chapter 6 shows that with optimal design of the adsorption beds, leaching of the catalyst can be prevented.

In this chapter the first experimental demonstration of combined RFA with a catalytic reaction is shown. However, recovery and reaction are not continuously performed in this initial study, since a batch type of reactor is selected. The goal of this chapter is to:

- Experimentally study the stability of Reverse Flow Adsorption (RFA),
- Evaluate the activity of the homogenous catalyst after several cycles of reversible adsorption/desorption of $PdCl_2$.

The Heck reaction is selected as a test reaction for catalyst activity. In a broad study Alonso et al. [5] gave a critical overview on the Heck reaction. The influence of the solvents, ligands, type of catalyst and reaction conditions is discussed. They point that tertiary phosphine ligands were used to ensure catalyst stability, but on the other hand broad research was done on ligandless carbon-carbon coupling. The first ligandless Heck reaction was independently reported by Beletskaya [6] and Jeffery [7,8]. Gundersen et al. [9] gave a simple catalytic system to couple vinylpurine with a range of aryliodides where palladium acetate in DMF is used as a catalyst precursor. Schmidt et al. catalyzed the reaction of bromobenzene and styrene also without presence of any ligand using $PdCl_2$ in DMF as a precursor [10].
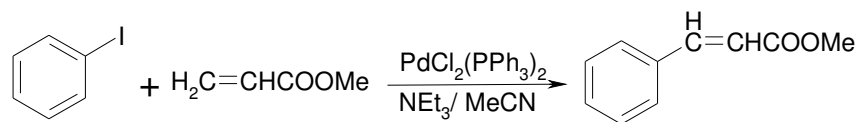

Figure 7.1. Iodobenzene vinylation with methyl acrylate

In this work iodobenzene vinylation with methylacrylate (Figure 7.1) is studied as proposed in the work of Zhao et al. [11]. In their work $Pd(OAc)_2$ was applied as a catalyst precursor. They studied beside reaction kinetics also the influence of solvent type and ligand/metal ratio. Since adsorption of palladium(II)chloride is studied in our previous work (Chapter 3) [3], $PdCl_2$ is also selected for this work to show both, the stability of the reversible adsorption/desorption cycles and the activity of the catalyst after several RFA cycles. The reversible adsorption/desorption cycles are stable without leaching of the metal and with a metal concentration after each desorption cycle equal to the initial feed concentration. First we demonstrate the stability of reverse flow adsorption after several continuous adsorption/desorption cycles of $PdCl_2$. The chapter continues with reproducing the results of Zhao et al. [11] and comparing their results with our catalytic system. Afterwards, the influence of the catalyst concentration on the reaction conversion is studied in order to find a region where the reaction conversion is directly dependant on the catalyst concentration. Finally, the results of the Heck reaction performed after several cycles of continuous adsorption/desorption of $PdCl_2$ are presented.

7.2   Material

Chemicals used in this work are palladium(II)chloride (99.9%, Sigma Aldrich), triphenylphopshine (PPh_3) (Sigma Aldrich), acetonitrile (MeCN) (99.9%, Sigma Aldrich), iodobenzene (98%, Acros Organics), methyl acrylate (99%, Acros Organics), 3-ethylamine (99%, Acros Organics), methyl cinnamate (99%, Sigma-Aldrich) and 3-(1-morpholino)propyl functionalized silica (Silicycle). Solvent was degassed before use, and all experiments were performed in an argon atmosphere. No preliminary treatment of the silica adsorbents (200-400 mesh, 60 Å, 500 m^2/g) was performed.

7.3   Experimental

7.3.1   *Reverse Flow experiments*

The set-up used for the reverse flow experiments is shown in Figure 7.2. It consists of two pumps (Smartline 1000 and Wellchrom K1001 produced by Knauer), two glass vessels, one heat exchanger (H.E.) and one column (for 20ºC temperature experiments: Media Flex, Dc=5mm, L=14-26 cm; for 50ºC experiments: homemade shell-

115

and-tube column, Dc=5 mm, L=40 cm). The flow directions are manually controlled with two valves.

The set-up is used for two types of RFA experiments:

- Both adsorption and desorption are performed at 20ºC;
- Adsorption is performed at 20ºC, while desorption at 33ºC and 50ºC.

For experiments at 20ºC no heat exchanger, H.E., was integrated in the set-up. For experiments performed at 33ºC and 50ºC, a heat exchanger is integrated to cool down the outlet solution after desorption.

Initially, 24cm of the column (L=40cm) is filled with 3-(1-morpholino)propyl-functionalized silica and the whole system is washed with clean solvent. 600 ml of a $PdCl_2$ solution in MeCN is pumped with a flow of 1 ml/min from Vessel 1 directly to the column to preload approximately half of the column with $PdCl_2$. After preloading pump P-1 is stopped. A sample is taken from Vessel 2 to analyze the outlet concentration. Then the direction of the valves is changed for the desorption process and pump P-2 started. 100 ml of pure solvent is pumped by P-2 (F=1mmol/l) back to the column to desorb $PdCl_2$. After desorption, the process is again stopped. Two samples are taken from Vessel 1 (app. 10 ml), one to analyze the outlet concentration (5ml), and one for performing the Heck reaction (5ml).
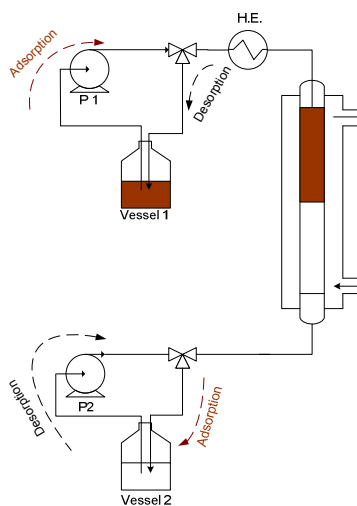

Figure 7.2. Reverse Flow set-up

116

Then 80 ml of the desorbed $PdCl_2$ solution is pumped back to the column where adsorption takes place. 10 ml of solvent remained in the Vessel 1 to prevent air entering the system. The adsorption/desorption process is repeated 4 times (5 times for experiments at 50 ºC). After each adsorption and desorption cycle a sample is taken to analyze the mean $PdCl_2$ concentration in the outlet solution.

7.3.2   Heck reaction

All the Heck reaction experiments were performed in a 50 ml three neck round bottom flask with water cooling on the top under an argon atmosphere. For each experiment reactants are added in the order: 20 mmol (4.08g) iodobenzene, 20 mmol (2.02g) triethyl amine and 20 mmol (1.72g) methyl acrylate. The catalyst is always added in a ratio $PPh_3/PdCl_2=2$, there amounts were varied depending on the desired catalyst concentration (e.g. 4 ml of 1mmol/l of PPh_3 and 2ml of 1mmol/l of $PdCl_2$ for 0.1 mmol/l total catalyst concentration). Pure solvent is added at the end to reach the total reaction volume of 20ml. Samples are taken at specific time intervals (15, 60 and 120 min) and reaction mixture is analyzed by GC-FID (Varian Chrompack CP 3800 GC). The column used for the analysis is Varian WCOT fused silica 50m x 0.32 mm ID column with CP-Sil 5CB DF 1.2 coating. $PdCl_2$ is analyzed by AAS (Varian SpectrAA 110 AAS). The measured absolute error in the conversion of the Heck reaction is 2%. This error increases up to 4% after its combination with the RFA experiments.

Characteristics of the analytical method by GC are given in Table 7.1. In Table 7.2 retention times of the Heck reactants and product are given. Since the Heck reaction products are analyzed immediately after taking a sample no internal standard is added. Methyl acrylate is used as an internal standard to quantitatively measure each sample because the initial concentration of methyl acrylate, $[MA]_0$, is always equal to the sum of methyl acrylate [MA] and methyl cinnamate [MC]:

$$[MA]_0 = [MA] + [MC] . \tag{7.1}$$

Therefore four samples were analyzed with different concentration ratios of MA and MC. Results show that there is a constant factor, F, between the concentration and the peak area ratio of MA and MC (Table 7.3). This factor is used to recalculate the concentration of MA and MC after the Heck reaction (Equations (2) and (1)):

$$[MA] = \frac{[MA]_0}{1 + F \cdot arearatio} . \tag{7.2}$$

Table 7.1. GC Settings for Quantitative Analysis

Separation Stage	Variable		
Injection	Injection temperature		280ºC
	Split ratio	On	1:20
Separation	Column Oven Temperature		190ºC
	Column Flow	He	2.0 ml/min
Detection	Varian FID		325ºC

Table 7.2. GC Separation: Retention Time Heck Reactants

Substance	Retention Time [min]
Acetone	2.87
Methyl acrylate	2.98
Triethylamine	3.09
Iodobenzine	4.78
Methyl cinnamate	9.42

Table 7.3. Quantification method of methyl acrylate and methyl cinemmate

[MA], (mmol/ml)	[MC], (mmol/ml)	Conc ratio, [MC]/[MA] (-)	Average area ratio (-)	Conc / area ratio, F, (-)
0.664	0.330	0.496	1.939	0.186
0.462	0.553	1.198	4.672	0.170
0.903	0.147	0.163	0.618	0.182
0.11	0.92	7.84	45.1	0.176
0.26	0.80	3.07	15.6	0.197
			Average conc / area ratio, F,	0.182
			Standard deviation	0.01

7.4 Results and Discussion

7.4.1 Reverse flow adsorption

The reverse flow adsorption (RFA) experiments are performed with an initial feed concentration of 1 mmol/l $PdCl_2$. The adsorption temperature is kept constant (20 ºC), while desorption temperature is varied: 20ºC, 33 ºC and 50ºC. At the end of each

adsorption and desorption cycle the concentration of the outlet $PdCl_2$ solution is measured. The results are shown in Figure 3. Initially, experiments are performed at 20ºC. After each adsorption cycle leaching of $PdCl_2$ is detected. Roughly 0.04 mmol/l of the $PdCl_2$ was not adsorbing. Already after the first desorption cycle a significant decrease in the outlet concentration is observed. In spite of the constant leaching, the outlet $PdCl_2$ concentration decreases compared to the feed concentration and remains constant with an increase of cycles ($\approx$0.5 mmol/l). This is caused by the initial preloading of the column. The decrease in the desorption concentration indicates a difference in adsorption and desorption equilibrium. To enhance desorption, the temperature of the column is increased to 33ºC and 50ºC during desorption cycles. Figure 7.3 shows an increase in the $PdCl_2$ concentration after desorption cycles with an increase of temperature. At a temperature of 33ºC the concentration of $PdCl_2$ after each desorption cycles remains approximately equal to the feed concentration. Increasing temperature to 50ºC, the outlet concentration of $PdCl_2$ after each desorption cycle is larger than the feed concentration ($\approx$1.5 mmol/l). This indicates that adjustment of desorption temperature is required to obtain the same concentration after each desorption cycle as the feed concentration.
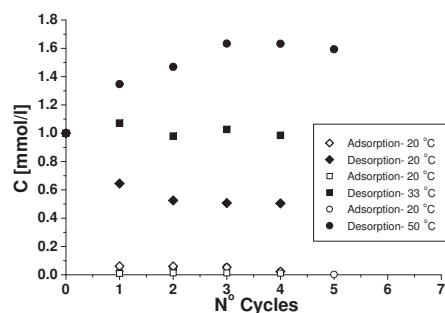

Figure 7.3. Concentration of PdCl2 after each adsorption and desorption cycle in the RFA experiments

Since adsorption is always performed at 20ºC a constant concentration of $PdCl_2$ appeared to be leaching after each adsorption cycle (0.04 mmol/l). To understand why this occurs, the adsorption isotherm of PdCl2 on morpholine functionalized silica is investigated for the lower concentration range (Figure 7.4). It is observed that part of the palladium is not adsorbing. This can be explained by the presence of different palladium species in a solution [12], where some form is probably not adsorbing. Therefore the

119

leaching observed in the RFA experiments is not due to inadequacy of the process, but due to a flaw in the adsorbate-adsorbent interaction.
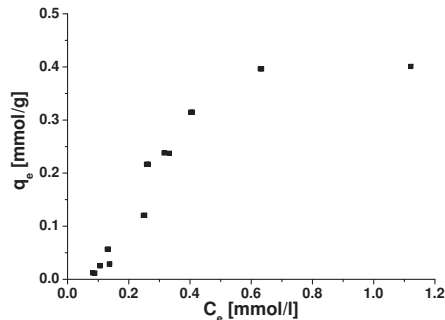

Figure 7.4. PdCl2 adsorption on 3-(1-morpholino)propyl functionalized silica at 20ºC

7.4.2   Heck reaction

7.4.2.1   Data reproducibility

The studied Heck reaction is selected from the work of Zhao et al. [11]. Initially a reproducibility experiment was performed to ensure that the experimental procedure is correct (Table 7.4). The Heck reaction is repeated under similar conditions as reported in the work of Zhao et al [11]. The conversion was 66.7% after one hour of reaction, indicating a good reproducibility [11]. Additionally, the precipitation of black palladium is observed as indicated in Zhao et al. [11].

Table 7.4. Reproducibility data of the Heck reaction after 1 hour

Catalyst / Concentration [mmol/l]		Solvent	Temperature [ºC]	Conversion [%]
$Pd(OAc)_2(PPh_3)_2$[11]	2.5	MeCN	75	65.5
$Pd(OAc)_2(PPh_3)_2$	2.5	MeCN	75	66.7

7.4.2.2   Concentration selection

To test the catalyst activity after the RFA experiments the Heck reaction experiments should be performed under conditions where the reaction conversion is directly dependent on catalyst concentration. This is important because during the RFA experiments possible deactivation of palladium may occur. Therefore the Heck reaction is performed for the following catalyst precursor concentrations: 0, 0.1, 0.2, 0.5, 1 and 2.5

mmol/l. The reaction conversion measured after 15, 60 and 120 min is shown in Figure 7.5. No reaction occurred without catalyst present. In the presence of the catalyst the Heck reaction needs a certain activation period. Therefore after 15 minutes no conversion is detected for catalyst precursor concentrations 0.1-0.5 mmol/l. For catalyst precursor concentrations 1 mmol/l and 2.5 mmol/l conversion is equivalent. Also for these concentrations part of the catalyst has precipitated in a form of palladium black. For lower concentrations (0.1-0.5 mmol/l) this is not observed. A clear dependence of the reaction conversion and catalyst concentration is observed for concentration ranges of 0.1-0.5 mmol/l. This dependence is still not in the linear range but sufficiently clear to identify when a part of the catalyst after desorption of $PdCl_2$ in the RFA is deactivated. Thus, 0.1 mmol/l is selected as a catalyst concentration for performing the Heck reaction experiments after the RFA experiment.
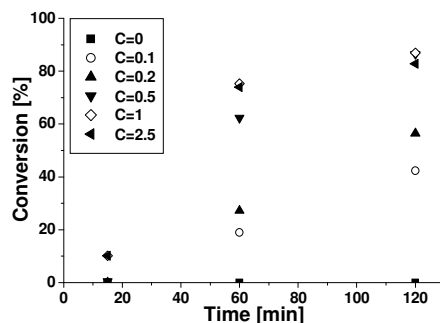

Figure 7.5. Selection of the catalyst concentration for the Heck reaction at 75ºC

7.4.2.3   Catalyst activity after RFA

After each RFA desorption cycle a sample is taken and the Heck reaction is performed. The results are shown in Figure 7.6. Conversions for the Heck reaction with non-recycled $PdCl_2$ after 15, 60 and 120 minutes are presented by the solid lines. With open and full symbols the conversions of the Heck reaction after each desorption cycles at 20ºC and 50ºC are presented respectively. Up to five cycles of reversible adsorption and desorption of the $PdCl_2$ no deactivation of the catalyst is observed.
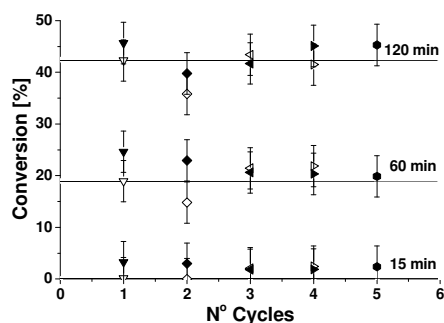
121

Figure 7.6. The Heck reaction conversion after the RFA experiments for desorption performed at 20ºC   (open symbols) and 50ºC (full symbols)

7.5   Conclusion

In this work the stability of reverse flow adsorption and the activity of the catalyst after multiple cycles of reversible adsorption/desorption of $PdCl_2$ are studied. The following conclusions are drawn:

- Leaching observed in the RFA experiments is not due to inadequacy of the process, but due to a flaw in adsorbate- adsorbent interaction.

- In spite of leaching, a constant concentration of $PdCl_2$ is reached at the outlet of the column during desorption after several adsorption/desorption cycles due to initial preloading of the column;

- The outlet concentration can be set to the feed concentration by adjusting the desorption temperature;

- After several cycles of the continuous adsorption/desorption of $PdCl_2$ there was no deactivation of the catalyst observed for the Heck reaction.

7.6   List of symbols

F -	Concentration and peak area ratio of MA and MC	[-]
MA -	Methyl acrylate	[-]
[*MA*]-	Concentration of methyl acrylate	[mol/l]
[*MA*]$_0$-	Initial concentration of methyl acrylate	[mol/l]
MC -	Methyl cinnamate	[-]
[*MC*]-	Concentration of methyl cinnamate	[mol/l]

7.7 Reference:

[1]   B. Cornils, W. A. Hermann, Applied Homogeneous Catalysis with Organometallic Compounds, Wiley-VCH, 2000

[2]   J.T. Scarpello, Nair D., et al., J. Membr. Sci. 5180 (2002) p. 1-15

[3]   T.Djekic, A.G.J. van der Ham, A.B. de Haan, J. Chrom. A 11420 (2007), p.32-38

[4]   T.Djekic, A.G.J. van der Ham, H. Bosch, A.B. de Haan, Chem. Eng. Sci. 62, (2007) p. 2032-2039

[5]   F.Alonso, I.P. Beletskaya, M. Yus, Tetrahedron 62 (2005) p.11771-11835

[6]   I.P.Beletskaya, J. Organomet. Chem. 1983,250, p.551-564

[7]   T. J. Jeffery, Chem. Soc., Chem. Commun. 1984 p. 1287-1289

[8]   T. J. Jeffery, Tetrahedron Lett., 1985,26, p. 2667-2670

[9]   A.. Brathe, L.L. Gundersen, F. Rise, A.B.Eriksen, , A.V. Vollsnes, L.Wang, Tetrahedron 1999,55, p.211-228

[10]   A. Scdmit , V.V. Smirnov, J. Mol. Catal. A:Chem, 2003, 203, p. 75-78

[11]   F. Zhao, B.M.Bhanage, M. Shirai, M. Arai, J. Mol. Catal. A, 142 (1999) p.383-388

[12]   D. Nicholls, Complexes and First –Row Transition Elements, The Whitefriars press Ltd., London and Tonbridge,1974

Conclusions and future outlook

The goal of this thesis was to evaluate a new concept for recovery and recycling of homogeneous catalysts: Reverse Flow Adsorption (RFA) Technology. The objective was to prevent leaching and deactivation of homogeneous catalysts in the recovery process. To achieve this four topics are studied in this work:

- Composition of metal complexes in solution;
- Selection of suitable adsorbents;
- Stability of the RFA (model and experimental);
- Activity of homogeneous catalysts after recovery of free metal by the RFA.

8.1 Composition of homogeneous catalysts in solution

The first step in understanding and modelling of the RFA concept is to obtain insight in the interactions of all species present in the liquid phase. Composition of homogeneous catalysts in solution is usually described by stability constants. In this work studied complex compounds are described with the 1:2 complexation model where concentration of each species present in the solution is calculated. The results show that even for very high values of the stability constants ($\approx 10^{14}$) with a ligand to metal ratio of 2 there is a still free metal present ($\approx 0.001\%$). If this amount of free metal is not included in the recovery process, a significant amount of metal can leach in time.

In this work we studied the composition of the different catalyst precursor forms. To apply RFA in the industrial process it is necessary to determine the composition of the catalyst forms in the catalytic cycle. In this way the real ratio of the active catalyst and other complex forms is known which can be applied in the modeling and optimization of the process. This approach is important since different interactions (e.g. reactant-catalyst, solvent-catalyst or product-catalyst interaction) can alter the equilibrium of the catalyst precursor forms.

8.2 Selection of suitable adsorbents

Selection of promising adsorbents for a selected homogeneous catalyst consists of a model design of adsorbent, a selection of functionalized groups on the adsorbent carrier, a competitive adsorption study of all complex species present in solution and a study of adsorption kinetics.

The modeling study of the adsorbent design showed that binding strength between adsorbing catalyst and selected adsorbent should be in the range of 0.8 l/mmol; adsorbent capacity and diffusion coefficient should be maximal; and particle size and bed porosity

minimal. Here should be also included material limitations such as surface area and particle shape, as well as process limitations such as allowed pressure drop.

Functionalized silica adsorbents are selected in our experimental work for adsorbent selection due to its rigid and uniform pore structure. Experiments demonstrate that a promising adsorbent for recovery of coordination complexes can be selected according to the Hard and Soft Acid Base theory. Besides the equilibrium studies the adsorption kinetic is evaluated in this thesis. The values of the effective diffusion coefficient are in the range of:

- pore size of 60Å: D_P=1.95·10^{-10}m^2/s,
- pore size of 90Å: D_P=5.8·10^{-10}m^2/s.

The particles with 90Å pore size should be selected for further research because they provide faster diffusion inside particles, and still have equivalent surface area as the one with 60 Å pore size (Chapter 5). In addition, we recommend studying adsorption kinetics of adsorbents with a pore size of 140 Ǻ. The decrease in surface area can be compensated with synthesizing bidentate type of adsorbents where the number of functionalized groups will be doubled. Due to the uniform pore structure and high effective diffusion coefficients it is experimentally shown that silica adsorbents are promising adsorbents for the Reverse Flow Adsorption application.

To recover homogeneous catalyst by the RFA all catalyst forms should be adsorbed. This was evaluated in Chapter 4 where competitive adsorption of different complex species (M, ML and ML$_2$) is studied. Results obtained by modeling the competitive adsorption isotherms illustrate that all complex forms (M, ML and ML$_2$) are adsorbed. In the future work this should be confirmed by studying an adsorbent surface after adsorption of homogeneous catalyst using techniques such as IR microscopy. In addition, selection of promising adsorbents should be studied at the conditions (e.g. temperature, pressure, type of solvent, presence of ligand) which will be applied for the specific studied reaction.

8.3   Design of reversible adsorption

Modeling the reversible adsorption/desorption process has shown that a stable operation for 500 cycles can be reached where no leaching of the catalyst species is noticed. The RFA process can be applied for wide ranges of the stability constants and becomes even more applicable for the recovery of homogeneous catalysts that have a lower metal concentration. In the simulation example, rhodium recovery in the BASF hydroformylation process requires a total adsorption bed volume of 6% of the reactor volume for the recovery of the metal part.

However, 96% efficiency of the recovery process is achieved in the experimental study of the reversible adsorption and desorption. This insufficiency was due to a flaw in the adsorbent-adsorbate interactions, where some form of the palladium present in the acetonitrile solution was not adsorbed. This outcome shows that the selected adsorbent must recover all present complex species, otherwise leaching can occur in spite of optimal design of the process. Although some leaching is detected, a constant concentration of $PdCl_2$ is reached at the outlet of the column after several adsorption/desorption cycles due to initial preloading of the column. This confirms that stable operation can be reached. Additionally, the outlet desorption concentration can remain equal to the feed concentration by adjusting the desorption temperature.

To improve the present RFA experiments, UV-Vis detectors should be integrated in the set-up to measure online catalyst concentration during adsorption and desorption. Furthermore, temperature effect and catalyst-solvent interaction should be studied in more details to provide a better insight into adsorption of all catalyst forms. In this way the current leaching can be prevented.

It is also recommended to demonstrate the stability of the complete Reverse Flow Adsorption concept by integrating a model for the reactor together with the models for recovery and recycling of homogenous catalyst which are given in Chapter 6. Furthermore, this model should be also experimentally validated.

8.4   Activity of homogeneous catalysts in the RFA

Finally, in this thesis the activity of the palladium catalyst after several cycles of reversible adsorption/desorption of $PdCl_2$ is studied. The Heck reaction is selected as a test reaction. After continuous adsorption/desorption of $PdCl_2$ for multiple cycles there was no deactivation of the catalyst observed.

The activity of a homogeneous catalyst should be fully studied after reversible adsorption and desorption of the active catalyst form and in the presence of reactants and products. During experimental demonstration of the RFA concept activity of the homogeneous catalyst should be continuously monitored for larger number of cycles.

8.5   Overall conclusion and outlook of RFA

In this thesis we demonstrated that Reverse Flow Adsorption can be a promising concept for recovery and recycling of homogenous catalysts. We studied adsorption of catalyst precursor forms and we achieved constant activity of the catalyst after recycling of its metal centre. Leaching of the metal is detected due to a flaw in adsorbate-adsobent interactions, and not due to a flaw in reverse flow adsorption experiments.

Prior to applying the RFA concept on industrial scale, a very selective silica based adsorbent should be chosen. This adsorbent should adsorb either all metal containing catalyst forms or free ligand, but be exclusive to solvent, reactants or products present in the feed. Also an economic evaluation of the concept should be conducted. Higher investment costs for the RFA application are expected due to the required preloading of the adsorption columns. Profit gained due to multiple recycling of the catalyst should be larger than an interest lost for investing in unused preloaded catalyst. This can be accomplished since multiple cycles can be reached by optimal design of the process where turnover number increases rapidly.

With a constant increase in the production, and herewith catalytic processes, profitable and complete recovery and recycling of homogeneous catalysts will be demanding. Reverse Flow Adsorption has all the potential to become one of the applied techniques.

List of publications

1. "*Determination of the stability constants for cobalt, nickel and palladium homogeneous catalyst complexes containing triphenylphosphine ligands*"   T. Djekic, Z. Zivkovic, A.G.J. van der Ham, A.B. de Haan, Applied Catalysis A: General, 308, pp. 144-152, 2006.

2. "*Evaluation of functionalized silica's for the adsorptive recovery of homogenous catalysts through interaction with the metal centre*" T. Djekic, A.G.J. van der Ham, A.B. de Haan, Journal of chromatography A, 1142, pp. 32-38, 2007

3. "*Adsorption of homogeneous catalysts over functionalized silica adsorbents: Modelling of the competitive adsorption isotherms*"   T. Djekić, A.G.J. van der Ham, H. Bosch, A.B. de Haan, J. Chem. Eng. Sci., 62, pp. 2032-2039, 2007

4. "*Effective* i*ntraparticle diffusion coefficient of CoCl$_2$ in mesoporous functionalized silica adsorbent by the Zero Length Column method*"   T. Djekić, V. Tripkovic, A.G.J. van der Ham, A.B. de Haan, Adsorption, (in press)

5. "*Silica Adsorbent Design and Process Evaluation for Recovery of Homogeneous Catalysts by Reverse Flow Adsorption*"   T. Dekic Zivkovic, A.B. de Haan, AIChE Journal, (submitted)

Curriculum vitae

Tanja Đekić Živković (maiden name Đekić) was born on the 8th January 1980 in Virovitica, Croatia. After finishing her secondary education at the VI Belgrade Gymnasium and St. Albans High School, WV, USA (1998) she studied Chemical Engineering at the University of Belgrade, Faculty of Technology and Metallurgy. After performing experimental work at the Separation Technology group, University of Twente, the Netherlands, she defended her diploma thesis at the University of Belgrade on 30th September 2003. Between March 2004 and February 2008 she accomplished her Ph.D. thesis "The Reverse Flow Adsorption Technology for the Process Integrated recycling of Homogeneous catalysts" under supervision of prof.dr.ir. Andre de Haan at the Separation Technology group, University of Twente and the Process Systems Engineering group, Eindhoven University of Technology.

-The End-